

# Advanced Techniques for Traffic Monitoring using Inductive Sensors

---

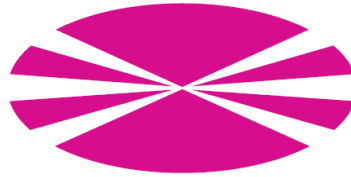
*José Juan Lamas Seco*



Department of Electronics and Systems  
Universidade da Coruña, Spain



Department of Electronics and Systems  
Universidade da Coruña, Spain



PHD THESIS

# Advanced Techniques for Traffic Monitoring using Inductive Sensors

José Juan Lamas Seco

17 de marzo de 2016

PhD Advisors:  
Adriana Dapena Janeiro  
Paula M. Castro Castro



Dña. Adriana Dapena Janeiro y Dña. Paula M. Castro Castro

CERTIFICAN:

Que el trabajo original titulado “Advanced Techniques for Traffic Monitoring using Inductive Sensors”, ha sido realizado por D. José Juan Lamas Seco bajo nuestra dirección en el Departamento de Electrónica y Sistemas de la Universidade da Coruña y concluye la tesis que presenta para optar al grado de Doctor.

A Coruña, 17 de marzo de 2016

Fdo: Dña. Adriana Dapena Janeiro  
Directora de la Tesis Doctoral  
Titular de Universidad  
Dpto. de Electrónica y Sistemas  
Universidade da Coruña

Fdo: Dña. Paula María Castro Castro  
Directora de la Tesis Doctoral  
Contratada Doctora  
Dpto. de Electrónica y Sistemas  
Universidade da Coruña



**Tesis Doctoral:** Advanced Techniques for Traffic Monitoring  
using Inductive Sensors

**Autor:** D. José Juan Lamas Seco

**Directores:** Dra. Adriana Dapena Janeiro y Dra. Paula M. Castro Castro

**Fecha:** 15 de junio de 2016

## **Tribunal**

Presidente:

Vocal:

Secretario:



*Cuando a mediados del siglo XIX el escocés James C. Maxwell presentó las Ecuaciones del Electromagnetismo, muy pocos fueron conscientes de que se encontraban ante un hito histórico, no sólo para la Ciencia, sino también para la humanidad. También es cierto que el gigante Maxwell se apoyó en otros gigantes: Coulomb, Gauss, Ampère, Faraday, etc. A principios del siglo XX el gigante Einstein se basó en las Ecuaciones de Maxwell del Electromagnetismo para elaborar su Teoría de la Relatividad Especial. Pero esto es Física. Hablemos de Ingeniería.*

*Mi primer contacto con los Detectores de Bucles Inductivos (ILDs, del inglés Inductive Loop Dectectors) fue, allá por el año 2000, cuando colaboré en el diseño de un detector de vehículos para su uso en las carreteras bajo competencia de la Xunta de Galicia. Se trataba de desarrollar un equipo al uso, capaz de contabilizar vehículos por carriles y medir sus velocidades y longitudes en los sistemas de doble bucle inductivo habituales en las carreteras de este país.*

*Tuvieron aún que transcurrir unos años, hasta el 2005, para que, de forma totalmente casual, entrase en contacto con las huellas inductivas de los vehículos. Fue por entonces cuando, con objeto de mejorar la precisión en la medida de la longitud de los vehículos, junto con mi hermano Carlos, que se encargaba del análisis informático de los datos, decidimos modificar el equipo detector para que capturase registros completos del paso de los vehículos, con el fin de ser usados en la optimización de umbrales. Mi sorpresa fue enorme al visualizar por primera vez las huellas inductivas de los vehículos y comprobar cuán diferentes eran según el tipo de vehículo y cuán similares para un mismo vehículo al pasar sobre los dos bucles sucesivos. En aquel momento pensé que estaba ante un tema muy interesante para un trabajo de investigación y quedó grabado así en mi memoria.*

*Cuando en el ao 2012, después de treinta años dedicado a la realización de desarrollos de ingeniería, sobre todo en el campo industrial, decidí retomar mi doctorado en la universidad, convencí a mis dos profesoras tutoras para iniciar una línea de investigación en el desarrollo de nuevas técnicas para la monitorización del tráfico de vehículos usando sensores inductivos, que espero se continúe y amplíe en el futuro a más investigadores.*

*Esta tesis resume mi trabajo de investigación de estos últimos cuatro años. Ha sido escrita en inglés para darle mayor difusión. Quiero anticipar al lector aquellos puntos a los que, por su mayor interés, recomiendo prestar una atención especial: en los capítulos 2 y 3, las comparativas entre ILDs resonantes y de amplitud; en el capítulo 4, el nuevo modelo de sensor inductivo multiespira (multi-loop en inglés), y en el capítulo 5, el descriptor en el dominio de la frecuencia para clasificación de vehículos con un único bucle.*

*Como no podía ser de otra forma, para su elaboración he tenido que recurrir a los gigantes. Se mencionan a lo largo de este trabajo a Maxwell, Fourier, Neumann, Cramer, Faraday, Ohm, Ampère, Laplace, Foucault, etc.*

*Hablemos de Ciencia ...*

# Agradecimientos

Cuando estás terminando tu tesis doctoral y vuelves la vista atrás eres consciente de cuánto tienes que agradecer a todas esas personas que, de un modo u otro, te han ayudado. Intentaré resumir en unas líneas mi gratitud a todas ellas y pido disculpas si hay alguna que se me quede olvidada.

En primer lugar, debo citar a mis dos directoras de tesis, las profesoras doctoras Adriana Dapena y Paula Castro, con las que, hace ya cuatro años, inicié una nueva línea de investigación, objeto de esta tesis, en el Grupo de Tecnología Electrónica y Comunicaciones (GTEC) del Departamento de Electrónica y Sistemas de la Universidad da Coruña. Tengo que agradecer a Adriana sus buenas ideas, que nos han proporcionado importantes aportaciones en este trabajo de investigación, y especialmente a Paula, por el enorme esfuerzo de pasarlo a Latex y la revisión meticulosa de todo el trabajo. Paula, un agradecimiento especial para ti.

También tengo que dar las gracias a otros miembros del GTEC: a Fran, por su disponibilidad y colaboración en las revisiones y en las traducciones al inglés, y a Julio, por su ayuda en el manejo de la herramienta Sim4Life para la obtención de los diagramas de corrientes inducidas. No olvido a los profesores del Máster en Tecnologías de la Información y Comunicaciones en Redes Móviles (TICRM), Luis, Carlos, José Antonio, etc., que, sin saberlo, pusieron la semilla para iniciar esta tesis.

No quiero tampoco olvidarme de agradecer la colaboración de Ricardo y Daniel de la empresa Dimaco S.C.G. de A Coruña, por su aportación en equipamiento y ayuda para la recogida de huellas inductivas de vehículos en varias localizaciones.

Mi mayor agradecimiento a mi familia, porque siempre estáis ahí incondicionalmente a mi lado, a las duras y a las maduras, para animarme a seguir adelante. Gracias especialmente a Marina, mi mujer, siempre pinchándome para no abandonar, creyendo en mis posibilidades más que yo mismo. Esta tesis también es tuya.

Mi eterno agradecimiento a todos.

*E ti vives no mundo, terra miña,  
berce da miña estirpe,  
Galicia, dóce mágoa das Españas,  
deitada rente ao mar, ise camiño,...*

Celso Emilio Ferreiro  
(Deitado frente ao mar)

# Resumen

El objetivo principal de este proyecto es el desarrollo de técnicas avanzadas para gestión del tráfico de vehículos usando un *Detector de Bucles Inductivos* (ILDs).

Para ello, en primer lugar se desarrolla e implementa un ILD que va a proporcionar huellas inductivas de los vehículos que transitan por una vía. Además de las funciones tradicionales de medida de aforamientos de tráfico, tales como densidad, ocupación y clasificación de vehículos, se pretende conseguir el reconocimiento de los mismos mediante el análisis de la señal de su huella. Basándose en la infraestructura existente en las carreteras para realizar los aforamientos de tráfico que usa fundamentalmente bucles inductivos, modificaciones de los equipos detectores van a permitir incluir además la función de re-identificación, para su uso en aplicaciones de control y supervisión de tráfico de vehículos. Por lo tanto, y aunque la tecnología de los detectores de bucles inductivos está totalmente extendida y en uso en este momento, se le añade una función de captura de las huellas inductivas del vehículo que permite aplicaciones adicionales de reconocimiento de los mismos para mejorar la clasificación, detección de velocidad con una sola espira, y re-identificación para aplicaciones de control y supervisión del tráfico rodado.

Este trabajo presenta un sistema completo para clasificación de vehículos compuesto de un detector de bucles inductivos y los correspondientes algoritmos *off-line*. El sistema detecta la presencia de vehículos mediante un desplazamiento en el periodo de oscilación del bucle seleccionado de forma que las huellas de los vehículos detectados se registran mediante la duración de un número prefijado de pulsos de oscilación. En este trabajo nos centraremos en la cuestión, todavía no resuelta a día de hoy, de contar el número de vehículos (clasificándolos en tres tipos, coches, furgonetas y camiones) que circulan por una carretera. El método clásico para tal propósito consiste en la estimación de la longitud del vehículo usando las huellas inductivas obtenidas en dos bucles y, a continuación, las clasifica de acuerdo con un umbral preestablecido.

Para la clasificación de los vehículos que circulan por una vía, presentamos un sistema bastante simple que usa esas huellas inductivas y la transformada rápida de Fourier (DFT, del inglés *Discrete Fourier Transform*). Para abordar el problema de clasificación en tres tipos de vehículos (como mencionábamos antes, coches, furgonetas y camiones) se propone un algoritmo heurístico basado en decisión por umbrales y en la magnitud del primer máximo espectral obtenido aplicando el análisis DFT a la huella inductiva del vehículo obtenida a partir de un único bucle. Además, el método aquí desarrollado puede aplicarse a huellas de vehículos capturadas con otros tipos de sensores. En este trabajo compararemos nuestro sistema con métodos de clasificación clásicos basados en la estimación de la longitud del vehículo obtenida a partir de dos bucles. Los resultados experimentales muestran que el criterio basado en la magnitud de la DFT exhibe un error

de clasificación más bajo que el alcanzado con dichos métodos, con la enorme ventaja de la utilización de un único bucle.

Por último, dado el elevado coste de estas pruebas en escenarios reales cada vez que una nueva técnica está siendo estudiada, hemos desarrollado un modelo avanzado del detector de bucles inductivos que claramente supera los modelos que se han usado tradicionalmente con unos resultados muy similares a los obtenidos directamente usando el prototipo de ILD que hemos desarrollado.

## Resumo

O obxectivo principal deste proxecto é o desenvolvemento de técnicas avanzadas para a xestión do tráfico de vehículos usando un *Detector de Bucles Inductivos* (ILD).

Así, desenvólvese e impleméntase un ILD que vai a proporcionar pegadas inductivas dos vehículos que transitan por unha vía. Ademáis das funcións tradicionais de medidas de aforamentos de tráfico, tales como densidade, ocupación e clasificación de vehículos, preténdese conseguir o recoñecemento dos mesmos mediante a análise do sinal da pegada. Baseándose na infraestrutura existente nas estradas para realizar os aforamentos de tráfico que usa fundamentalmente bucles inductivos, modificacións dos equipos detectores permiten incluír ademáis a función de re-identificación, para o seu uso en aplicacións de control e supervisión de tráfico de vehículos. Polo tanto, e aínda que a tecnoloxía dos detectores de bucle inductivos está totalmente extendida e en uso neste momento, engádese unha función de captura das pegadas inductivas do vehículo que permite aplicacións adicionais de recoñecemento dos mesmos para mellorar a clasificación, detección de velocidade cunha soa espira, e re-identificación para aplicacións de control e supervisión do tráfico rodado.

Este traballo presenta un sistema completo para clasificación de vehículos composto dun detector de bucles inductivos e dos correspondentes algoritmos *off-line*. O sistema detecta a presenza de vehículos mediante un desprazamento no período de oscilación do bucle seleccionado de xeito que as pegadas dos vehículos detectados se rexistran mediante a duración dun número prefixado de pulsos de oscilación. Neste traballo imos focalizarnos na cuestión, aínda non resolta a día de hoxe, de contar o número de vehículos (clasificándoos en coches, furgonetas e camións) que circulan por unha estrada. O método clásico para este propósito consiste na estimación da lonxitude do vehículo usando as pegadas inductivas obtidas en dous bucles e, a continuación, clasificalas dacordo a un umbral preestablecido.

Para a clasificación dos vehículos que circulan por unha vía, presentamos un sistema bastante sinxelo que usa esas pegadas inductivas e a transformada rápida de Fourier (DFT, do inglés *Discrete Fourier Transform*). Para abordar o problema de clasificación en tres tipos de vehículos (como comentabamos antes, coches, furgonetas e camións) propónse un algoritmo heurístico baseado en decisión por umbrais e na magnitude do primeiro máximo espectral obtido aplicando a análise DFT á pegada inductiva do vehículo obtida a partir dun único bucle. Ademáis, o método proposto pode aplicarse a pegadas de vehículos capturadas con outros tipos de sensores. Neste traballo compararemos o noso sistema a métodos de clasificación clásicos baseados na estimación da lonxitude do vehículo obtida a partir de dous bucles. Os resultados experimentais amosan que o criterio baseado na magnitude da DFT presenta un erro de clasificación máis baixo que o que acadan estes métodos, coa enorme vantaxe da súa utilización dun único bucle.

Por último, dado o elevado custo das probas realizadas en escenarios reais cada vez que unha nova técnica está baixo estudo, desenvolvemos tamén un modelo avanzado de detector de bucles inductivos que claramente supera os modelos que se están a usar tradicionalmente con esta finalidade cuns resultados moi similares aos obtidos directamente usando o prototipo de ILD proposto neste traballo.

# Summary

The main goal of this work is the development of advanced techniques for vehicle traffic monitoring using *Inductive Loop Detectors* (ILD).

Thus, we develop an implementation of an ILD that will provide vehicle inductive signatures passing on a road. Several traditional functions of traffic monitoring are intensity, density or vehicle classification, but moreover we want to identify those vehicles using their inductive signatures. Based on the infrastructure already available under the road pavements for traffic applications using inductive sensors, some modifications on the detector equipments allow us to include re-identification functions to be used for vehicle traffic control and management. Therefore, although the technology of inductive loop detectors is widely used in many countries, we will add a module for capturing the inductive signatures leading to additional applications of vehicle recognising to improve the classification, the vehicle detection, and their re-identification useful for vehicular traffic control and surveillance tasks.

This work presents a complete system for vehicle classification composed by an inductive-loop detector and the corresponding off-line algorithms. The system detects the presence of vehicles by means of a shift in the oscillation period of the selected loop so that the signature of the detected vehicles is registered by measuring the duration of a fixed number of oscillator pulses. We focus on the open issue of counting the number of vehicles (classified into cars, vans and trucks) on a roadway. The classical method for such purpose consists of estimating the vehicle length using the inductive signatures obtained from two loops and, subsequently, it classifies them taking into account a prefixed threshold.

We present a simple system to classify vehicles travelling along a road using inductive signatures and the *Discrete Fourier Transform* (DFT). We focus on the problem of classifying those vehicles into three types (cars, vans, and trucks) using a heuristic algorithm based on threshold decision and on the magnitude of the first spectral maximum obtained applying the DFT analysis to the vehicle inductive signature from only one loop. Moreover, the method here developed can be applied to vehicle signatures captured with other types of sensors. In this dissertation we will compare our system to classical methods based on estimating the vehicle length obtained from two loops. Experimental results show that the magnitude of the DFT exhibits a lower classifying error rate than that achieved using the length-based method, with the enormous advantage of requiring only one loop.

Finally, due to the high cost of testing in real scenarios each new technique under study, we also develop an advanced model of an ILD that clearly outperforms the traditional ones with similar results to those directly obtained from the hardware prototype

XIV

of ILD proposed in this work.

# Index

<b>List of figures</b>	<b>XIX</b>
<b>List of tables</b>	<b>XXIII</b>
<b>1. Introduction</b>	<b>1</b>
1.1. Problem Overview . . . . .	1
1.2. Main Contributions . . . . .	2
1.2.1. Publications . . . . .	3
1.3. Thesis Overview . . . . .	4
1.4. Notation . . . . .	5
<b>2. Vehicle Inductive Sensors</b>	<b>7</b>
2.1. Preliminary Traffic Concepts . . . . .	7
2.2. Introduction to Traffic Sensors . . . . .	9
2.2.1. Passive Sensors . . . . .	9
2.2.2. Active Sensors . . . . .	12
2.3. Inductive Loop Traffic Sensors . . . . .	17
2.3.1. Resonant ILDs . . . . .	19
2.3.2. Amplitude ILDs . . . . .	24
2.4. Conclusions . . . . .	27
<b>3. Design of an Inductive Sensor</b>	<b>29</b>
3.1. Colpitts Oscillator . . . . .	29
3.2. Pulse Counter . . . . .	30
3.3. Measurement . . . . .	34
3.4. Registration . . . . .	34
3.5. Real Capturing of Inductive Signatures . . . . .	36
3.6. Impact of Noise on Digital Detectors . . . . .	39
3.6.1. Impact of Noise on Resonant Detectors . . . . .	40
3.6.2. Impact of Noise on Amplitude Detectors . . . . .	40

3.7.	Conclusions . . . . .	43
<b>4.</b>	<b>Modelling of an Inductive Sensor</b>	<b>45</b>
4.1.	Induced Currents by Rectangular Coils . . . . .	46
4.1.1.	Induced Currents for the Standard Approach . . . . .	47
4.1.2.	Induced Currents for the Proposed Approach . . . . .	48
4.2.	Standard Modelling Approach . . . . .	49
4.2.1.	Experiment Results . . . . .	53
4.3.	Proposed Modelling Approach . . . . .	59
4.3.1.	Calculation of the Mutual Inductances $M_i$ and $M_{ij}$ . . . . .	60
4.3.2.	Calculation of the Self-inductance $L_C$ . . . . .	60
4.3.3.	Calculation of the Multi-loop Self-inductances $L_i$ . . . . .	60
4.3.4.	Experiment Results . . . . .	62
4.4.	Comparison of Performances using Real Inductive Signatures . . . . .	68
4.4.1.	Experiment 1: Real Inductive Signatures . . . . .	68
4.4.2.	Experiment 2: Real Loop Sensitivity . . . . .	69
4.5.	Conclusions . . . . .	73
<b>5.</b>	<b>Advanced Methods for Vehicle Traffic Monitoring</b>	<b>75</b>
5.1.	Model for Time Estimation . . . . .	76
5.2.	Speed Estimation . . . . .	77
5.2.1.	Standard Method . . . . .	78
5.2.2.	Proposed Method . . . . .	78
5.2.3.	Speed Estimation Results . . . . .	79
5.3.	Vehicle Classification . . . . .	87
5.3.1.	Standard Method . . . . .	88
5.3.2.	Proposed Method . . . . .	88
5.3.3.	Vehicle Classification Results . . . . .	96
5.4.	Conclusions . . . . .	100
<b>6.</b>	<b>Conclusions and Future Work</b>	<b>103</b>
6.1.	Conclusions . . . . .	103
6.2.	Future Work . . . . .	104
6.2.1.	Multi-loop Model for Non-Flat Profiles . . . . .	105
6.2.2.	Capturing of Vehicle Profiles from Inductive Signatures . . . . .	105
6.2.3.	Increasing Classification Categories . . . . .	105
6.2.4.	Re-identification and Travel Time Estimation . . . . .	105
<b>A.</b>	<b>Calculation of the Mutual Inductance of Two Rectangular Loops</b>	<b>107</b>

<b>B. Calculation of the Inductance of a Single-layer Rectangular Coil of <math>N_C</math> Turns</b>	<b>111</b>
<b>C. DFT Descriptor Properties</b>	<b>115</b>
C.1. Independence on Speed . . . . .	115
C.2. Independence on Lateral Displacement . . . . .	116
<b>D. Resumen extendido</b>	<b>119</b>
<b>E. List of Acronyms</b>	<b>127</b>
<b>References</b>	<b>129</b>



# List of figures

2.1. Relationship speed-density per lane ( <b>upper left</b> ), speed-flow per lane ( <b>upper right</b> ), and flow-density per lane ( <b>bottom left</b> ), extracted from [1].	8
2.2. Traffic monitoring by video camera (see [2]).	10
2.3. Microphone for traffic monitoring (see [3]).	11
2.4. Seismic sensor (see [4]).	11
2.5. Magnetic sensor for traffic monitoring (extracted from [1]).	12
2.6. Microwave radar (see [5]).	13
2.7. Doppler radar (see [6]).	13
2.8. Laser radar (extracted from [1]).	14
2.9. Active infrared sensor for traffic monitoring (extracted from [1]).	15
2.10. Ultrasonic sensor (extracted from [1]).	15
2.11. Emerging technologies for traffic monitoring (extracted from [1]).	16
2.12. Sensor combining passive infrared and Doppler microwave radar sensors (extracted from [1]).	16
2.13. Inductive loop detector.	17
2.14. Inductive traffic sensor (see [7]).	18
2.15. Road loop (see [8]).	18
2.16. Parallel resonant circuit.	21
2.17. 8-loop vehicle inductive detector (Afortes-Dimaco).	23
2.18. Amplitude RLC circuit.	24
2.19. Magnitude of the transfer function for frequencies from $f = 50$ kHz to 100 kHz and inductances $L = 90, 92, 94, 96, 98, 100 \mu\text{H}$ .	25
2.20. Magnitude of the inverse transfer function for inductances $L$ from 90 $\mu\text{H}$ to 100 $\mu\text{H}$ and frequencies $f = 76, 77, 78, 79, 80$ kHz.	26
3.1. Circuit for the Colpitts oscillator.	30
3.2. Measurement method by using comparison and capture.	31
3.3. Multiplex system with eight inductive loops.	32
3.4. Interconnections for AT89C51RE2.	33
3.5. Photo of the hardware prototype.	33

3.6.	Flowchart of attention at T2 interruption. . . . .	35
3.7.	A photo of the measurement location, with GPS coordinates: 43.235941 (Lat.); -8.464462 (Long.). . . . .	36
3.8.	Interconnections from the inductive loop to the detector. . . . .	37
3.9.	Interface of the signature visor. . . . .	37
3.10.	From left to right, the upper figures show the photo of a private car and the respective signatures obtained with the loops 3 and 4. The figures in the middle of the picture show a truck and its corresponding signatures captured also using the loops 3 and 4. The lower figures display the photo of a bus and two signatures obtained with the first and the second loop, respectively. . . . .	38
3.11.	Block scheme of a resonant detector. . . . .	39
3.12.	Inductive signature of the resonant detector with and without noise. . . . .	41
3.13.	Block scheme of an amplitude detector. . . . .	41
3.14.	Inductive signature of the rms amplitude detector with and without noise. . . . .	42
3.15.	Inductive signature of the detector with synchronous demodulator with and without noise. . . . .	42
3.16.	Output SNR for resonant and amplitude detectors. . . . .	44
4.1.	Induced Foucault currents (extracted from [1]). . . . .	47
4.2.	Rectangular coil and induced currents. . . . .	48
4.3.	Eddy current distribution on a 4 m × 1.5 m aluminium plate centred on a 2 m × 2 m coil with a distance $d = 25$ cm between them. . . . .	49
4.4.	Eddy current density in the longitudinal axis $x$ . . . . .	50
4.5.	Eddy current density in the transversal axis $y$ . . . . .	50
4.6.	Inductive loop and vehicle model. . . . .	51
4.7.	Equivalent circuit coil-vehicle undercarriage. . . . .	51
4.8.	Resonant oscillation circuit used for vehicle detection. . . . .	52
4.9.	Sensitivity (in %) as a function of the distance between the road loop and the vehicle undercarriage (in cm) for three different coverages of the vehicle on the loop (25%, 50%, and 100%). . . . .	54
4.10.	Vehicle profile. . . . .	55
4.11.	Inductive signatures as a function of the vehicle width. . . . .	56
4.12.	Inductive signatures as a function of the vehicle distance. . . . .	56
4.13.	Inductive signatures as a function of the vehicle length. . . . .	57
4.14.	Inductive signatures as a function of the vehicle speed. . . . .	58
4.15.	Inductive signatures as a function of the vehicle acceleration. . . . .	58
4.16.	Road Inductive loop and multi-loop currents. . . . .	59
4.17.	Multi-loop equivalent circuit. . . . .	61

4.18. Sensitivity (in %) as a function of the distance $d$ in cm between the road loop and the vehicle undercarriage for a vehicle with a length $l = 200$ cm and three widths: $b = 50$ cm, $100$ cm and $200$ cm. . . . .	63
4.19. Multi-loop current distributions. . . . .	64
4.20. Inductive signatures for different values of the number of loops $N$ . . . . .	65
4.21. Inductive signatures for different values of the vehicle length $l$ , with $N = 200$ . . . . .	65
4.22. Inductive signatures for different values of the distance $d$ , with $N = 200$ . . . . .	66
4.23. Inductive signatures for different values of the vehicle width $b$ , with $N = 200$ . . . . .	67
4.24. Inductive signatures for different values of the vehicle speed $v$ , with $N = 200$ . . . . .	67
4.25. Inductive signatures for different values of the vehicle acceleration $a$ , with $N = 200$ . . . . .	68
4.26. Rectangular single-layer coil with $N_C$ wire turns on an insulating core, with length $a$ , width $w$ , and axial length $a_l$ , with a flat parallel plate of length $l$ and width $b$ . . . . .	69
4.27. Inductive signatures for different values of the loop distance $d$ ( $d = 2.5, 3.5, 4.5, 5.5$ cm), for a plate of $25$ cm $\times$ $16$ cm. . . . .	70
4.28. Inductive signatures for different values of the plate length $l$ ( $l = 9, 16, 25$ cm), with $b = 16$ cm and $d = 2.5$ cm. . . . .	70
4.29. Inductive signatures for different values of the plate length $l$ ( $l = 9, 16, 25$ cm), with $b = 16$ cm and $d = 3.5$ cm. . . . .	71
4.30. Inductive signatures for different values of the plate width $b$ ( $b = 9, 16, 25$ cm), with $l = 16$ cm and $d = 2.5$ cm. . . . .	71
4.31. Inductive signatures for different values of the plate width $b$ ( $b = 9, 16, 25$ cm), with $l = 16$ cm and $d = 3.5$ cm. . . . .	72
4.32. Maximum sensitivity (in %) as a function of the distance $d$ between the experimental inductive loop and the $25$ cm $\times$ $16$ cm aluminum plate. . . . .	72
5.1. Scheme for dual loop time. . . . .	76
5.2. Sign of $e_M - e_P$ : positive (1), zero (0), or negative (-1), considering $v_N = 100$ km/h and $T = 10$ ms. . . . .	80
5.3. Sign of $e_M - e_P$ : positive (1), zero (0), or negative (-1), considering $v_N = 100$ km/h and $T = 4$ ms. . . . .	80
5.4. Histogram of speeds $v_I$ and $v_O$ . . . . .	81
5.5. Time index distributions of mean speeds considering data of Río Anllóns station. . . . .	81
5.6. Histogram of speeds $v_M$ and $v_P$ . . . . .	82

5.7. Average error (%) in speed estimation. . . . .	84
5.8. Influence of acceleration on speed estimation. . . . .	87
5.9. Software simulator: Examples of profiles ( <b>Top</b> ), signatures ( <b>Middle</b> ) and normalized DFT ( <b>Bottom</b> ) for two vehicles of 4 m and 6 m in length and for different speeds. . . . .	90
5.10. Software simulator: Signature descriptor for vehicle length from 4 m to 10 m, and speed from 20 km/h to 120 km/h. . . . .	91
5.11. Impact of additive white Gaussian noise on the DFT descriptor. . . . .	92
5.12. Vehicle profile. . . . .	92
5.13. Inductive signatures in the frequency domain as a function of the vehicle length. . . . .	93
5.14. Experimental results: Examples of captured signatures. . . . .	97
5.15. Experimental results: DFT descriptor versus vehicle length, computed from acquired signatures. . . . .	98
5.16. Experimental results: Success rates for different threshold values. . . . .	98
A.1. Pictures of the multiloop inductive model. . . . .	107
B.1. Picture of two identical rectangular loops. . . . .	111
B.2. Rectangular coil and one loop at a $z$ position. . . . .	112

# List of tables

1.1. General notation. . . . .	5
5.1. Statistical parameters for $\mathbf{v}_M$ and $\mathbf{v}_P$ distributions . . . . .	83
5.2. Statistical hypothesis tests . . . . .	84
5.3. $R^l[\omega_n]$ parameter for vehicles without acceleration and 50 km/h of speed as a function of the vehicle length (in m) . . . . .	93
5.4. $R^l[\omega_n]$ parameter as a function of the vehicle width (in cm) . . . . .	93
5.5. $R^l[\omega_n]$ parameter as a function of the distance vehicle-road loop (given by the profile in Fig. 5.12) . . . . .	94
5.6. $R^l[\omega_n]$ parameter as a function of the vehicle speed (in km/h) . . . . .	94
5.7. $R^l[\omega_n]$ parameter as a function of the vehicle acceleration (in $\text{m/s}^2$ ) . . . . .	94
5.8. $R^l[\omega_n]$ for a plate width of $w = 16$ cm and a distance between plate and loop of $d = 2.5$ cm, as a function of the plate length $l$ . . . . .	95
5.9. $R^l[\omega_n]$ for a plate length of $l = 16$ cm and a distance between plate and loop of $d = 2.5$ cm, as a function of the plate width $w$ . . . . .	95
5.10. $R^l[\omega_n]$ for a plate length of $l = 16$ cm and a plate width of $w = 16$ cm, as a function of the distance $d$ between plate and loop. . . . .	95
5.11. Confusion matrices for AC-523 road. . . . .	99
5.12. Confusion matrices for AC-415 road. . . . .	99
5.13. Comparison with other related literature works in terms of success rates. . . . .	100



# Chapter 1

## Introduction

### 1.1. Problem Overview

One of the most important aspects of *Intelligent Transportation Systems* (ITS) is vehicle traffic monitoring, essentially those applications whose aim is to count the number of vehicles on a roadway or to know their speed, occupancy, or structural characteristics like density and type. Although different sensors have been used for vehicle detection, like *Inductive Loop Detectors* (ILDs) [9], magnetometers [10] or infra-red thermal image sensors [11], since their introduction in the 1960s, ILDs are the more commonly used sensors in traffic management systems. ILDs have been widely used for tasks such as vehicle classification [12–16], vehicle re-identification [17–20], and speed estimation with a single loop [21].

Several works set the basis for the theoretical study of ILDs. In [22, 23] an approximate model for an ILD is shown, and an equivalent circuit model is detailed in [23]. Klein et al. presented in [1] a detailed study on the sensitivity of an inductive loop and the response time to changes in inductance of different digital detectors. Cheevarunothai et al. [24] addressed the sensitivity problems in dual loops and proposed software and hardware implementation solutions to identify and correct them. In [25] three-dimensional maps illustrating the sensitivity of various inductive loops located under the asphalt surface of roads are obtained.

These works have led to different implementations of ILDs. In the US4680717A patent [26] a multiplex system for vehicular traffic detection with a single oscillator is presented. A multiple vehicle detection system incorporating low-cost oscillators and an algorithm to calibrate the device following changes in environmental conditions is proposed in [27]. However, although both works allow the detection of the presence of vehicles, none of them register their inductive signatures. In [28] a system to detect multiple vehicles is also developed, but it requires multichannel acquisition of analogue

signals which makes it overly complex. Furthermore, due to the function not being fully multiplexed and to the use of the same frequencies in near loops, such development causes significant interferences between channels (also known as *crosstalk*).

As mentioned before, ILDs are the most commonly active sensors used in traffic management systems [9,12–14,17,21,29,30]. These sensor systems mostly need accuracy and reliability when estimating vehicle speed with a minimum delay in control strategies. The estimate obtained from dual loop detectors is usually accurate [31–34], but it requires a proper maintenance of both loops, which implies that it is not the optimum solution in terms of cost. Moreover, only one loop is available in most of traffic systems. Although some algorithms have already been developed for single-loop classification [35–37] and single-loop speed estimation [38, 39], how to achieve enough accuracy using only one loop is still an open question.

## 1.2. Main Contributions

Taking into account the drawbacks identified in the previous section, in this work we propose a multiplex system for the *Simple Detection of Inductive Vehicle Signatures* (SiDIVS). Our proposal implies a fully multiplexed system that avoids the interference between loops (also called *inter-loop interference*) thanks to a very simple and almost fully automatic digital measurement process. Therefore, it does not require neither the use of complex and expensive analog processing circuits nor of analog signal acquisition methods. Based on *Time-Division Multiplexing* (TDM) with multiple oscillators, one for each inductive loop, the system detects the presence of vehicles by means of a shift in the oscillation period of the selected loop and registers the signature of the detected vehicles.

Additionally, we develop an inductive sensor model based on that presented in [1]. The main advantage of sensor modelling is that it provides us useful prior information before the actual testing in a real scenario, thus reducing the necessary time and resources. However, this model does not consider neither the penetration depth of the Foucault currents induced in the road coil nor also both the influence of the coil pieces of the vehicle undercarriage that are not on the road coil and the influence of the neighbouring coils. For that reason, we propose a new sensor model which includes all the aforementioned effects and that clearly better fits under all the possible scenarios to the real sensor behaviour.

Moreover, we will present an advanced method for vehicle identification based on analysing the inductive signatures in the frequency domain instead of working in the time domain, as usual. The proposed descriptor in the transform domain will be used for vehicle classification by means of a simple threshold-based method.

Thus, we will show some experimental results obtained with these methods. The first set of experiments has been performed using the inductive sensor model proposed by

us, which provides useful information about several traffic parameters; and the second one uses our hardware prototype capable of obtaining simultaneous inductive signatures of vehicles travelling on a road with minimal cost. This work will show that the *Discrete Fourier Transform* (DFT) is an adequate tool to classify vehicles from inductive signatures because of the spectral features extracted from the frequency domain analysis. This analysis exhibits interesting properties. Firstly, it can be used with only one loop, as it is shown in Chapter 5. Secondly, the DFT has been demonstrated to be independent to variations in the vehicle speed. Moreover, the experimental results performed with real signatures captured with our inductive sensor prototype have shown that the proposed DFT-based criterion obtains a significant reduction of the total error percentage when compared with the standard criterion based on estimating both speed and length of passing vehicles with two loops and with other methods in the literature.

### 1.2.1. Publications

The publications presented below exhibit the acceptance of the work proposed by the Ph.D. student in the field in recent years.

#### ■ Patents

1. José Juan Lamas-Seco, Adriana Dapena, Paula M. Castro, “Identificación automática de vehículos mediante RFID con Detector de Bucles Inductivos”, número de solicitud P201200846, fecha de prioridad: 29/08/2012. Oficina Española de Patentes y Marcas, ámbito nacional.

#### ■ Journal papers

1. José J. Lamas-Seco, Paula M. Castro, Francisco J. Vazquez-Araujo, Adriana Dapena, “SiDIVS: Simple Detection of Inductive Vehicle Signatures with a Multiplex Sensor System” submitted to *Sensors*, Jan. 2016.
2. José J. Lamas-Seco, Paula M. Castro, Adriana Dapena, Francisco J. Vazquez-Araujo, “Multi-Loop Inductive Sensor Model” submitted to *IEEE Sensor Letters*, Dec. 2015.
3. José J. Lamas-Seco, Paula M. Castro, Adriana Dapena, Francisco J. Vazquez-Araujo, Begoña Garcia-Zapirain, “Influence of Vehicle Characteristics on an Inductive Sensor Model for Traffic Applications” accepted to be published at *International Journal of Simulation: Systems, Science & Technology*, Nov. 2015. Factor SJR: 0,187 (Q4/T3 SJR 187/219 Computer Science: Modeling and Simulation).

4. José J. Lamas-Seco, Paula M. Castro, Adriana Dapena, Francisco J. Vazquez-Araujo, “Vehicle Classification using the Discrete Fourier Transform with Traffic Inductive Sensors”, *Sensors*, 15(10), 27201-27214, 2015; ISSN: 1424-8220, doi:10.3390/s151027201. Impact factor in 2014: 2.245 (Q1/T1 10/56 INSTRUMENTS & INSTRUMENTATION).

■ **International and national conferences**

1. José J. Lamas-Seco, Paula M. Castro, Adriana Dapena, Francisco J. Vazquez-Araujo, Begoña Garcia-Zapirain, “SimSiVIDS: Modelling of an Inductive Sensor for Traffic Applications”, UKSim-AMSS 9th European Modelling Symposium on Mathematical Modelling and Computer Simulation, Oct. 6-8, 2015, Madrid, Spain.
2. José J. Lamas-Seco, Adriana Dapena, Francisco J. Vazquez-Araujo, Paula M. Castro, “A Novel Criterion for Vehicle Classification using Inductive Vehicle Signatures”, Third International Conference on Advances in Computing, Electronics and Communication (ACEC 2015), Oct. 2015, Zurich, Switzerland.
3. José J. Lamas-Seco, Adriana Dapena, José P. González-Coma, Paula M. Castro, Francisco J. Vazquez-Araujo, “System for Vehicle Classification: Hardware Prototype and Off-line Signal Processing”, IEEE Region 8 EuroCon 2015 Conference, Sept. 2015, Salamanca, Spain.
4. José J. Lamas-Seco, Paula M. Castro, Adriana Dapena, Francisco J. Vazquez-Araujo, “Sistema de clasificación basado en magnitud-FFT usando huellas inductivas de vehículos”, XXX Symposium Nacional de la Unión Científica Internacional de Radio (URSI 2015), Sept. 2015, Pamplona, Spain.
5. José J. Lamas-Seco, Paula M. Castro, Francisco J. Vazquez-Araujo, Adriana Dapena, “Sistema múltiplex para la detección sencilla de huellas inductivas de vehículos”, XXIX Symposium Nacional de la Unión Científica Internacional de Radio (URSI), Valencia, Spain, Sept. 2014.

### 1.3. Thesis Overview

This thesis is organized as follows:

In Chapter 2, we present different types of sensors used for traffic applications. A theoretical study of ILDs is also included in this chapter.

Next, Chapter 3 shows the practical implementation of our prototype using a multiplex sensor with eight channels.

In Chapter 4, we model this inductive sensor thus avoiding expensive tests in real scenarios.

In Chapter 5, we propose an advanced technique in the frequency-domain for traffic classification. Several simulation results will show the good performance of our proposal.

Finally, Chapter 6 is dedicated to the conclusions and future work.

## 1.4. Notation

In this section we introduce the notation used throughout this work.

Real scalar	$x$
Absolute value	$ \cdot $
Matrix	$\mathbf{X}$
Column vector	$\mathbf{x}$
Element at row $j$ and column $k$	$[\mathbf{X}]_{j,k}$
All-zeros vector	$\mathbf{0}$
Transpose	$(\cdot)^T$
Matrix inverse	$\mathbf{A}^{-1}$

Table 1.1: General notation.



# Chapter 2

## Vehicle Inductive Sensors

A sensor is a device capable of detecting physical or chemical magnitudes, called instrumentation variables, and transform them into electrical variables. Instrumentation variables can be temperature, light intensity, distance, acceleration, tilt, displacement, pressure, force, torque, humidity, motion, pH, etc. An electrical quantity can be a resistor, an electrical capacity, a voltage, an electric current, etc.

Sensors are needed in modern traffic monitoring systems, since maximizing the efficiency and capacity of existing transport networks is crucial due to the exponential increase in traffic volume in last years and limited construction of new roads. The strategies leading to an efficient use of existing infrastructures are known as *Intelligent Transportation Systems* (ITS), which make use of a wide variety of sensors and technologies for traffic control and monitoring, and also for information sharing.

This chapter is organized as follows. First, we introduce some fundamental traffic concepts. Since different types of sensors have been used for traffic applications in recent years, this chapter follows with a review of the most used ones to end with a detailed description of the inductive sensors on which we will focus our work: the *Inductive Loop Detectors* (ILDs).

### 2.1. Preliminary Traffic Concepts

The *traffic intensity* or *traffic flow* is defined as the number of vehicles passing through a fixed section of the road per time unit, and is expressed in vehicles/h (time intensity) or vehicles/day (daily intensity).

The *traffic density* is defined as the number of vehicles that occupy a stretch of road with a given length in a concrete moment. It is usually measured in vehicles/km. The maximum density value takes place when all the vehicles are in a row without gaps between them, and logically depends on the average length of the vehicle.

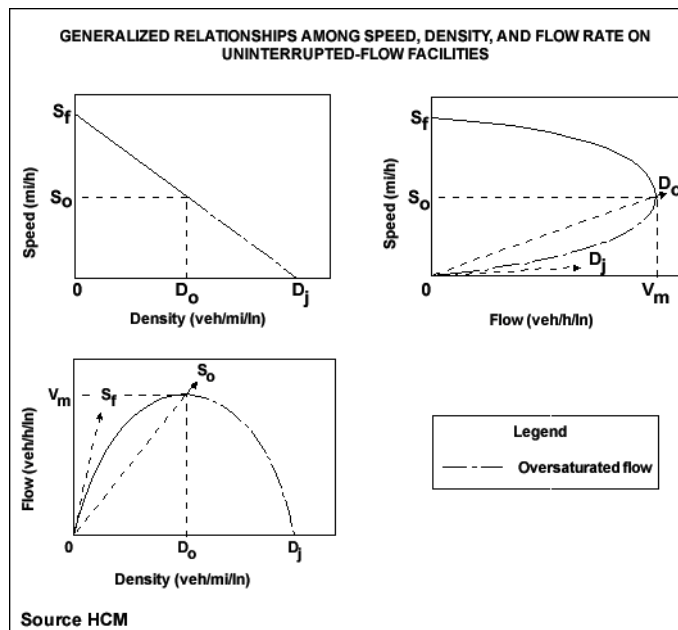


Figure 2.1: Relationship speed-density per lane (**upper left**), speed-flow per lane (**upper right**), and flow-density per lane (**bottom left**), extracted from [1].

The *travel time* is defined as the time employed by a vehicle to travel between two fixed points spaced a certain length. The *travel speed* is the ratio between the travel length and the travel time.

The density can be calculated using both the average travel speed and the traffic density, which are more easily measured, as follows

$$v = s \cdot D, \quad (2.1)$$

where  $v$  is the traffic intensity expressed in vehicles/h,  $s$  is the average travel speed in km/h, and  $D$  is the traffic density, expressed in vehicles/km. You can see in Fig. 2.1 the relationship between all these parameters.

In traffic control systems it is frequently used the parameter of road occupation instead of traffic density because it is easier to be measured. The *space occupancy* is defined as the proportion of the road length covered by vehicles, and the *time occupancy* is defined as the time proportion that a cross section is occupied by vehicles. Therefore, the space occupancy could be calculated as the product of the traffic density by the average vehicle length, and the time occupancy as the traffic intensity by the average time that the vehicle takes to pass through a cross section of the road, so that it can be measured by adding the times used by all the vehicles to traverse a section for a while.

The maximum traffic flow of a road is known as *capacity*. The density at which this

occurs is referred to as *critical density*, denoted as  $D_0$ , and the speed at which it happens is referred to as *critical speed*, denoted as  $s_0$  (see Fig. 2.1).

The aforementioned traffic concepts are related to the basic parameters of speed, length, and times of passing of each vehicle, which are registered by the detector equipments.

## 2.2. Introduction to Traffic Sensors

Nowadays there are a great variety of devices for collecting data on traffic conditions (which are known as detectors or traffic sensors). Most of them are capable of measuring some traffic parameters like the number of vehicles (strength), speed of movement, the vehicle type, and the track occupancy as a percentage of time presence.

Sensors can be classified accordingly to their location in the road, i.e. as in-roadway and over-roadway sensors. In general, problems of installation and maintenance are suffered by in-roadway sensors and of blocking of *Line-Of-Sight* (LOS) by weather conditions or obstacles by over-roadway sensors.

However, the more frequently-used classification of sensors is accordingly to the existence (or not) of an external energy source. Thus, we can talk of active and passive sensors, respectively. Both types and the corresponding technologies to collect the aforementioned parameters as well as their strengths and weaknesses will be presented in the following subsections of the chapter.

### 2.2.1. Passive Sensors

Passive sensors measure reflected radiation that has been emitted from the surrounding environmental elements. Therefore, they do not need any additional energy source and directly convert the external stimulus to electric energy. For that reason, they do not influence each other in the case of proximity.

For traffic applications, we can mainly find the following passive sensors.

#### Image Processing-based Sensors

Its operation is based on the treatment of images captured by a *TeleVision* (TV) camera (see Fig.2.2). The camera images are digitized and processed by algorithms that identify changes in the background image, determining whether a vehicle is in the area of interest. Analysing successive images we can determine many parameters like intensity, speed or vehicle length.

The main advantage of this type of detectors is the possibility of using slow video image in case of incidents, the possibility of automatic incident detection, there are no

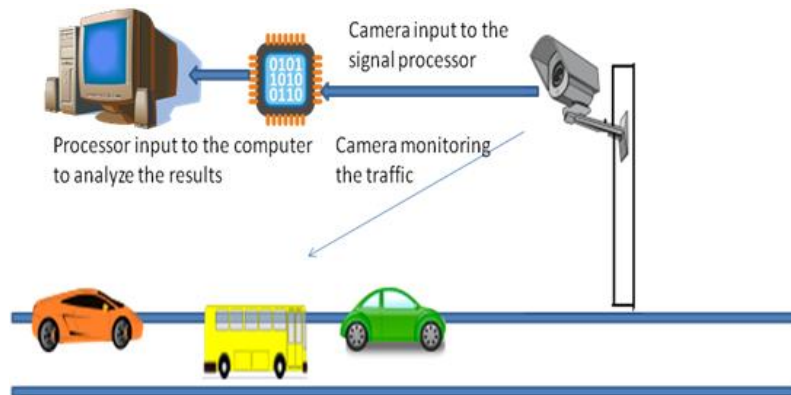


Figure 2.2: Traffic monitoring by video camera (see [2]).

intruders on the pavement of the road, do not suffer wear by vehicles passing or road maintenance, and have high reliability. However, this sensor has a high installation cost, requires a cone of vision as perpendicular as possible to the area to be measured, and its operation can be altered by the visibility of the road (fog, night..), and usually a single camera measures only one lane. Moreover, the obstacles between source and sensors could difficult the vehicle detection.

Other technologies based on image processing are the image processing via satellite or via thermal *InfraRed* (IR) sensors, which could be necessary in the case of coverage of wide areas or under dark conditions, respectively, although the treatment of the thermal noise can complicate the detection in the case of passive IRs.

### Acoustic Sensors

Acoustic signals are captured by microphones and therefore, the type of microphones selected to be used for such purposes is critical. With these sensors, typically installed at ground level but outside the travel lines, we can avoid the limitations of both in-roadway and over-roadway sensors. However, bad atmospheric conditions or acoustic noise may seriously affect vehicle detection. Such reasons limit the use of this technology for vehicle classification tasks. The microphone could be affected by reflections from its support, although these interferences are better avoided when the support is behind the microphone (see Fig. 2.3).

### Seismic Sensors

These sensors detect the vibrations produced by moving vehicles. We can see in Fig. 2.4 a picture of a seismic sensor. This detector has 3 channels of 24 bits with up to 2 000 *samples per second* (sps). We can classify them accordingly to the measured

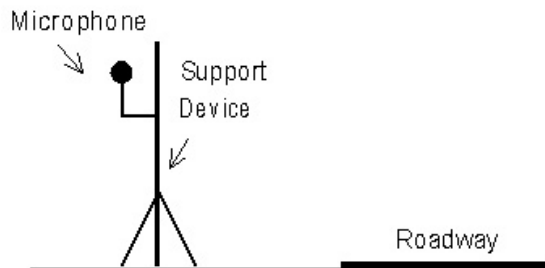


Figure 2.3: Microphone for traffic monitoring (see [3]).



Figure 2.4: Seismic sensor (see [4]).

ground motion, i.e. ground velocity (geophone) or ground acceleration (accelerometer). Contrary to acoustic traffic sensors, they are not so sensitive to weather conditions due to the earth propagation but lower frequencies than that used by the seismic device strongly disturb vehicle detection and also the type of terrain where they are buried or the depth are determining factors in their proper operation for traffic monitoring tasks.

### **Magnetic Sensors**

Magnetic sensors detect the distortion of the Earth local magnetic field produced by the passage of a ferromagnetic metal mass, i.e. the vehicles, over them. It can be seen in Fig. 2.5 how this sensor works when a vehicle is passing over it. Magnetic sensors consist of a metal tube inside which there is an iron core with a coil connected to an amplifier.

Such detectors have the advantage of an easy replacement and being passive, but conversely are severely disturbed by power lines, railways, lightning, etc. Moreover, these detectors do not detect non-ferromagnetic metals, like as aluminium or copper, which

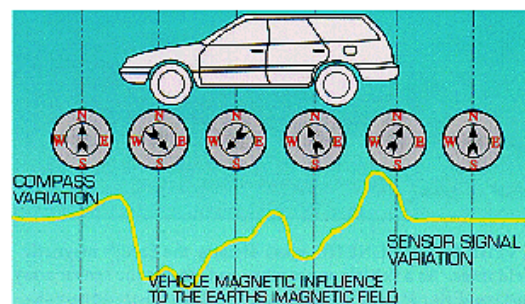
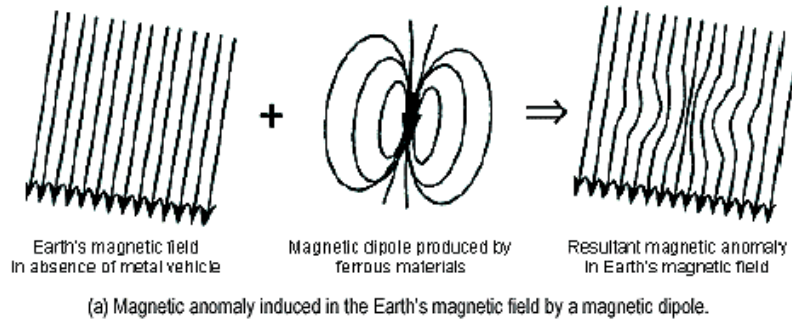


Figure 2.5: Magnetic sensor for traffic monitoring (extracted from [1]).

are present on the vehicle undercarriages.

### 2.2.2. Active Sensors

Active sensors require its own source of excitation and its sensor measures the reflected energy. Again, we will discuss in this section the most frequently used active sensors for traffic applications.

#### Radar Sensors

Vehicle detectors using *R*Adio *D*etection *A*nd *R*anging (RADAR) sensors emit microwave energy at high frequencies in the direction in which vehicles travel (see Fig. 2.6). With this technique it is possible to determine both the intensity and speed of vehicles by means of the change in frequency of the emitted signal due to the Doppler effect, which is proportional to the vehicle speed (see Fig. 2.7). The most prominent error for police radar “gun is the cosine error, caused by the radar beam arriving with a certain angle to the path of the target vehicle. The effect is the measurement of a lower speed than that of the target vehicle passing on the road.

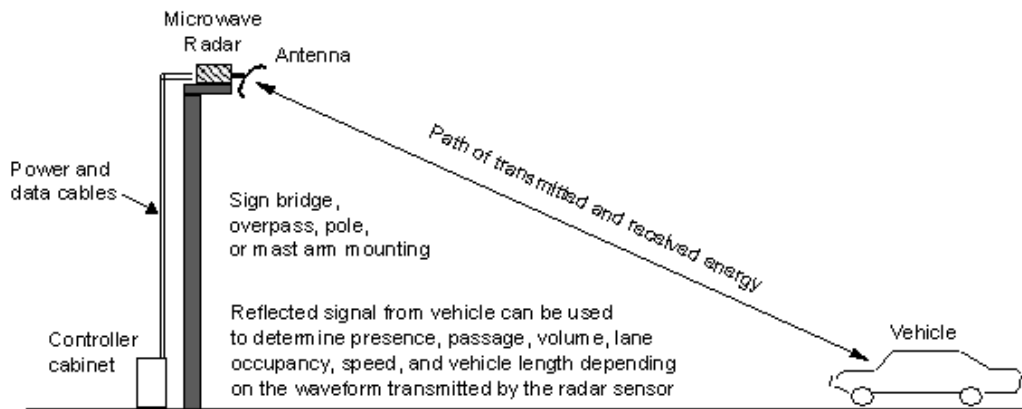


Figure 2.6: Microwave radar (see [5]).

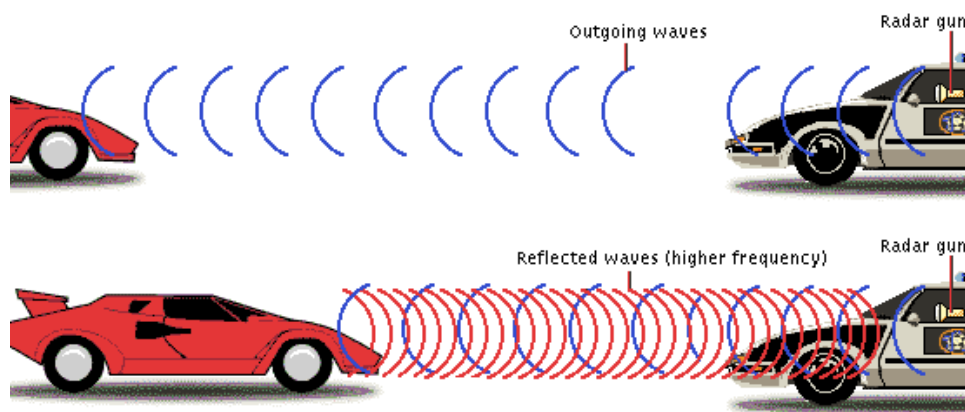


Figure 2.7: Doppler radar (see [6]).

The main advantages of such sensors are that they are transportable and very accurate in the speed measurement, are no intruders on the road and have good performance with bad weather. However, in the case of stationary vehicles or low speed ( $\leq 10$  km/h) the information provided by radar sensors is not reliable since the road would appear as empty as result of their measurements. However, that problem has been eliminated in recent years, although the cost and also maintenance and surveillance of such devices is still expensive. Moreover, one radar per lane is required.

### Laser Sensors

*Light Detection And Ranging* or *Laser Imaging Detection And Ranging* (LIDAR) is a technology that allows to determine the distance from a laser emitter to an object

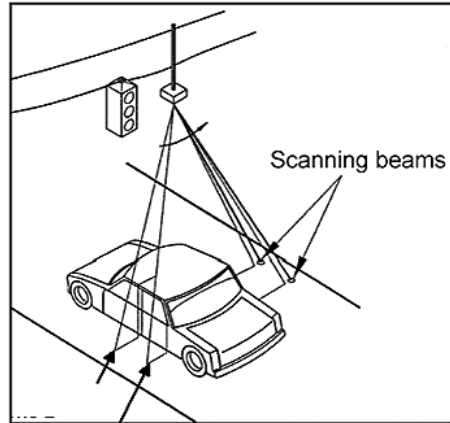


Figure 2.8: Laser radar (extracted from [1]).

using a pulsed laser beam (see Fig. 2.8). The distance to the object is determined by measuring the time delay between the pulse transmission and its detection through the reflected signal. Laser radar uses a laser light beam in the infrared band.

Some advantages of LIDAR against radar are its faster, with a narrower beam, its greater portability and lower maintenance, and its lower cost. However, one limitation is that LIDAR has to be static, i.e. it can not be moved during the measurement.

### Infrared Sensors

The IR detection systems are based on the use of a photon sensor placed on a pole or bridge along the lane to be monitored and measure the energy in the IR band emitted by the road. When a vehicle enters the detection zone causes a change in the radiated energy due to its temperature. In this case we have only a passive detector that measures the traffic intensity. Moreover, if the detector emits energy in the infrared spectrum, a portion of this energy will reflect with the passage of vehicles and thus will allow us to measure their speed, and therefore this would be an active detector (see Fig. 2.9).

Such detectors are not intruders in the road, but have not been very popular because of its low accuracy since they do not detect vehicles at low speed. Again, installation and maintenance costs are important drawbacks of this technology.

### Ultrasound Sensors

Ultrasound sensors emit ultrasonic sound waves perpendicular to the road (see Fig. 2.10). The presence of a vehicle is determined by the difference in time to get the reflected wave in the case to do it on the floor or on a vehicle. The frequency of the emitted waves lies in the range of 25 to 50 KHz, above the audible frequency band. They are

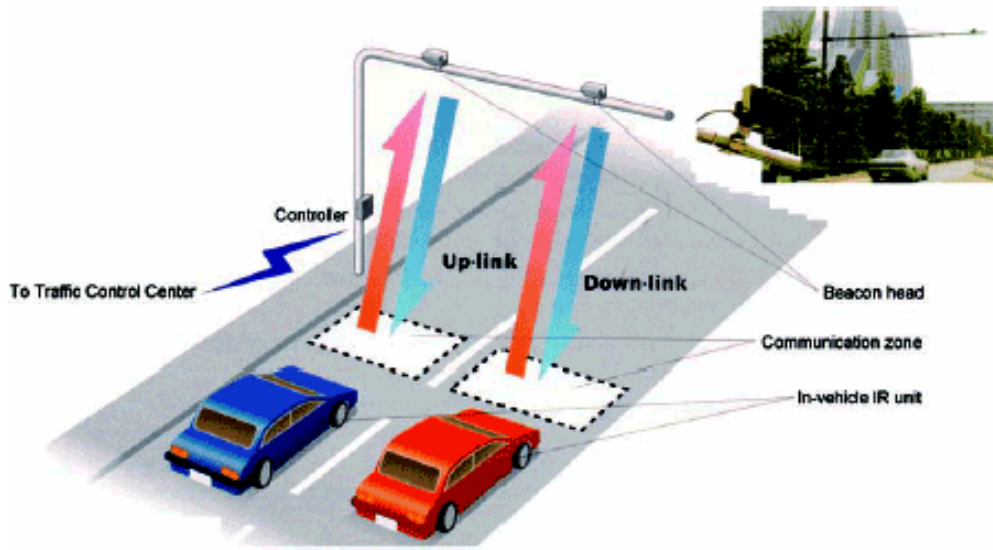


Figure 2.9: Active infrared sensor for traffic monitoring (extracted from [1]).

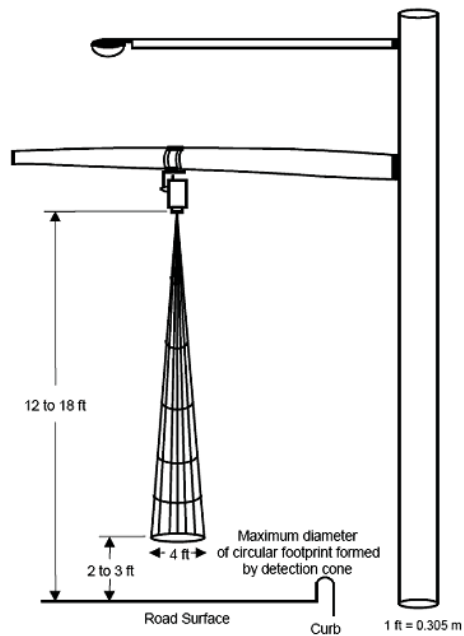


Figure 2.10: Ultrasonic sensor (extracted from [1]).

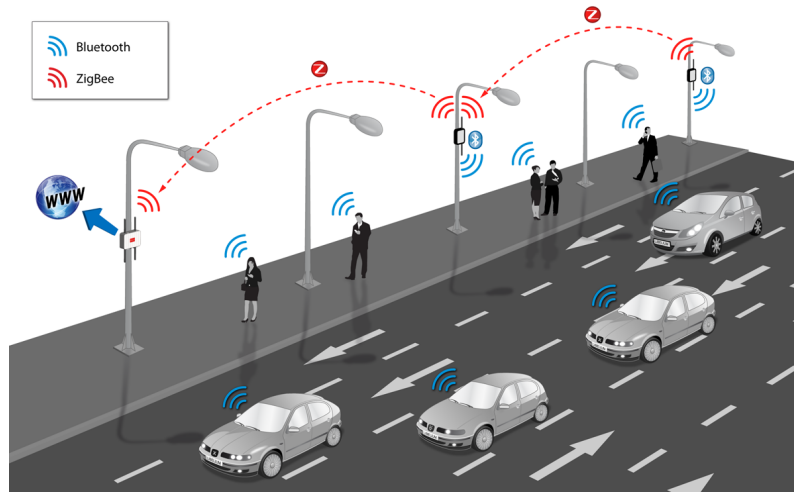


Figure 2.11: Emerging technologies for traffic monitoring (extracted from [1]).

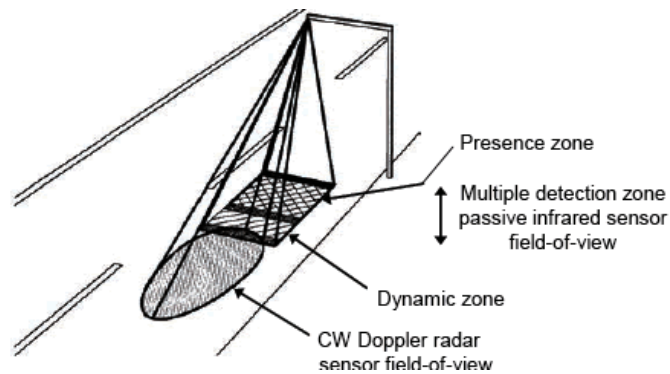


Figure 2.12: Sensor combining passive infrared and Doppler microwave radar sensors (extracted from [1]).

very sensitive to temperature and wind, which make them inadequate for their operation, specially in our region, Galicia, although they are very easy to install.

### Emerging Sensors

Recent technologies like the standard communication protocols Bluetooth or Zigbee also allow to detect mobile devices like cars in a road.

It is basically a high-range Bluetooth/Zigbee device that is able to detect the *Media Access Control* (MAC) addresses (unique device identifier) of the devices installed in the mobile targets, i.e. the vehicles passing on the road (see Fig. 2.11).

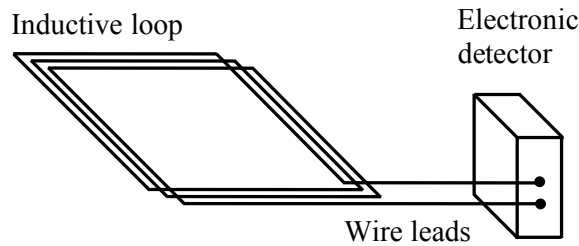


Figure 2.13: Inductive loop detector.

### Inductive Loop Sensors

Inductive loop sensors are based on the principle of electromagnetic induction. On the pavement a few cuts are made into squares of 2 m side, as we can see in Fig. 2.15. A coil is created burying cable in these cuts and then filled with epoxy resin, for example.

When a vehicle is passing, its metal mass induces a Foucault current that is interpreted as the passage of a vehicle. The duration of the current could be used to measure the lane occupation. Also the vehicle speed can be easily calculated. Double loop detectors also measure the vehicle length allowing us to classify the vehicles accordingly to the types established in advance. This type of inductive loop detectors are those that have greater presence in Spain, since it is a highly developed technology, of simple operation, unaffected by environmental conditions, and low installation cost. Although those inductive sensors present a complicated replacement in case of breakage, a need for regular calibration, and the inevitable interruption of traffic in case of maintenance tasks, its flexible design can adapt to a enormous variety of applications, even making use of a single loop, providing better accuracy in traffic classification than other commonly used techniques.

## 2.3. Inductive Loop Traffic Sensors

Figures 2.13 and 2.14 depict the elements of an ILD. It consists of one or more coils with one or more turns (usually 3 to 5) embedded in the road pavement (see Fig. 2.15); isolated cables for the connection from the coils to the control cabinet; and the electronic equipment (i.e., the detector) inside the cabinet.

The sensitivity  $S$  of an inductive loop is a measurement of its ability to detect small changes in inductance and is defined as the ratio between the change in inductance due to passing traffic and the initial inductance (i.e., the inductance when a vehicle is not present). Thus, we can express the sensitivity as

$$S = \frac{\Delta L}{L_{nv}} = \frac{L_{nv} - L_v}{L_{nv}}, \quad (2.2)$$

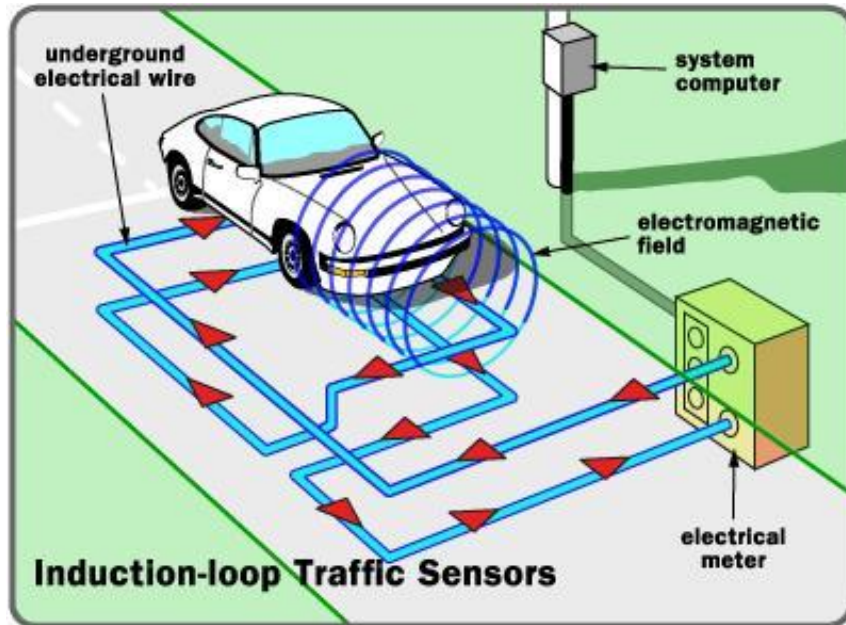


Figure 2.14: Inductive traffic sensor (see [7]).



Figure 2.15: Road loop (see [8]).

where  $L_{nv}$  is the initial inductance when no vehicle is present, and  $L_v$  is the inductance when a vehicle is present.

The *threshold sensitivity* can be defined as the smallest inductance change that can be distinguished by the detector device. The system sensitivity must be equal to or greater than the sensitivity threshold of the electronics unit. *National Electrical Manufacturers Association* (NEMA) Standards specify the sensitivity threshold for three classes of test vehicles when they are centred in a single  $1.8 \text{ m} \times 1.8 \text{ m}$  three-turn loop with 30.5 m of lead-in cable. Those vehicle classes are

- Class 1: 0.13 percent in inductance change (small motorcycle).
- Class 2: 0.32 percent in inductance change (large motorcycle).
- Class 3: 3.2 percent in inductance change (automobile).

Modern inductive detectors of vehicle presence are digital because they provide more reliable, accurate, and precise measurements than analogue detectors. Currently, the majority of ILDs indirectly measure variations in inductance as indicated in Eq. 2.2. These variations are caused by the presence of a vehicle in the detection area of the inductive loop, which produces a decrease of inductance. Two methods are used to measure such variations: the first one, based on measuring the frequency or period changes of an oscillator resonant circuit, and the second one, based on measuring the voltage amplitude changes of a RLC circuit operating at a fixed frequency.

We will briefly describe in the following subsections both ILD types, known as *resonant ILDs* and *amplitude ILDs*, respectively.

### 2.3.1. Resonant ILDs

Resonant ILDs are based on the measurement of changes of oscillation frequency or period. The oscillator frequency is controlled by the parallel resonant circuit of Fig. 2.16, also called *tank circuit*, which is constituted by a non-ideal loop inductance in parallel with a capacitance placed in the detector. The complex impedance of this circuit is given by

$$\mathbf{Z}(jw) = \frac{R(1 - w^2LC) + w^2RLC + j(wL(1 - w^2LC) - wR^2C)}{(1 - w^2LC)^2 - w^2R^2C^2}. \quad (2.3)$$

Since for a resonant circuit it verifies  $\text{Im}[\mathbf{Z}(jw)] = 0$ , we have that  $w_0L(1 - w_0^2LC) - w_0R^2C = 0$ , which gives us the resonant angular frequency  $w_0$

$$w_0 = \sqrt{\frac{L - R^2C}{CL^2}}. \quad (2.4)$$

Since  $R \approx 1 \Omega$ ,  $L \geq 50 \mu\text{H}$ , and  $C \leq 100 \text{nF}$ ,  $L \gg R^2C$ , and the oscillation frequency  $f_0$  can be approximated by

$$f_0 = \frac{\omega_0}{2\pi} \cong \frac{1}{2\pi\sqrt{LC}}. \quad (2.5)$$

It is important to note that the oscillation frequency depends on the inductance as  $f_0 = kL^{-1/2}$ , and the frequency change is given by  $\Delta f = f_v - f_{nv}$ , being  $f_v$  the oscillation frequency with vehicle presence, and  $f_{nv}$  the oscillation frequency without its presence. Thus, we have

$$f_v = kL_v^{-1/2} = k(L_{nv} - \Delta L)^{-1/2} = KL_{nv}^{-1/2} \left(1 - \frac{\Delta L}{L_{nv}}\right)^{-1/2} = f_{nv} \left(1 - \frac{\Delta L}{L_{nv}}\right)^{-1/2}, \quad (2.6)$$

and

$$\frac{\Delta f}{f_{nv}} = \frac{f_v - f_{nv}}{f_{nv}} = \frac{f_v}{f_{nv}} - 1 = \frac{1}{\sqrt{1 - \frac{\Delta L}{L_{nv}}}} - 1. \quad (2.7)$$

Since  $\Delta L/L_{nv}$  is very small,  $\Delta f/f_{nv}$  can be approximated by the first two terms of the Taylor series, i.e.

$$\frac{\Delta f}{f_{nv}} \approx \frac{1}{2} \frac{\Delta L}{L_{nv}} = \frac{1}{2} S, \quad (2.8)$$

where  $S$  is the sensitivity of the inductive loop (see Eq. 2.2). This sensitivity can thus be approximated by

$$S = \frac{\Delta L}{L_{nv}} \approx 2 \frac{\Delta f}{f_{nv}} = 2 \frac{f_v - f_{nv}}{f_{nv}} = 2 \frac{T_{nv} - T_v}{T_v} = 2 \frac{\Delta T}{T_v}, \quad (2.9)$$

where  $T_v$  is the period of oscillation if a vehicle is over the coil, and  $T_{nv}$  denotes the period of oscillation otherwise. Experimental results have shown that the loop sensitivity  $S$  is extremely repeatable for fixed sizes and geometries of both the loop and the vehicle and for a fixed distance between them, as can be verified from Eqs.(2.2) and (2.9).

Depending on whether the inductive loop measures changes on the frequency or on the period of the waveform, the characteristics of the detector are different, which will be explained in the following.

### ILDs using Frequency Shift (*Type I/II*)

*Type I* detectors measure frequency shifts  $\Delta f$  and *type II* detectors measure relative frequency shifts  $\Delta f/f$ . Both types have requirements in measurement time that can not be assumed in practical systems for acquisition of inductive signatures [1].

*Type I* detectors compare a value proportional to the frequency of the loop oscillator with a reference frequency periodically taken when vehicles are not present. When the counter exceeds the reference in a threshold value a vehicle is detected.

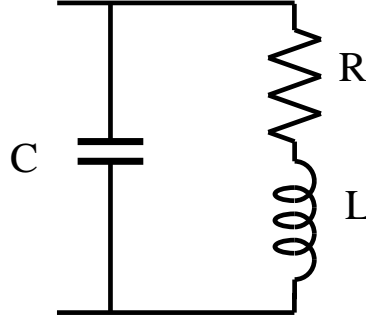


Figure 2.16: Parallel resonant circuit.

The reference value is given by  $N_{nv}$  as follows

$$N_{nv} = f_{nv}T_c = \frac{f_{nv}}{f_c}, \quad (2.10)$$

where  $T_c$  and  $f_c$  are respectively fixed counting times and frequencies.

On the other hand, with the presence of a vehicle over the loop the number of cycles is calculated as

$$N_v = f_vT_c = \frac{f_v}{f_c}. \quad (2.11)$$

The shift  $\Delta N$  can then be calculated as the difference between the values given by Eqs. (2.10) and (2.11) as

$$\Delta N = N_{nv} - N_v = \frac{f_{nv} - f_v}{f_c} = \frac{\Delta f}{f_c}. \quad (2.12)$$

Equating this value to the minimum detection threshold, denoted as  $N_t$ , gives us

$$\Delta N = \frac{\Delta f}{f_c} = N_t \quad \rightarrow \quad \Delta f = N_t f_c. \quad (2.13)$$

Thus, from Eq. 2.9 we obtain the threshold sensitivity  $S_t$  in the way

$$S_t \cong 2 \frac{\Delta f}{f_{nv}} = 2 \frac{N_t f_c}{f_{nv}} = 2 \frac{N_t}{N_{nv}}. \quad (2.14)$$

Then, due to  $N_{nv}$ , the characteristics of the oscillation loop (determined by  $L$  and  $C$ ) have a great influence on the threshold sensitivity in *type I* detectors.

*Type II* detectors work similarly to *type I* ones but maintaining approximately constant the counting value  $N_c = f/f_c$  of the oscillation frequency  $f$ , and therefore being  $T_c$  variable. For this case, the threshold sensitivity  $S_t$  is given by

$$S_t \cong 2 \frac{N_t}{N_c}. \quad (2.15)$$

Thus, as we can see from Eq. 2.15, ILDs using relative frequency shift measurements, i.e.  $\Delta f/f_{nv}$ , provide a threshold sensitivity that is approximately constant, independent from the measured frequency, and therefore, from  $L$  or  $C$  of the parallel resonant circuit of Fig. 2.16

### ILDs using Period Shift (*Type III/IV*)

Detectors whose operation is based on period changes (i.e., based on period shifts  $\Delta T$ ), known as *type III* or *type IV*, in which period shifts or relative period shifts are measured, respectively, present a measurement time that is short enough for their use in applications of inductive signature capturing, although the characteristics of the oscillation loop have influence on the threshold sensitivity.

*Type III* detectors based on period shift use a reference clock signal whose frequency is of several MHz, typically between 20 and 1000 times greater than the oscillation frequency of the inductive loop we are interested in measuring. The period of the oscillation signal is calculated as the number of cycles  $N$  of the reference clock signal in  $m_c$  cycles of the oscillation signal. When a vehicle stops or passes over the loop the oscillation frequency increases, so the period (and thus the number of cycles  $N$ ) decreases. The counter of clock signal periods without vehicles involved is given by

$$N_{nv} = \frac{mT_{nv}}{T_r}, \quad (2.16)$$

where  $T_r$  is the period of the reference clock signal. On the other hand, with the presence of a vehicle over the loop the number of cycles is calculated as

$$N_v = \frac{mT_v}{T_r}. \quad (2.17)$$

The shift  $\Delta N$  can then be calculated as the difference between the values given by (2.16) and (2.17) as

$$\Delta N = N_{nv} - N_v = \frac{m}{T_r} (T_{nv} - T_v) = m \frac{\Delta T}{T_r}. \quad (2.18)$$

Equating this value to the minimum detection threshold  $N_t$  gives us

$$\Delta N = m \frac{\Delta T}{T_r} = N_t \quad \rightarrow \quad \Delta T = \frac{N_t T_r}{m}, \quad (2.19)$$

so from Eq.2.9 we obtain the threshold sensitivity  $S_t$  as

$$S_t \cong 2 \frac{\Delta T}{T_v} = 2 \frac{N_t T_r}{m T_v} = 2 \frac{N_t}{N_v}. \quad (2.20)$$



Figure 2.17: 8-loop vehicle inductive detector (Afotres-Dimaco).

From this equation, it can be seen that for *type III* detectors there is a loss in threshold sensitivity for high oscillation frequencies, although this loss can be easily reduced by increasing the frequency  $f_r$  corresponding to the reference clock signal.

*Type IV* detectors work similarly to *type III* ones but maintaining approximately constant the threshold sensitivity by selecting a value for  $N_t$  of  $S_t N_v$ , so that the sensitivity is constant and expressed as

$$S \cong 2 \frac{N_t}{N_v} = 2S_t. \quad (2.21)$$

ILDs using relative period shift measurements provide a threshold sensitivity that does not depend on the measured period.

Most digital detectors can operate with four or more loops. The problem of crosstalk for resonant ILDs is solved by separating the loops using *Time-Division Multiplexing* (TDM) [26, 28]. These multiplexed models sequentially feed and analyse the channels more than 100 times per second using period shift detectors which, as mentioned before, are fast enough to allow these scanning rates.

Our practical implementation is based on a *type III* detector using TDM, as we will detail in the next chapter. We can see in Fig. 2.17 a real vehicle inductive detector of 8 loops.

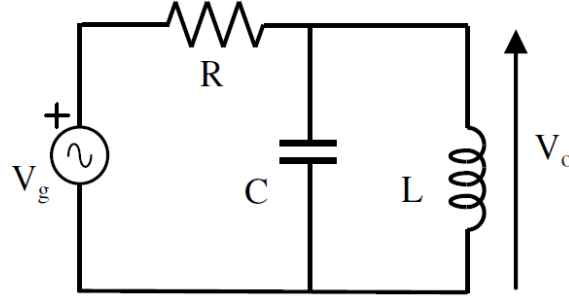


Figure 2.18: Amplitude RLC circuit.

### 2.3.2. Amplitude ILDs

Amplitude ILDs are based on the measurement of changes in voltage amplitude of a RLC circuit to which a fixed frequency signal is applied [31,40,41]. Figure 2.18 shows the RLC circuit formed by the loop inductance  $L$  and both the resistance  $R$  and the capacity  $C$  in the detector, connected to the sinusoidal voltage generator  $V_g$  operating at a fixed frequency  $f = \omega/2\pi$ . The amplitude of the output voltage  $V_o$  changes with the value of the loop inductance  $L$ .

The complex transfer function  $V_o/V_g$  is given by

$$\frac{V_o}{V_g} = \frac{1}{1 - jR \left( \frac{1}{\omega L} - \omega C \right)}, \quad (2.22)$$

and the magnitude of  $V_o/V_g$ , i.e.  $|V_o/V_g|$  is

$$\frac{|V_o|}{|V_g|} = \frac{1}{\sqrt{1 + R^2 \left( \frac{1}{\omega L} - \omega C \right)^2}}. \quad (2.23)$$

Figure 2.19 shows six magnitude transfer curves obtained for  $R = 1 \text{ k}\Omega$ ,  $C = 50 \text{ nF}$ ,  $f \in [50, 100] \text{ kHz}$ , and six inductance values  $L = 90, 92, 94, 96, 98, 100 \text{ }\mu\text{H}$ . Figure 2.20 shows the magnitude of the inverse transfer function obtained for  $R = 1 \text{ k}\Omega$ ,  $C = 50 \text{ nF}$ , inductance  $L \in [90, 100] \text{ }\mu\text{H}$ , and five frequency values  $f = 76, 77, 78, 79, 80 \text{ kHz}$ .

It is important to note that the voltage amplitude depends on the inductance as follows

$$V = \frac{1}{k_1 L + k_2}, \quad (2.24)$$

and the amplitude change is given by

$$\Delta V = V_v - V_{nv}, \quad (2.25)$$

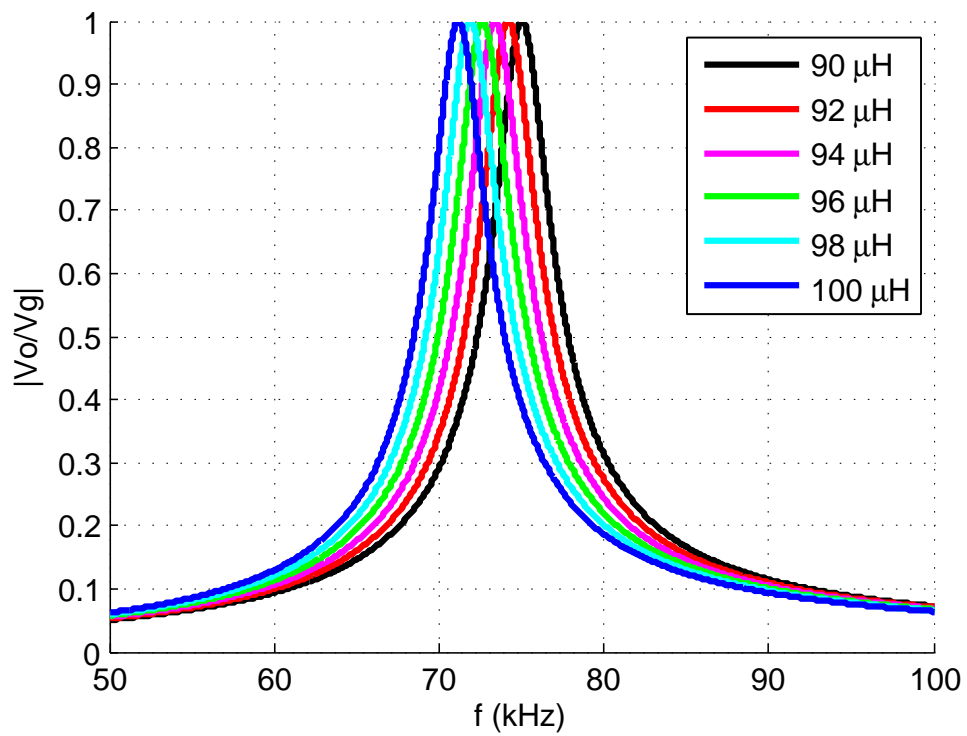


Figure 2.19: Magnitude of the transfer function for frequencies from  $f = 50$  kHz to 100 kHz and inductances  $L = 90, 92, 94, 96, 98, 100$   $\mu\text{H}$ .

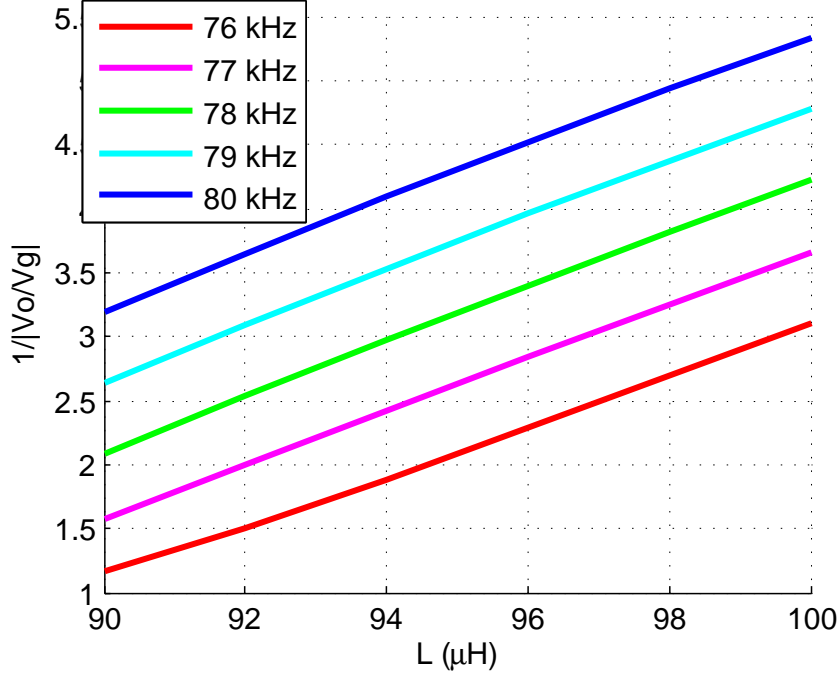


Figure 2.20: Magnitude of the inverse transfer function for inductances  $L$  from  $90 \mu\text{H}$  to  $100 \mu\text{H}$  and frequencies  $f = 76, 77, 78, 79, 80 \text{ kHz}$ .

being  $V_v$  the voltage amplitude with vehicle presence, and  $V_{nv}$  the voltage amplitude without that presence. Thus, we have:

$$\Delta V = V_v - V_{nv} = \frac{1}{k_1 L_v + k_2} - \frac{1}{k_1 L_{nv} + k_2} = \frac{k_1 (L_{nv} - L_v)}{(k_1 L_v + k_2)(k_1 L_{nv} + k_2)},$$

$$\frac{\Delta V}{V_v} = \frac{k_1 (L_{nv} - L_v)}{k_1 L_{nv} + k_2} = \frac{k_1 (L_{nv} - L_v) / L_{nv}}{k_1 + (k_2 / L_{nv})} = \frac{k_1}{k_1 + (k_2 / L_{nv})} S. \quad (2.26)$$

Since  $L_{nv}$  is constant, then the sensitivity  $S$  is

$$S = \frac{\Delta L}{L_{nv}} \cong k \frac{\Delta V}{V_v}, \quad (2.27)$$

i.e., the changes in the inductance of the inductive loop due to the vehicle presence modulate the amplitude of the input signal with a fixed frequency carrier. In other words, the output voltage signal is *Amplitude Modulated* (AM) by the vehicle signature. Therefore, the demodulation of the AM waveform gives that vehicle signature and also, by means of an *Analogue-to-Digital Conversion* (ADC), the signature data. The bandwidth of the vehicle signature is mainly a function of the vehicle speed, the loop geometry, and the vehicle undercarriage features.

Let  $n$  be the bit number for ADC, and therefore  $N = 2^n$  the state counter. Let also  $N_t$  be the count threshold, and then the threshold sensitivity is expressed as

$$S_t \cong k \frac{N_t}{N}. \quad (2.28)$$

The problem of crosstalk for the amplitude ILDs with four or more loops [41]] is solved by a RLC circuit per loop with the carrier frequencies of each loop spaced enough to include the signature bandwidth, and using a synchronous demodulator tuned to each carrier frequency.

## 2.4. Conclusions

This chapter presents different sensors for traffic applications. ILDs show an adequate compromise between reliability and cost, which determines that such sensors have been widely used for traffic monitoring in Spain during last years.

For that reason, we will focus our work in the improvement of ILDs, taking into account both aspects, their hardware design and also the development of signal processing methods for traffic monitoring.



# Chapter 3

## Design of an Inductive Sensor

In this chapter we present our implementation of the inductive signatures detector, including the hardware and software elements and the procedures for both measurement and registration of signatures. Our implementation has eight channels, allowing the registration of signatures of up to four lanes with dual loops in each lane or of up to eight lanes with simple loops in each lane. This covers most of the existing types of roads and makes the system easy to build thanks to the availability of a large number of standard circuits with eight channels, like multiplexers, decoders, buffers, etc.

Sections from 3.1 to 3.4 describe the hardware prototype, and Section 3.5 shows the capture of real inductive signatures using this hardware. Finally, Section 3.6 validates the proposed detector in noisy environments and compares its performance to that obtained with the amplitude detectors explained in Chapter 2.

### 3.1. Colpitts Oscillator

The oscillation circuit employed in the proposed implementation is the well-known Colpitts oscillator, since it is the simplest resonant LC oscillator. Figure 3.1 shows the schematic of a Colpitts oscillator based on a pnp transistor in common base configuration connected to a tank circuit formed by the inductance  $L_1$  of the inductive loop and the capacitors  $C_1$  and  $C_2$  that form the capacitive divider of the feedback loop [42, 43].

The oscillation frequency is determined by the parallel resonant circuit formed by the inductance  $L_1$  and the equivalent capacitor  $C_T$  obtained from the serial connection of  $C_1$  and  $C_2$ , i.e.

$$f_0 = \frac{1}{2\pi\sqrt{L_1 C_T}}, \text{ with } C_T = \frac{C_1 C_2}{C_1 + C_2}. \quad (3.1)$$

In our implementation,  $C_1 = C_2 = 100$  nF. For example, for an inductance of  $L_1 = 100$   $\mu$ H, this results in an oscillation frequency of 71, 18 kHz. The circuit has been

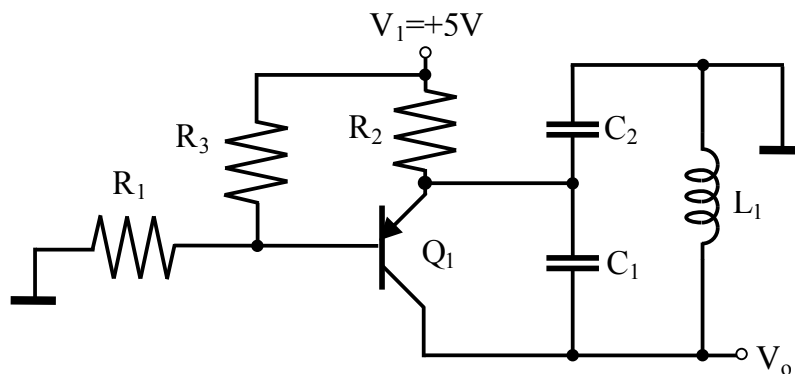


Figure 3.1: Circuit for the Colpitts oscillator.

designed for oscillation frequencies within the range [25 kHz, 100 kHz] i.e., for coils with inductances between 50  $\mu\text{H}$  and 800  $\mu\text{H}$ . Therefore, it is not necessary that the frequency of the LC oscillators have to be adjusted (which is known as *tuning*).

## 3.2. Pulse Counter

Figure 3.2 shows a block diagram of the comparison and capture process necessary to measure the oscillation period automatically. The pulses from the oscillation loop that has been selected as input are carried to a counter input, so that when a fixed number of pulses  $m$  is reached, the measured value  $N$  is captured from a timer working at the frequency  $f_r$  of the reference clock signal. Since the basic measurement process is performed by hardware using interruptions, the delay time of interruption attention (known as *latency*) is not critical.

Figure 3.3 shows the practical implementation of the multiplex system with eight coils. It consists of eight Colpitts oscillators connected to eight inductive loops and an analogue multiplexer which selects, at each instant, the oscillation signal of one of the loops using a decoder circuit. The use of eight oscillators instead of a single one allows us to avoid the introduction of an analogue multiplexer into the oscillation loop, which would be an additional error source.

The output signal of the multiplexer is carried to a shaping circuit, which converts the sinusoidal signal at its input into a digital pulse. That digital pulse is the input at the counter in the micro controller, which manages the entire system.

Due to the large amount of data captured by the system, a *Compact Flash* (CF) memory is employed for the recording of the signatures that will be subsequently analysed by a computer using signal processing algorithms. This off-line processing will allow us to perform vehicle classification and measurement of parameters such as speed or length,

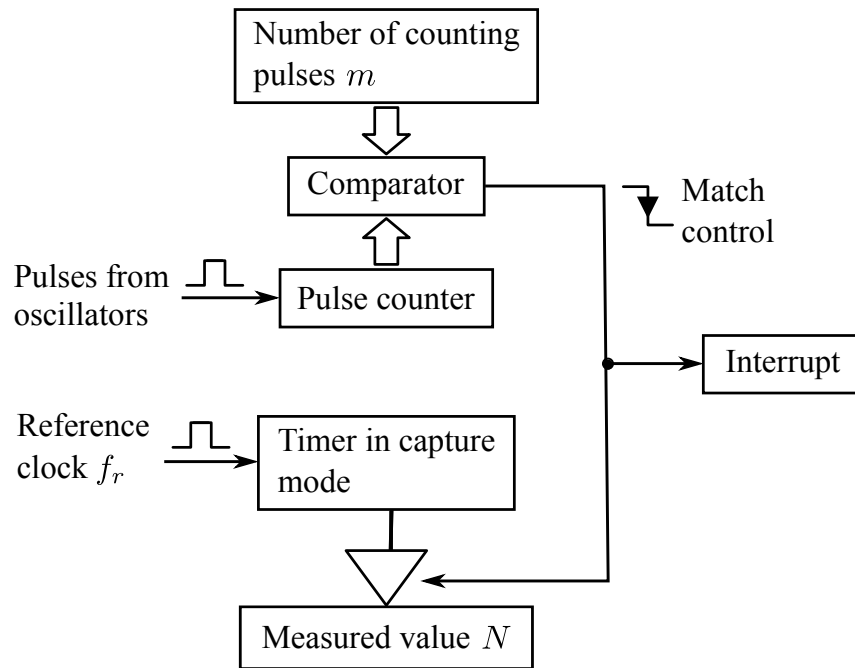


Figure 3.2: Measurement method by using comparison and capture.

and even vehicle re-identification for monitoring and control applications of vehicular traffic.

For the implementation of our system we have chosen the AT89C51RE2 micro controller since, firstly, it incorporates the comparison and capture unit needed in our application; and secondly, it can be easily interconnected to a CF memory bus. Figure 3.4 shows the interconnections for the AT89C51RE2 micro controller in our system. The output of the multiplexer is connected to the EC1 input, the CEX0 comparison output is carried to the T2EX input for capturing/interrupting, and the T2 timer is in capture mode.

Figure 3.5 shows a picture of the implemented hardware prototype. The left side of the board includes the eight oscillation circuits with multiplexing and a 16-pin connector for the connection of the eight inductive coils. The right side contains the micro controller and a *Real-Time Clock* (RTC) circuit with a lithium battery providing the date and time. The CF memory card used for the storage of the captured signatures can be seen at the bottom. One of the main advantages of the proposed system is that it can be implemented at a very low cost, thanks to its simplicity.

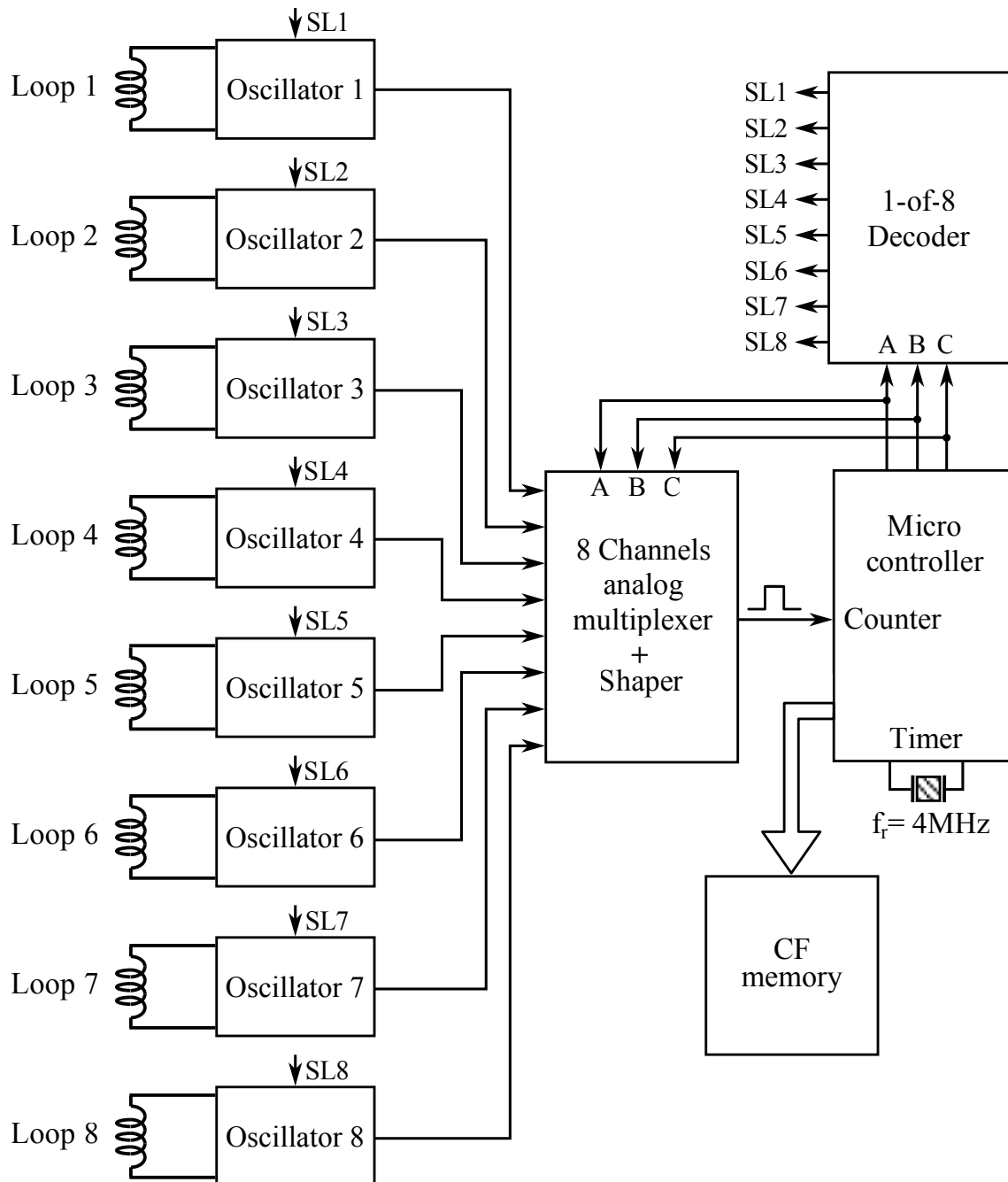


Figure 3.3: Multiplex system with eight inductive loops.

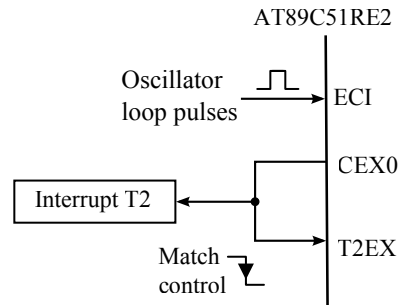


Figure 3.4: Interconnections for AT89C51RE2.

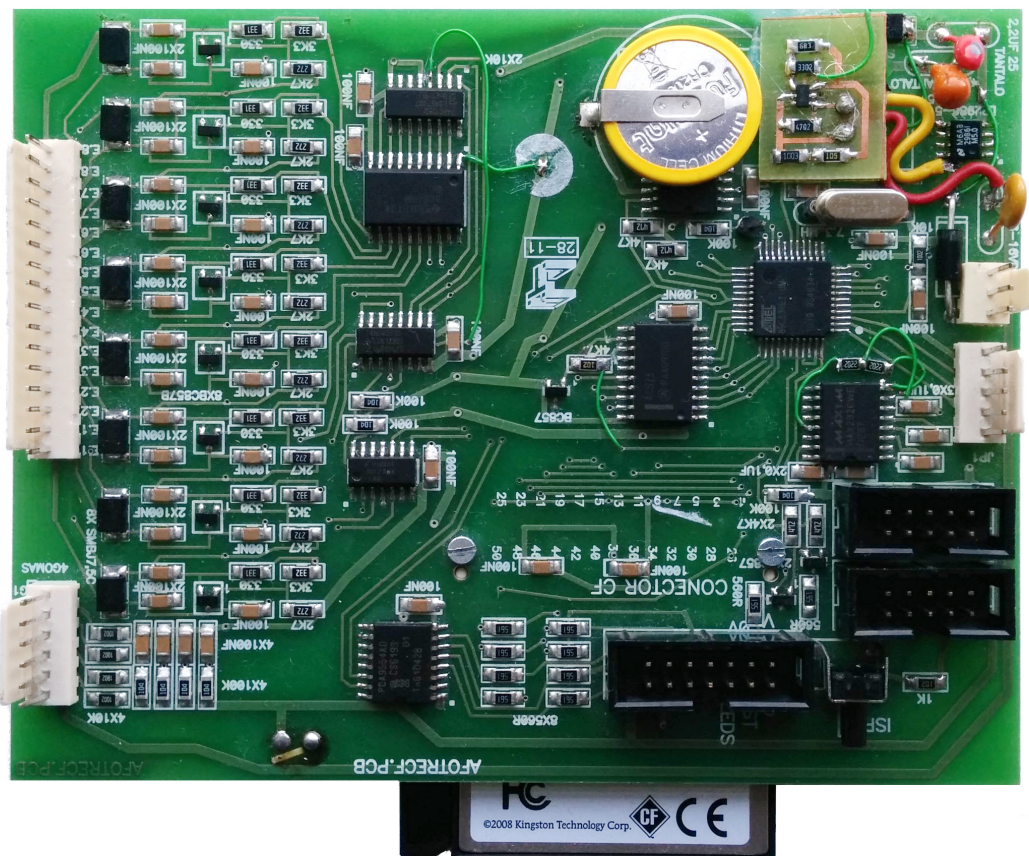


Figure 3.5: Photo of the hardware prototype.

### 3.3. Measurement

As explained previously, the period of the oscillation signal in each loop is calculated as the number of cycles  $N$  of the reference clock signal in  $m$  cycles of the oscillation signal of that loop. The measurement of  $N$  is made by means of T2 interruptions generated by overflow (TF2) and by hardware automatic capture (T2EX). An initial number of oscillation cycles  $m_i$  corresponding to the stability time of the oscillator start are discarded.

Figure 3.6 shows a flowchart describing the process of the T2 interruptions attention. The measurement of each loop starts with the interruption by T2 overflow due to the delay time between loops required for the oscillation of the previous loop to completely disappear (the branch with number 1 in the figure). At that point, a new measurement loop is selected, the  $m_i$  value is initialized to the number of initial start cycles, the maximum time for the measurement is established, and the corresponding oscillator is started.

Next, the branch marked with 2 in the figure is executed, so that the time  $N_i$  at initial start cycles is measured and the number  $m$  of counting cycles to be measured is loaded.

Finally, the measurement process finishes with the interruption by T2 capture when  $m$  is reached, which corresponds to branch 3 in Fig. 3.6. In this moment, the time interval between loops is loaded and the oscillation loop stops and saves the measured time  $N$  obtained after subtracting the value  $N_i$  of step 2.

Branch 4 only occurs on the unlikely situation in which the loop has problems with the start of the oscillation. In such a case, the inter-loop waiting time is loaded and  $N$  is set to zero, which indicates that the loop is not oscillating.

### 3.4. Registration

The oscillation period of the coils is continuously measured to determine the reference value of each coil at rest, i.e., without the presence of a vehicle. With the goal of adapting to the variations in the environmental conditions suffered by the coils, an adaptive algorithm, similar to the one described in [27], is employed. This algorithm tries to correct the reference value according to such external factors.

When the measured period of a coil is less than its reference value, which means that a vehicle is over the coil, the corresponding entry is made in the internal memory, storing the inductive signature of the vehicle.

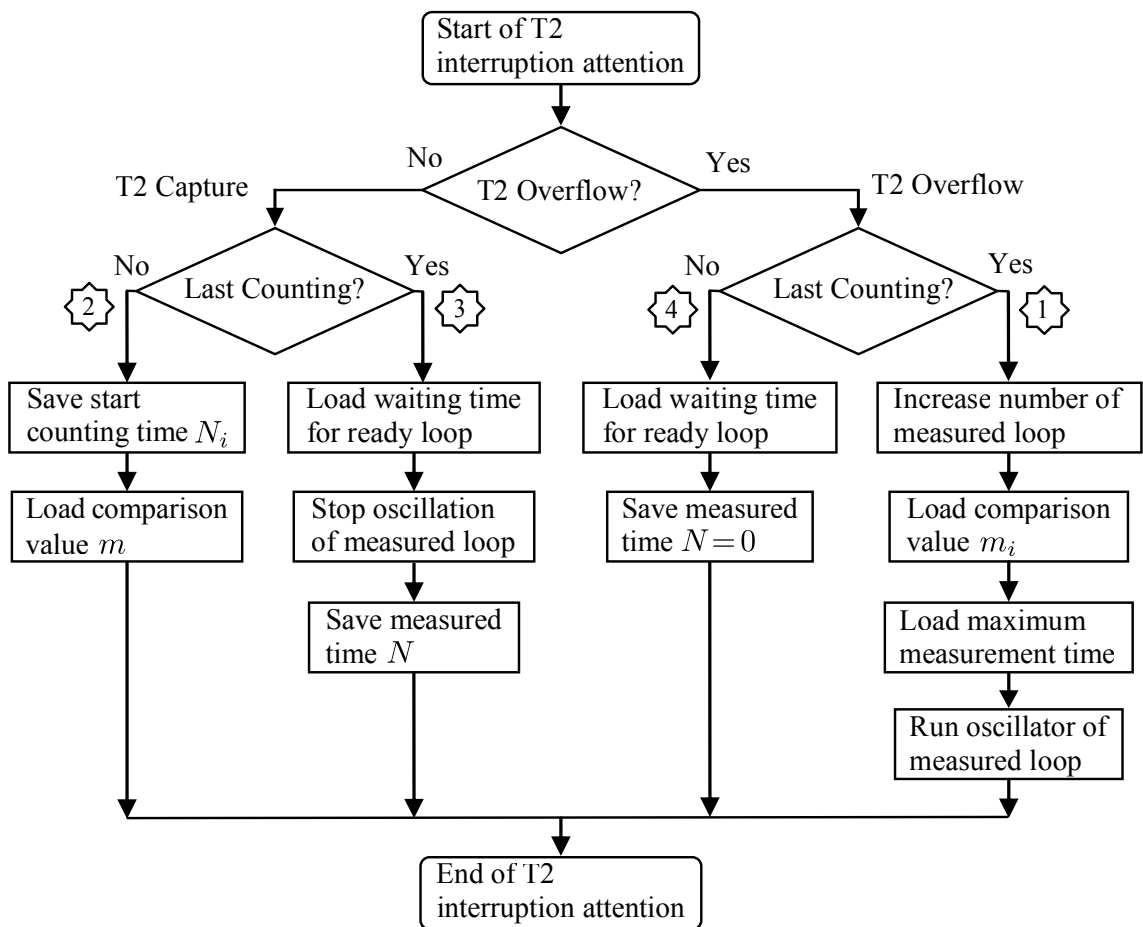


Figure 3.6: Flowchart of attention at T2 interruption.



Figure 3.7: A photo of the measurement location, with GPS coordinates: 43.235941 (Lat.); -8.464462 (Long.).

### 3.5. Real Capturing of Inductive Signatures

In order to test the hardware prototype we captured more than one thousand inductive signatures on the AC-523 road (Ledoño-Meirama, Spain), kilometre 7. A picture of this location is shown in Fig. 3.7. The detector equipment was located inside the cabinet of the Río Anllóns station, also shown in the photo.

Since the road is two lanes wide (one for each direction) we placed four inductive loop sensors, two in each side of the road. These sensors are squares with a side length of 2 m and a distance between their centres of 5 m. Figure 3.8 shows the interconnection of the four inductive loops to the measurement equipment. Notice that two inductive signatures are obtained from each passing vehicle. These inductive signatures will be very similar, although there can be small differences due to the fact that they are taken in different loops and time instants, and, in general, also for different positions and accelerations of the vehicle.

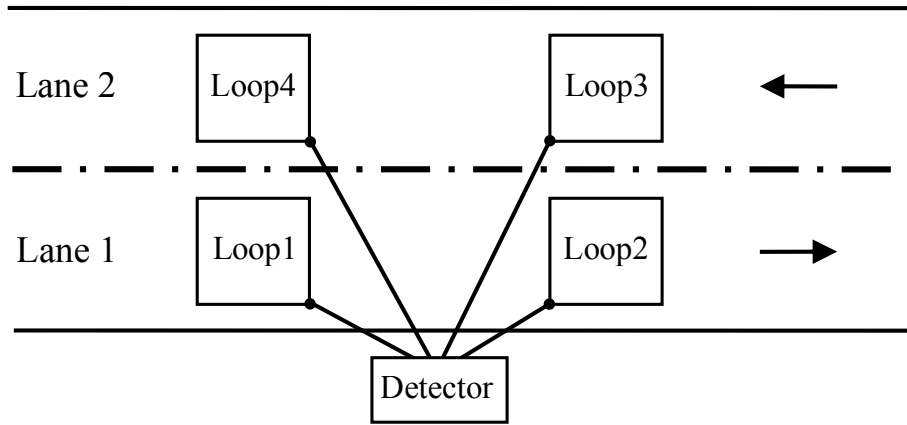


Figure 3.8: Interconnections from the inductive loop to the detector.

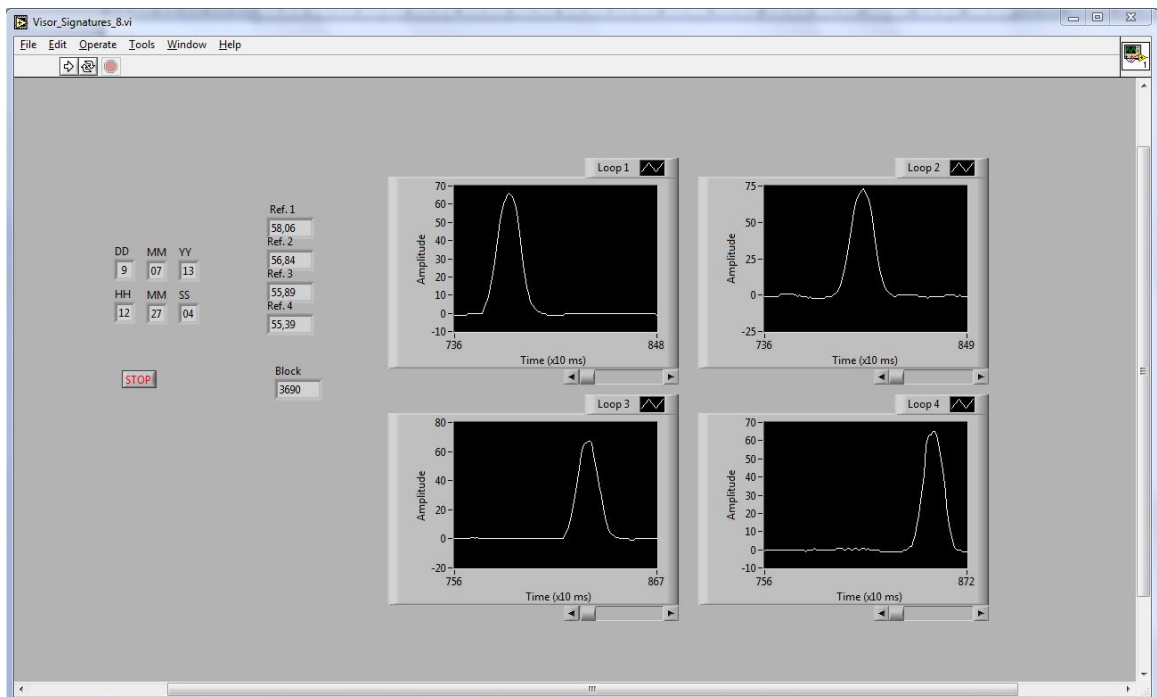


Figure 3.9: Interface of the signature visor.

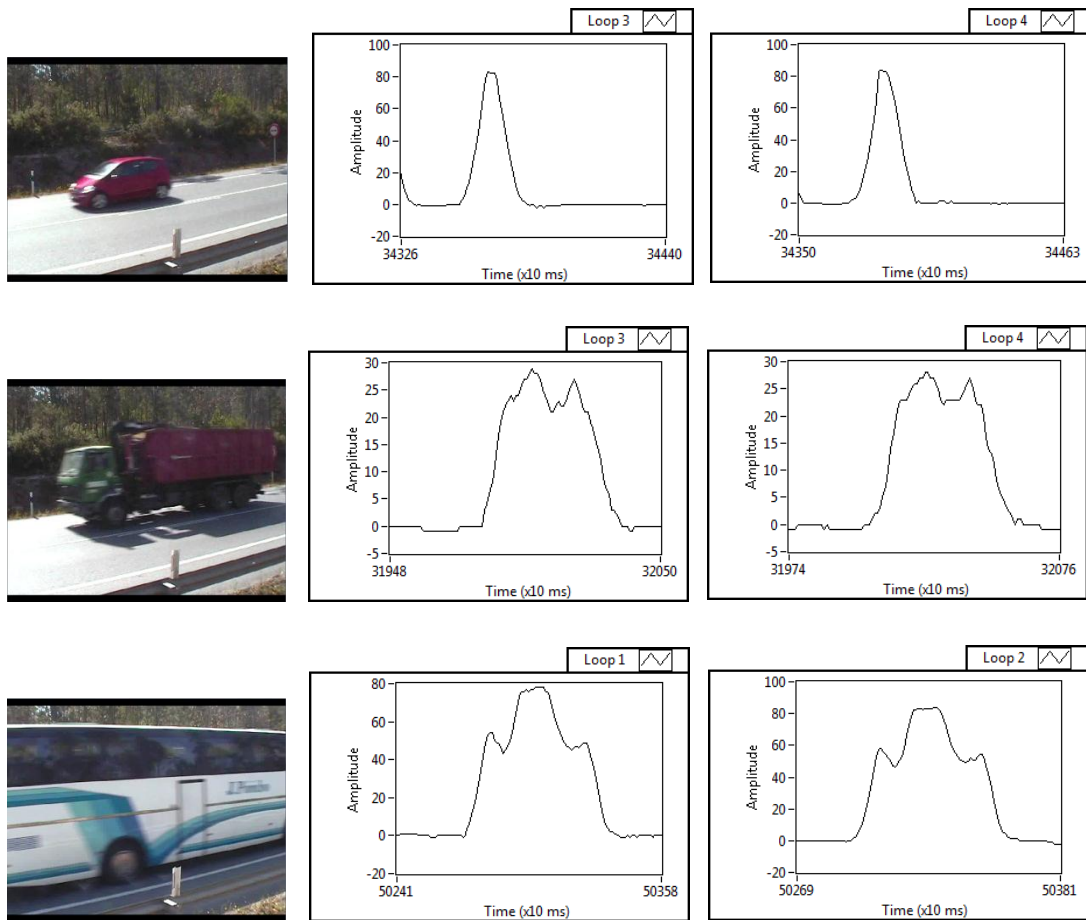


Figure 3.10: From left to right, the upper figures show the photo of a private car and the respective signatures obtained with the loops 3 and 4. The figures in the middle of the picture show a truck and its corresponding signatures captured also using the loops 3 and 4. The lower figures display the photo of a bus and two signatures obtained with the first and the second loop, respectively.

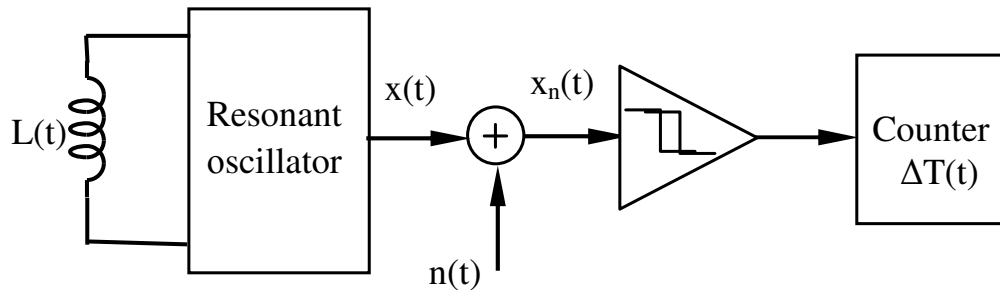


Figure 3.11: Block scheme of a resonant detector.

We have developed a software tool using Labview to display the signatures registered on the detector. This tool allows us to download the file containing the signatures from the CF card. Figure 3.9 shows the user interface of this tool, in which we can see some parameters of the outdoor experiment carried out in the previous scenario. These parameters are the captured signatures, the reference frequencies in the first four channels, data and time values, and the number of blocks stored in the CF memory. The amplitude of the signatures was determined by means of the difference between the measured value  $N$ , obtained every 10 ms, and that obtained at rest, which is calculated and registered by the measurement equipment. The cursors located below the graphics in Fig. 3.9 allow us to move forward or backward in time in order to display the signatures of each one of the vehicles passing over the coil.

At the same place where the inductive signatures were being captured we placed a video camera for the recording of the passing vehicles, so we could associate each vehicle to its corresponding inductive signature. As an example of the more than one thousand inductive signatures captured with our system, Fig. 3.10 shows the photos of three different vehicles and their corresponding inductive signatures obtained in the dual loops. As it can be seen in the figure, there is a great similarity between the pair of signatures of any of the vehicles, in contrast with the significant difference in the signatures obtained for different types of vehicles. Thus, each type of vehicle (private car, truck, bus...) can be classified under an unique inductive signature, which will depend on the parameters that define each of them, such as size, distribution of the metal mass, engine and axles location, spacing between the undercarriages and the road, etc.

### 3.6. Impact of Noise on Digital Detectors

In this section we will study the impact of noise on both types of detectors, i.e. resonant and amplitude detectors, which have been introduced in Chapter 2.

### 3.6.1. Impact of Noise on Resonant Detectors

Figure 3.11 shows the block scheme of a resonant detector. Let  $L(t)$  be the equivalent inductance in ends of the parallel resonant circuit constituted by this inductance and the equivalent capacity  $C_T$ . The oscillation frequency is given by Eq. 3.1 and therefore, we have

$$f(t) = \frac{1}{2\pi\sqrt{L(t)C_T}}. \quad (3.2)$$

Thus, the signal at the oscillator output is expressed as

$$x(t) = A\sin(2\pi f(t)). \quad (3.3)$$

We will consider interferences caused by *Additive White Gaussian Noise* (AWGN), denoted as  $n(t)$ , induced in the loop by ambient noise, like power lines, emissions from mobile phones, and so on. Therefore, at the comparator input we have

$$x_n(t) = x(t) + n(t), \quad (3.4)$$

where  $x_n(t)$  is the signal plus noise. This signal is approximately sinusoidal, although must be converted, previously to be carried out to the counter input, to a digital pulse train. This conversion is performed by the comparator with hysteresis, which acts as a wave shaper. Then, the counter receives and counts the  $m$  counting cycles and measures the time interval  $\Delta T$ , which provides the vehicle inductive signature.

Figure 3.12 shows the real vehicle inductive signature obtained, using the resonant detector of Fig. 3.11, with noise (for a *Signal-to-Noise Ratio* (SNR) of 15 dB) and no presence of noise in the system. As we can see in the figure, even for 15 dB of SNR the shape of the noisy inductive signature is quite similar to that obtained with no noise at the detector input, which verifies that our resonant detector is quite robust against environmental noise.

### 3.6.2. Impact of Noise on Amplitude Detectors

Figure 3.13 shows the block scheme of an amplitude detector. Let  $v(t)$  be the signal at the output of the RLC circuit. Its module is given by

$$|v(t)| = |V_g| \frac{2\pi f(t)L(t)}{\sqrt{R^2(1 - (2\pi f(t))^2 L(t)C)^2 + (2\pi f(t)L(t))^2}}. \quad (3.5)$$

Again, if we consider interferences produced by AWGN, denoted as  $n(t)$ , the signal at the output of the RLC circuit is given by  $v_n(t)$  as follows

$$v_n(t) = v(t) + n(t). \quad (3.6)$$

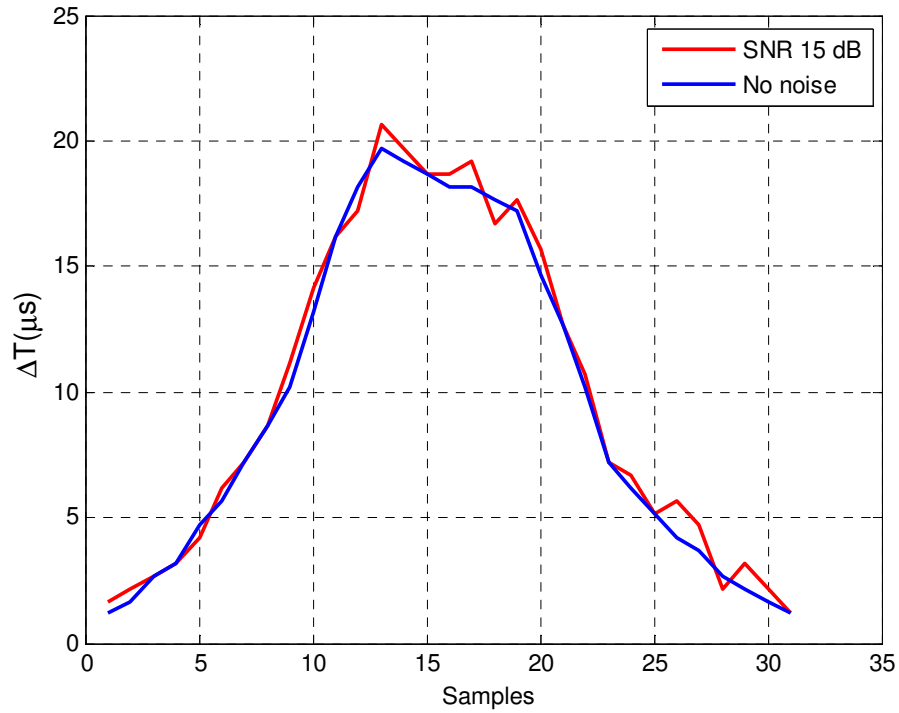


Figure 3.12: Inductive signature of the resonant detector with and without noise.

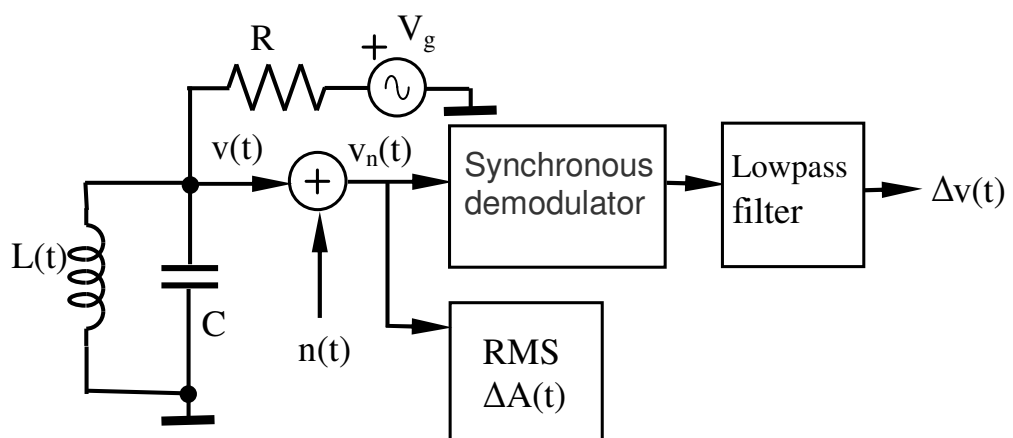


Figure 3.13: Block scheme of an amplitude detector.

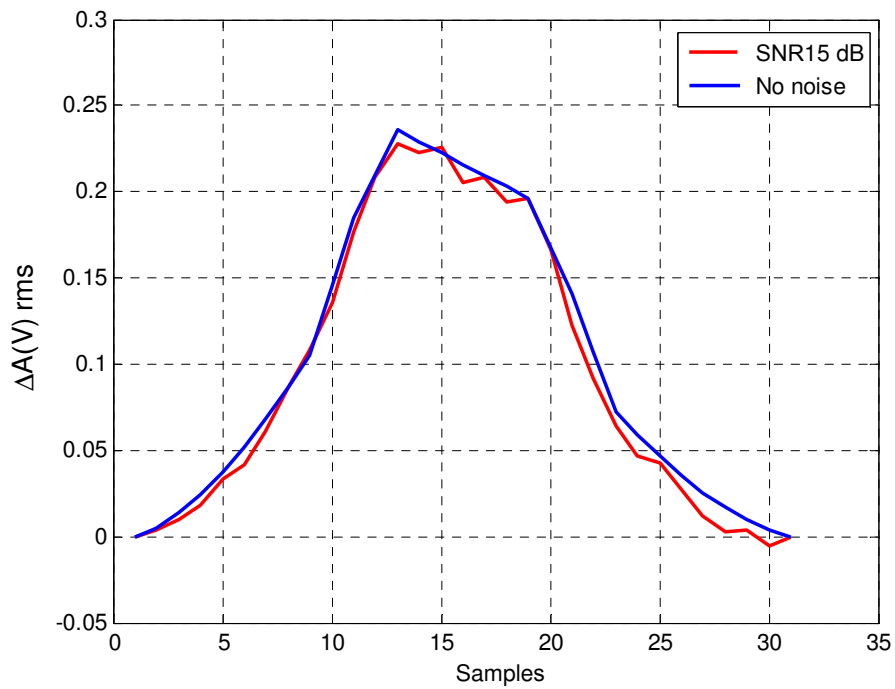


Figure 3.14: Inductive signature of the rms amplitude detector with and without noise.

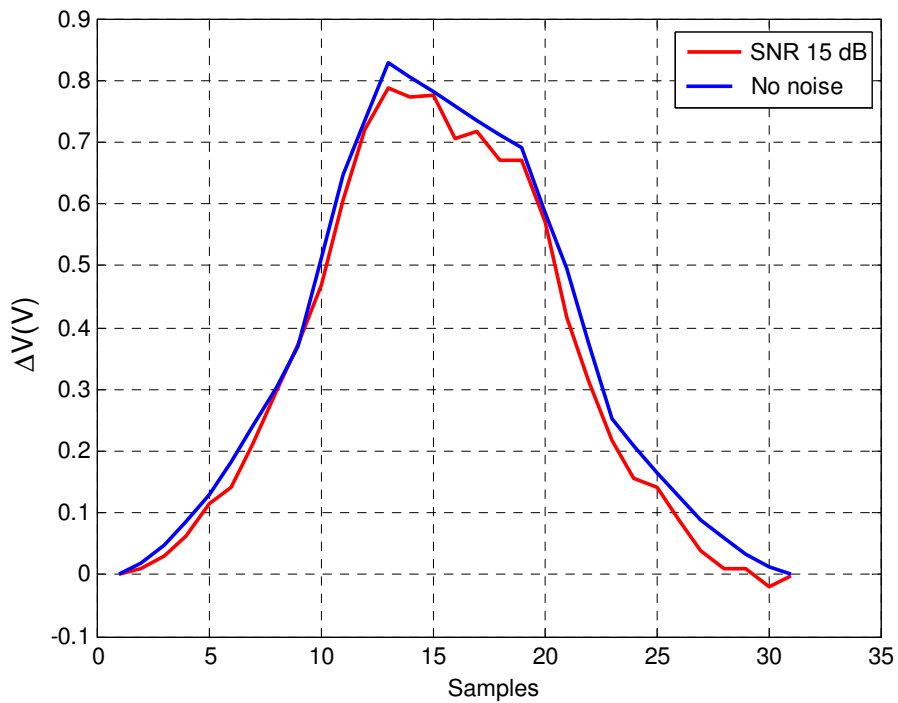


Figure 3.15: Inductive signature of the detector with synchronous demodulator with and without noise.

This signal is approximately sinusoidal and its *root mean square* (rms) value provides the inductive signature of amplitude  $\Delta A(t)$ . It can be seen in Fig. 3.14 the impact of noise on these amplitude detectors.

### Synchronous Demodulator (SD)

The signal modulated by the inductive signature  $s(t)$  can be written as

$$x(t) = (A + s(t)) \cos wt, \quad (3.7)$$

and multiplying  $x(t)$  by the carrier,  $\cos wt$ , we have

$$y(t) = (A + s(t)) \cos^2 wt, = \frac{1}{2} (A + s(t)) + \frac{1}{2} (A + s(t)) \cos 2wt. \quad (3.8)$$

With a low-pass filter, we can eliminate the component of frequency  $2w$ , so that, also removing the *Direct Current* (DC) component, the inductive signature  $\Delta v(t) = s(t)/2$  is obtained (see Fig. 3.13). You can see the influence of the noise on these detectors using the synchronous demodulator in Fig. 3.15.

Finally, we will compare the performances of both detectors, i.e. resonant and amplitude detectors, in terms of SNR at the detector output. For this purpose, we will calculate the output SNR as follows: firstly, we determine the level of signature signal without noise, i.e.  $\sum \Delta x_f$ ; then, this level with noise is obtained, i.e.  $\sum \Delta x$ , and finally, the output SNR is calculated as

$$\text{SNR} = 20 \log \frac{\sum \Delta x_f}{\sum \Delta x - \sum \Delta x_f}. \quad (3.9)$$

Figure 3.16 shows a good behaviour against noise of the resonant detector for input SNR greater than 15 dB, even better than that obtained for the amplitude detector. However, for SNRs lower than 15 dB the resonant detector is very sensitive to noise and therefore, not useful for the purposes described in this work.

## 3.7. Conclusions

In this chapter we have presented a simple module for the capture of inductive vehicle signatures based on *Time-Division Multiplexing* (TDM). The implemented system performs a sequential scanning using analogue multiplexing of up to eight oscillators and detects the presence of a vehicle by means of a shift in the period of the signals from the selected oscillator. It subsequently captures the inductive signature of the detected vehicle by measuring the time it needs to count a fixed number of pulses.

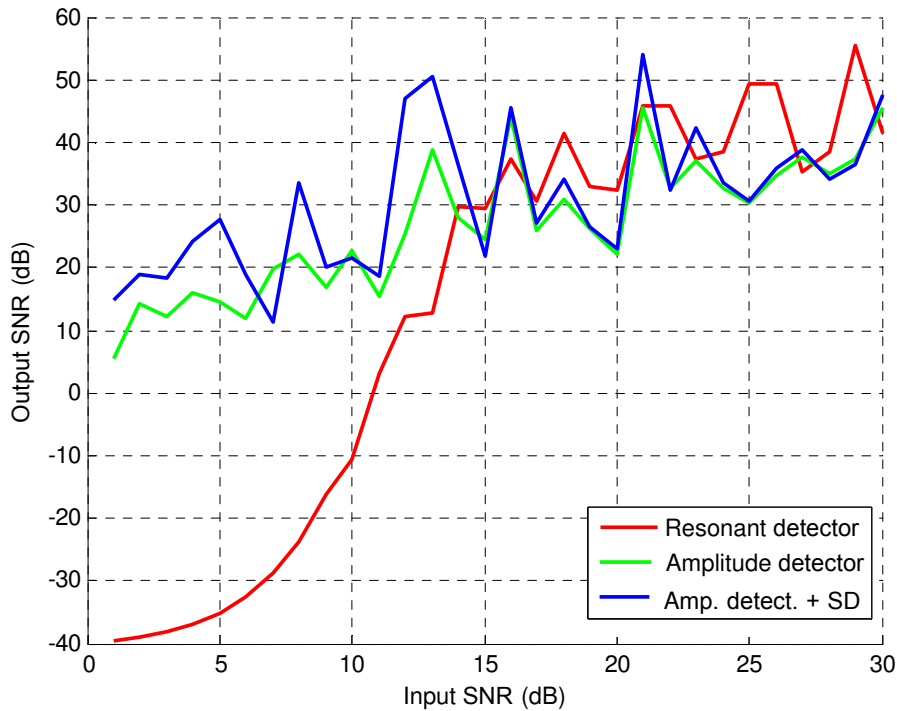


Figure 3.16: Output SNR for resonant and amplitude detectors.

In the experimental results obtained from measurements in a real scenario using dual loops, we observed a good similarity between the pair of signatures obtained from the same vehicle and a significant difference between the signatures corresponding to different vehicles, which validates the good performance of our implementation and enables its use in applications such as vehicle classification, speed and length measurement using only one loop, and re-identification of vehicles for supervision and control tasks in vehicular traffic.

Moreover, the performance of the resonant detector proposed in this work is validated in presence of AWGN determining an input SNR higher than 15 dB.

# Chapter 4

## Modelling of an Inductive Sensor

The high cost associated with testing every new development in real environments leads to the need of an appropriate model of the inductive sensor so that a simulator can be employed to assess their performance without wasting time and resources. In [22] an approximate model for an *Inductive Loop Detector* (ILD) is shown, and an equivalent circuit model is detailed in [23]. This model has been widely used in the literature [1,44].

Firstly, we will present a model of the inductive loop sensor proposed in the previous chapter based on [1] that will be employed to study the influence of parameters such as vehicle speed, acceleration, height, width and length in vehicle classification strategies.

Such standard sensor model does not take into account neither the shape of the induced currents in the vehicle undercarriage, that is the rectangular concentric, nor both the vehicle longitudinal and transversal displacement on the road coil and the influence of the vehicle undercarriage pieces not directly on the road coil. Thus, we will also develop a sensor model more sophisticated than the former one and that better fits the real sensor behaviour under all the possible scenarios. This model for inductive loop detectors is based on rectangular multi-loops employed on the acquisition of vehicle signatures in traffic management systems. We will show that our proposed model exhibits better performance than the standard modelling approach.

This chapter is organized as follows. Section 4.1 describes how currents are induced by rectangular coils. Section 4.2 details the standard model for the inductive sensor based on those standard approaches employed by simulators. Section 4.3 shows the advanced multi-loop model proposed for vehicle inductive sensors. Section 4.4 shows a comparison of the performances achieved with both approaches using real inductive signatures. Finally, Section 4.5 is devoted to conclusions and final remarks.

## 4.1. Induced Currents by Rectangular Coils

When a conductor is located in a time-varying magnetic field, eddy currents, also called Foucault currents, are induced. In this section, we will show how these currents have been traditionally considered in the literature and, as opposed to that, we propose a different induced current distribution which will be validated throughout several computer simulations.

When a conductor is located in a time-varying magnetic field, eddy currents, also called Foucault currents, are induced. Faraday's law of induction says that a time-varying magnetic field  $\mathbf{B}$  produces an electric field  $\mathbf{E}$  so that

$$\nabla \times \mathbf{E} = -\frac{\partial \mathbf{B}}{\partial t}, \quad (4.1)$$

where  $\nabla \times$  is the curl operator.

This induced electric field  $\mathbf{E}$  produces an eddy current density, denoted as  $\mathbf{J}$ , which is given by Ohm's law as follows

$$\mathbf{J} = \sigma \mathbf{E}, \quad (4.2)$$

where  $\sigma$  is the conductivity of the conductor, assumed to be homogeneous and isotropic. The field lines of  $\mathbf{J}$  are closed since  $\nabla \cdot \mathbf{J} = 0$ .

Since the wavelengths corresponding to the used frequencies are large enough compared to the coil dimensions, the problem can be considered as quasi-stationary and the displacement currents can be neglected. Ampère's law relates the current density  $\mathbf{J}$  with the magnetic field  $\mathbf{B}$  as follows

$$\mathbf{J} = \frac{1}{\mu} \nabla \times \mathbf{B}, \quad (4.3)$$

where  $\mu$  is the magnetic permeability of the homogeneous and isotropic conductor.

From Eqs. 4.2 and 4.3 and using the properties of the Nabla operator, we have

$$\nabla \times \mathbf{E} = \nabla \times \frac{\mathbf{J}}{\sigma} = \nabla \times \nabla \times \frac{\mathbf{B}}{\sigma\mu} = \frac{1}{\sigma\mu} (\nabla (\nabla \cdot \mathbf{B} - \nabla^2 \mathbf{B})), \quad (4.4)$$

where  $\nabla^2$  is the Laplace operator. Since  $\nabla \cdot \mathbf{B} = 0$  and using Eq. 4.1, we have

$$-\frac{1}{\sigma\mu} \nabla^2 \mathbf{B} = -\frac{\partial \mathbf{B}}{\partial t}. \quad (4.5)$$

Therefore, the magnetic field  $\mathbf{B}$  in the conductor can be obtained from the following expression

$$\nabla^2 \mathbf{B} = \sigma\mu \frac{\partial \mathbf{B}}{\partial t}, \quad (4.6)$$

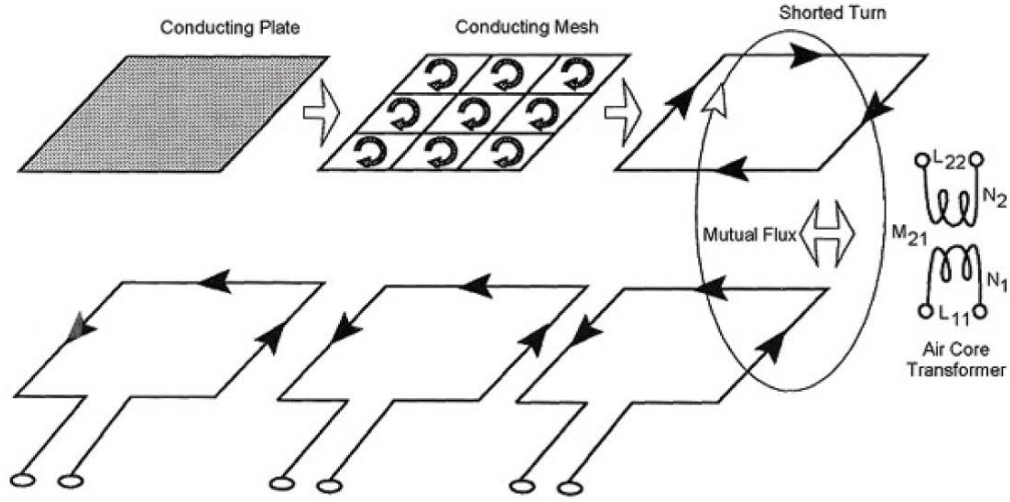


Figure 4.1: Induced Foucault currents (extracted from [1]).

and the Cartesian components of the eddy current density  $\mathbf{J} = (J_x, J_y, J_z)$  given by Eq. 4.3 are

$$\begin{aligned}
 J_x &= \frac{1}{\mu} \left( \frac{\partial B_z}{\partial y} - \frac{\partial B_y}{\partial z} \right), \\
 J_y &= \frac{1}{\mu} \left( \frac{\partial B_x}{\partial z} - \frac{\partial B_z}{\partial x} \right), \\
 J_z &= \frac{1}{\mu} \left( \frac{\partial B_y}{\partial x} - \frac{\partial B_x}{\partial y} \right) = 0.
 \end{aligned} \tag{4.7}$$

Using Eqs. 4.6 and 4.7 some analytical methods allow us to obtain the induced currents for simple problems, such as rectangular coils of  $a \times w$  dimensions, traversed by a sinusoidal current  $I(t) = Ie^{j\omega t}$  parallel to a semi-infinite conductor plane located at a distance  $d$  from the coil (see Fig. 4.2).

#### 4.1.1. Induced Currents for the Standard Approach

The classical inductive loop is simply a buried wire loop connected to an alternating current source, which also creates an alternating magnetic field. The operation of an ILD is based on an oscillation generated by the electronic detector at a frequency typically between 25 kHz and 100 kHz which is controlled by the coil inductance. A vehicle stopping or moving over the coil induces Foucault currents, which reduce the coil inductance and change the oscillation frequency. The classical approach considers that these induced currents have the distribution shown in Fig. 4.1.

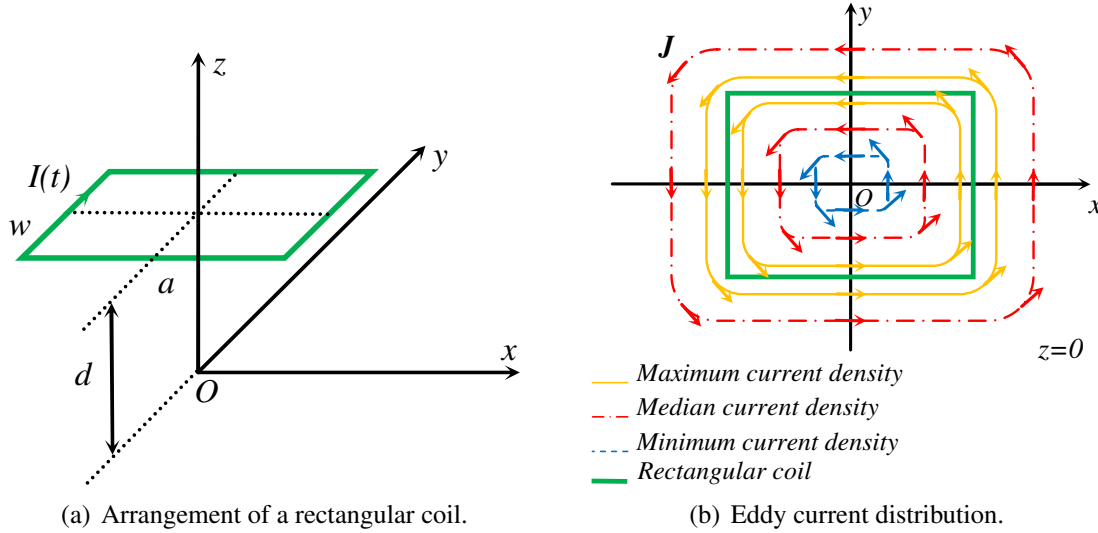


Figure 4.2: Rectangular coil and induced currents.

#### 4.1.2. Induced Currents for the Proposed Approach

Figure 4.2(a) shows the arrangement of a rectangular coil with a sinusoidal current  $I(t)$  that is placed parallel to a semi-infinite conductor plane. In [45–47], the expressions for the eddy current density  $J$  and also the distribution of the current on the conductor plane are provided. All these publications agree with the rectangular path currents, also rounded in the corners, and with the maximum induced values (see the yellow path lines depicted in Fig. 4.2(b)) just in the vicinity of the coil, represented as a green rectangular in this figure. Moreover, the work in [48] shows that for frequencies greater than 1 kHz and therefore, our working frequencies, the influence of the speed on the eddy current distribution of a moving conductor is negligible.

Computationally complex problems, even non-linear, can be numerically simulated using differential equations and solved in a relatively short time period using fine discretization. Three well-known methods are used for this purpose: the *Finite Element Method* (FEM), the *Boundary Element Method* (BEM), and the *Finite Difference Method* (FDM), although FEM is mainly used for calculations. Thus, the *Quasi-Static ElectroMagnetic Solvers* (P-EM-QS) obtained using the commercial Sim4Life software enable the efficient modelling of static and *Quasi-Static* (QS) *ElectroMagnetic* (EM) regimes by applying this numerical method on graded voxel meshes and optimizing for an approximation of Maxwell's equations. The method used in the QS solvers is the Galerkin FEM using linear nodal basis functions on a rectilinear grid [49]. In our case, P-EM-QS was used to calculate the distributions of the eddy current induced on aluminium plates parallel placed on rectangular coils.

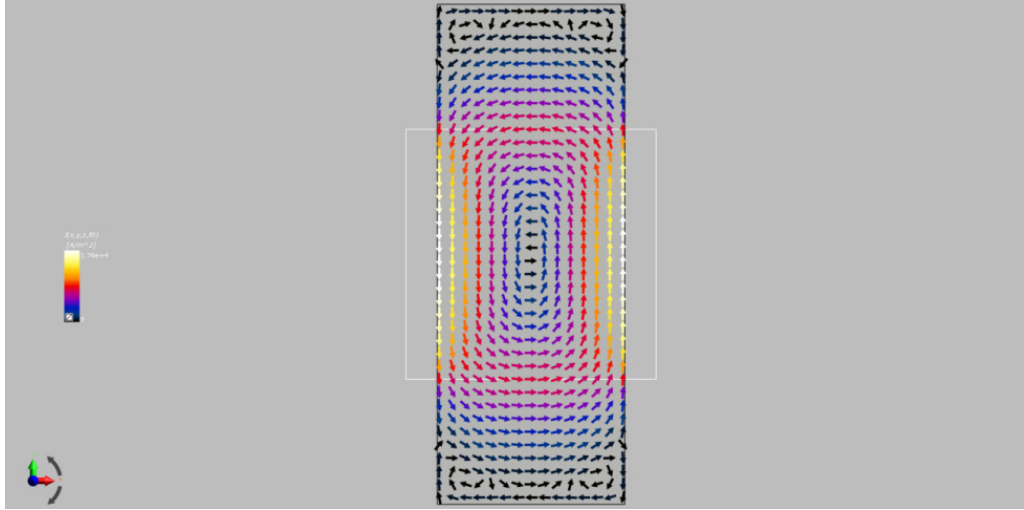


Figure 4.3: Eddy current distribution on a  $4\text{ m} \times 1.5\text{ m}$  aluminium plate centred on a  $2\text{ m} \times 2\text{ m}$  coil with a distance  $d = 25\text{ cm}$  between them.

Figure 4.3 shows the quasi-rectangular distribution of the currents induced in an aluminium plate of 2 mm thick and 4 m long and 1.5 m wide, placed centred on a square coil constituted by 5 turns of  $2\text{ m}$  long, with a sinusoidal current with a frequency of 56 kHz. As we can see in this figure, the white path lines correspond to greater induced current densities on the plate, which occurs in the vicinity of the coil. The lower values are represented in black, and as expected, the areas farthest from the coil exhibit those minimum values. This effect can be better observed in Figs. 4.4 and 4.5, in which the induced current density  $J$ , expressed in dB, is represented for the plate x-axis and y-axis, respectively. Thus, the maximum values are respectively achieved for  $x = -1\text{ m}$  and  $x = +1\text{ m}$ , or  $y = -0.75\text{ m}$  and  $y = +0.75\text{ m}$ , near the coil, and the minimum ones on its longitudinal borders and just on the centre of the plate.

## 4.2. Standard Modelling Approach

The equivalent model of the set constituted by the inductive loop and the vehicle is shown in Fig. 4.6. In the figure,  $A_1$  denotes the cross sectional area of the coil,  $l_1$  is the axial length of the coil,  $A_2$  is the area corresponding to the vehicle undercarriage,  $l_2$  is the axial length of its equivalent coil in short circuit, and  $d$  is the distance between the coil and the vehicle undercarriage [1, 22, 23].

The assembly formed by the coil and the vehicle undercarriage is modelled by an air core transformer in which the primary coil inductance, denoted by  $L_1$ , is excited by the sinusoidal generator at the oscillation frequency; the secondary, which represents the

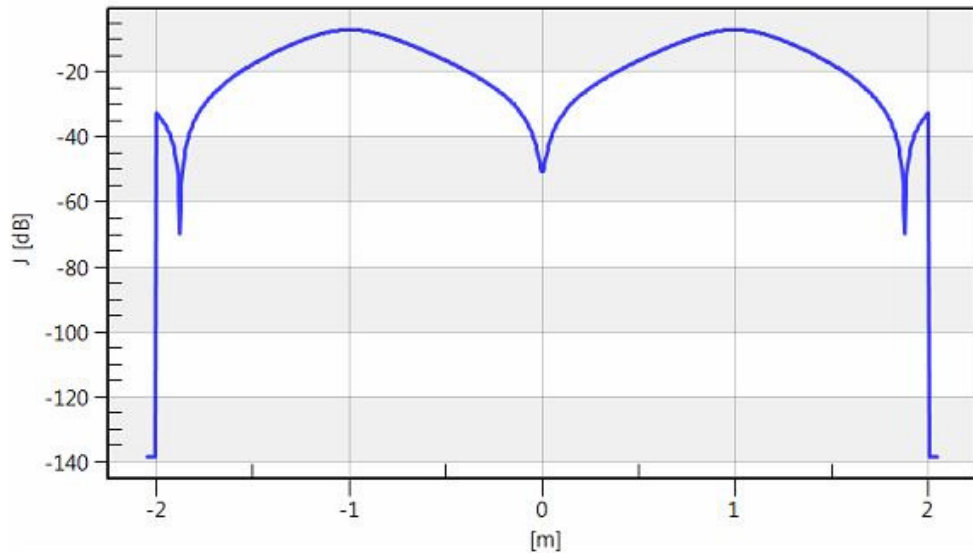


Figure 4.4: Eddy current density in the longitudinal axis  $x$ .

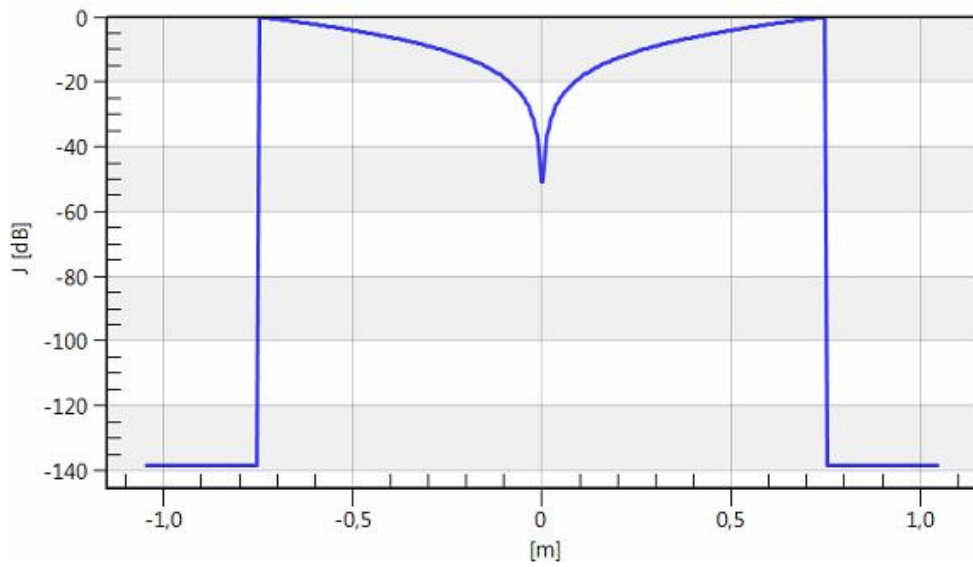


Figure 4.5: Eddy current density in the transversal axis  $y$ .

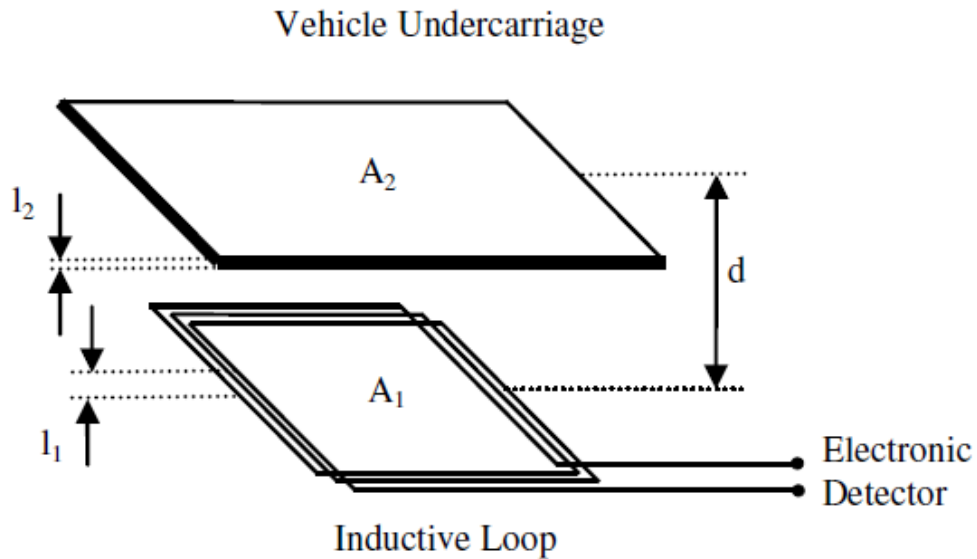


Figure 4.6: Inductive loop and vehicle model.

vehicle undercarriage, is modelled by a turn in short circuit with an inductance denoted by  $L_2 = L_2(t)$ , whose value changes with the vehicle position on the coil located under the road pavement; and finally, the coupling coil-vehicle is modelled by the mutual inductance denoted by  $M = M(t)$ , which also depends of the position of the vehicle on the road coil. This equivalent circuit is shown in Fig. 4.7.

From the mesh equations obtained in sinusoidal steady-state

$$\begin{aligned} v_i &= i_1 j\omega L_1 - i_2 j\omega M, \\ 0 &= -i_1 j\omega M + i_2 j\omega L_2, \end{aligned} \tag{4.8}$$

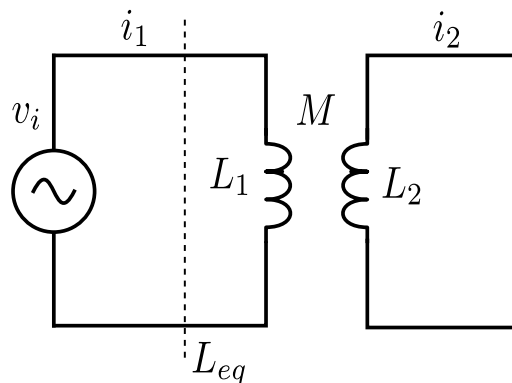


Figure 4.7: Equivalent circuit coil-vehicle undercarriage.

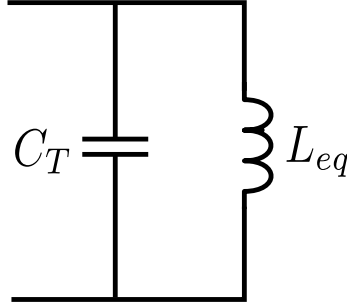


Figure 4.8: Resonant oscillation circuit used for vehicle detection.

we determine the input impedance

$$Z_i = \frac{v_i}{i_1} = j\omega \left( \frac{L_1 L_2 - M^2}{L_2} \right) = j\omega L_{eq}, \quad (4.9)$$

where

$$L_{eq} = \frac{L_1 L_2 - M^2}{L_2}, \quad (4.10)$$

obtained from the air core transformer model of the system formed by the inductive loop and the vehicle undercarriage.

Most detectors of inductive loops do not directly measure changes in  $L_{eq}$  but changes in period or frequency of a resonant oscillating circuit used for vehicle detection (see Fig. 4.8). The oscillator frequency is controlled by a parallel resonant circuit, also called tank circuit, which consists of the inductance  $L_{eq}$  of the loop in parallel with a capacity, denoted by  $C_T$ , located at the detector.

The oscillation frequency is given by

$$f_0 = \frac{1}{T} = \frac{1}{2\pi\sqrt{L_{eq}C_T}}, \quad (4.11)$$

and thus the difference in the oscillation period with a vehicle over the loop and without it the shift in the oscillation period (which gives us the inductive signature), determined as follows

$$\Delta T = 2\pi \left( \sqrt{L_1 C_T} - \sqrt{L_{eq} C_T} \right). \quad (4.12)$$

The self inductance of a loop, as in our case the coil placed under the road pavement, and denoted by  $L_1$ , is given by the following expression [1],

$$L_1 = \frac{\mu_0 N_1^2 A_1 F_1}{l_1}, \quad (4.13)$$

where  $\mu_0 = 4\pi \times 10^{-7}$  H/m,  $N_1$  is the number of turns, and  $F_1$  is a factor used to consider the non uniform flux in the roadway inductive loop.

Both the vehicle inductance, denoted by  $L_2(t)$ , and the mutual inductance, denoted by  $M(t)$ , depend on the position of the vehicle over the road loop and therefore, on the time instant  $t$ . At that time instant  $t$ , the vehicle covers a loop area,  $A_2(t)$ , given by

$$A_2(t) = l_v(t) \times w, \quad (4.14)$$

where  $l_v(t)$  is the road loop length covered by the vehicle at such instant, with  $w$  being the loop width. The average distance from this road loop to the vehicle undercarriage is denoted by  $d(t)$ . With such notation, and considering only one turn  $N_2 = 1$ , we can compute the vehicle inductance as follows

$$L_2(t) = \frac{\mu_0 A_2(t) F_2(t)}{l_2}, \quad (4.15)$$

where  $F_2(t)$  is the same factor as  $F_1$  but referred to the vehicle inductive loop.

The mutual inductance between the two coils is then given by [1]

$$M(t) = \frac{\mu_0 N_1 A_2(t) F_1}{d(t)}. \quad (4.16)$$

Using this standard model, the sensitivity given by Eq. 2.2 of Chapter 2 can be expressed as follows

$$\begin{aligned} S &= \frac{\Delta L}{L_{nv}} = \frac{L_{nv} - L_v}{L_{nv}} = \frac{L_1 - L_{eq}}{L_1} = \\ &= \frac{L_1 - \frac{L_1 L_2(t) - M(t)^2}{L_2(t)}}{L_1} = \frac{M(t)^2}{L_1 L_2(t)} = \frac{A_2(t) l_1 l_2 F_1}{A_1 d^2 F_2}, \end{aligned} \quad (4.17)$$

where  $L_2(t)$  and  $M(t)$  are respectively given by Eqs. 4.15 and 4.16. As it can be seen from (4.17), the sensitivity of the loop is affected by several parameters. Moreover, since there is a relationship with the inverse of the distance  $d$  squared, the sensitivity decreases very quickly when the separation between the coil and the metal surface of the vehicle undercarriage increases, as we can see in Fig. 4.9 in which three different coverages of the vehicle on the loop are considered (25%, 50%, and 100%). From (4.17) we can also observe the influence on the sensitivity of the ratio between  $A_2(t)$  and  $A_1$  which, in practice, is limited to the maximum value of 1, i.e. 100 %.

### 4.2.1. Experiment Results

In this section we have developed some experiments to show the performance of this model. In all of them, the inductive signature is obtained with the following procedure. The vehicle profile is placed at the different positions of the vehicle on the road loop,

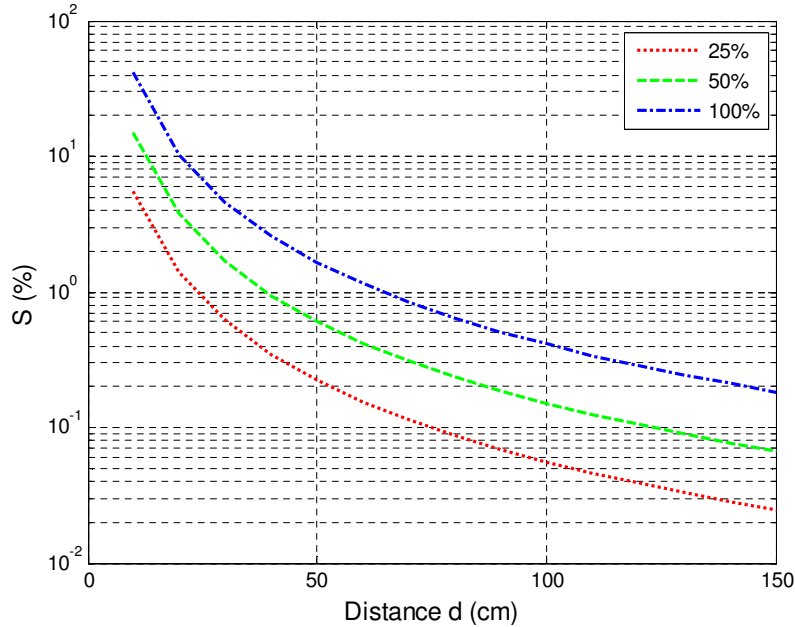


Figure 4.9: Sensitivity (in %) as a function of the distance between the road loop and the vehicle undercarriage (in cm) for three different coverages of the vehicle on the loop (25%, 50%, and 100%).

accordingly to the sampling frequency, vehicle and loop lengths, or vehicle speed and acceleration.

Let the origin for the length measurement be that on which the vehicle comes into the loop and  $t = 0$  the initial time instant corresponding to that event. Thus, we can write that the distance travelled by the vehicle during a total time period  $t$  is given by

$$x(t) = v_i t + \frac{1}{2} a t^2, \quad (4.18)$$

where  $v_i$  is the initial speed at the time instant  $t = 0$  and  $a$  is the vehicle acceleration, assumed to be constant and straight-line.

From this expression of  $x(t)$ , we can directly obtain the vehicle length covering the loop, which is given by  $l_v(t)$ . The vehicle inductance  $L_2(t)$  can be easily obtained from Eqs. 4.14 and 4.15. Also from  $l_v(t)$  we can determine the mean distance  $d(t)$  so that the mutual inductance is directly derived using Eq. 4.16.

Taking into account that the loop inductance  $L_1$  is calculated as given in Eq. 4.13, the equivalent inductance and the shift in the oscillation period  $\Delta T$  can be obtained using Eqs. 4.10 and 4.12, respectively. As said before,  $\Delta T$  gives us the amplitude of the inductive signature for the vehicle passing on the loop under the road pavement, which will be plotted in the figures corresponding to the experiments shown in the next subsections.

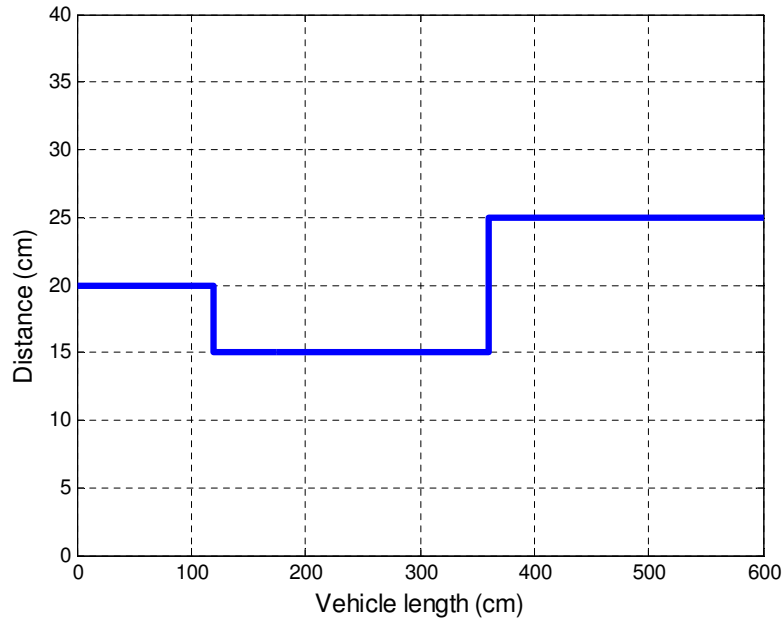


Figure 4.10: Vehicle profile.

In our simulation experiments, we have used the following parameters:  $N_1 = 4$ ,  $A_1 = 4 \text{ m}^2$ ,  $l_1 = 7.5 \text{ cm}$ ,  $l = 600 \text{ cm}$ ,  $w = 180 \text{ cm}$ ,  $l_2 = 2.5 \text{ cm}$ , and  $C_T = 50 \text{ nF}$ .

The behaviour of this model in the time domain against changes affecting different vehicle characteristics, such as width, distance between the vehicle undercarriage and the coil under the pavement, length, speed or acceleration, will be analysed in the following. Fig. 4.10 shows the profile of a vehicle of 6 m in length used for those simulations.

### **Influence of the Vehicle Width**

First of all, we want to analyse the influence of the vehicle width on the inductive signatures generated using the procedure explained before. Fig. 4.11 shows the inductive signatures obtained for a vehicle with the profile of Fig. 4.10 travelling at a speed of 50 km/h without acceleration. We can see the good linearity of this model against width changes. As shown in the figure, a good proportionality for all the time range of the inductive signature is maintained.

### **Influence of the Distance Vehicle-Loop**

Next, we will analyse the influence of the distance between the vehicle undercarriage and the loop under the road pavement for four different profiles: first, for the profile given in Fig. 4.10, and then for three profiles directly obtained from that after multiplying such

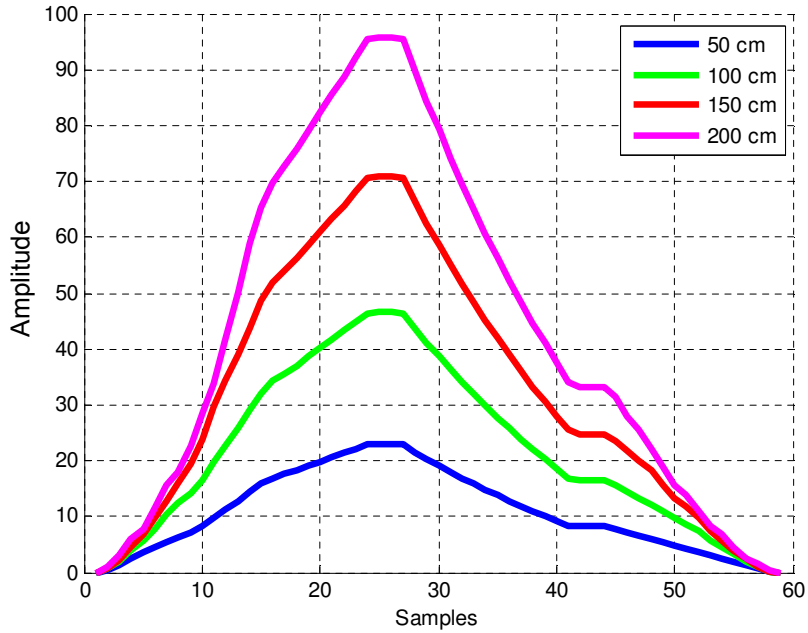


Figure 4.11: Inductive signatures as a function of the vehicle width.

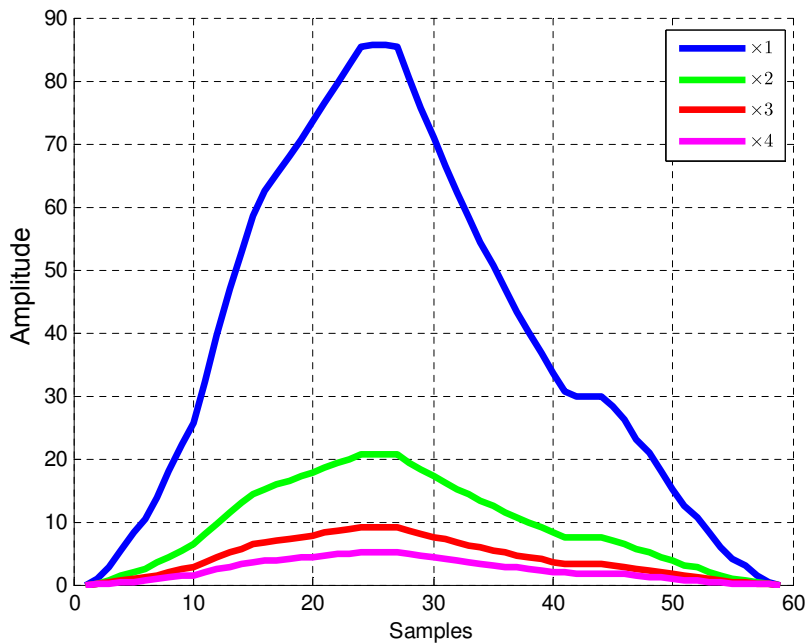


Figure 4.12: Inductive signatures as a function of the vehicle distance.

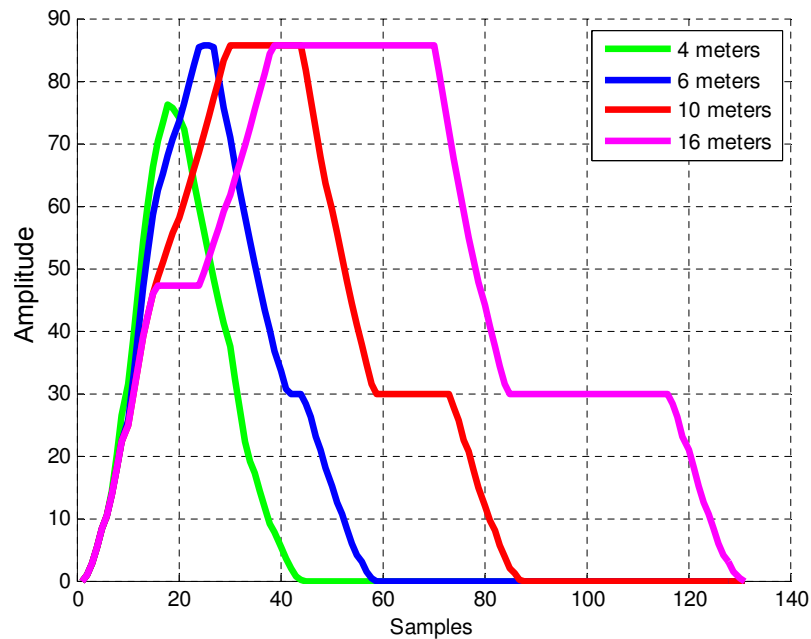


Figure 4.13: Inductive signatures as a function of the vehicle length.

a distance by a factor of 2, 3 and 4. For all the cases the vehicle speed is 50 km/h, without acceleration. Again, a good proportionality can be observed, but now with the inverse of the squared distance, since the amplitude of the inductive signature is highly sensitive to distance changes.

### Influence of the Vehicle Length

We will study now how the vehicle length influences on the inductive signature. For this purpose, the profile of Fig. 4.10 is scaled for vehicles of 4, 6, 10 and 16 meters in length without acceleration and travelling at 50 km/h. From Fig. 4.13, we can conclude that the vehicle length strongly affects the signature for a fixed profile.

### Influence of the Vehicle Speed

With the purpose of analysing the effect of the vehicle speed on the inductive signatures, we have obtained the signatures corresponding to the profile of a vehicle of 6 m in length (see Fig. 4.10) for constant speeds of 50, 100, 150 and 200 km/h with  $a = 0 \text{ m/s}^2$ . Fig. 4.14 shows the corresponding scaled replicas in time resulting from those variations in speed.

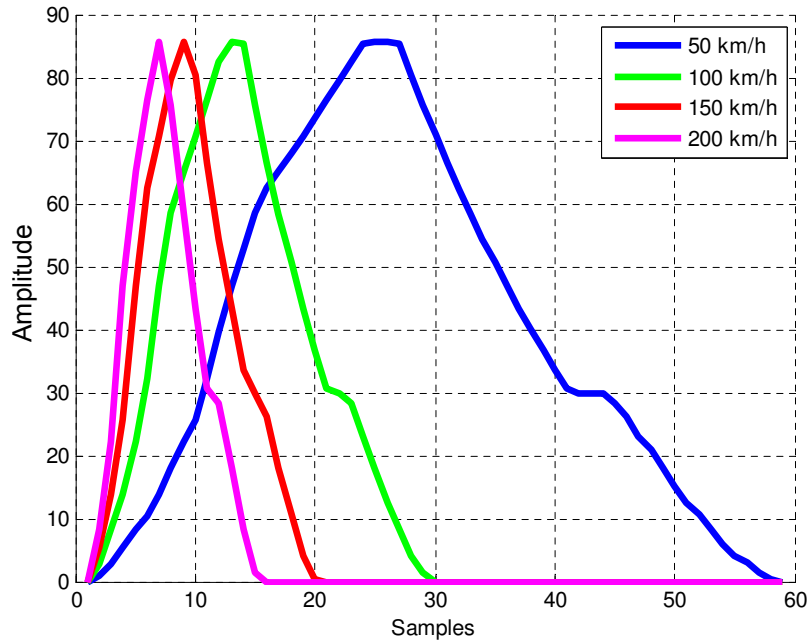


Figure 4.14: Inductive signatures as a function of the vehicle speed.

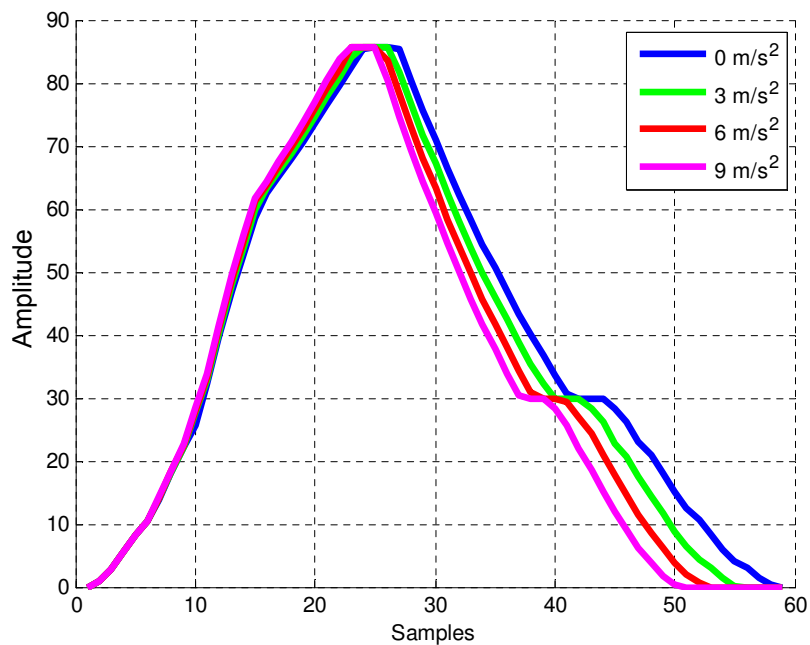


Figure 4.15: Inductive signatures as a function of the vehicle acceleration.

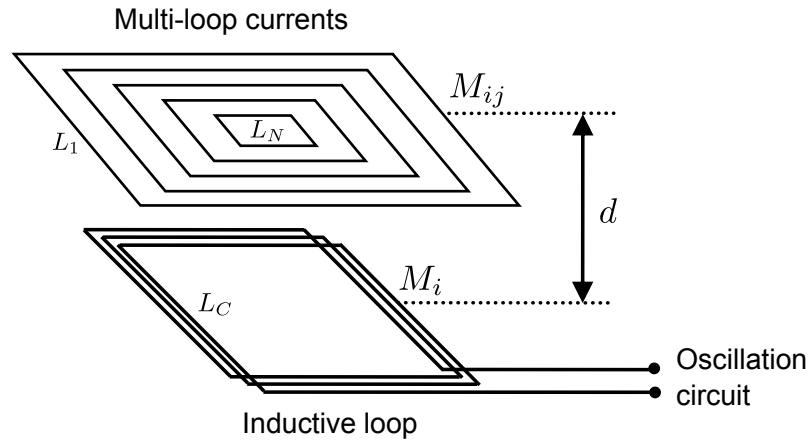


Figure 4.16: Road Inductive loop and multi-loop currents.

### Influence of the Vehicle Acceleration

Finally, the impact of the vehicle acceleration on the inductive signatures is shown in Fig. 4.15. We have simulated inductive signatures for the vehicle whose profile is given in Fig. 4.10 and whose acceleration is 0, 3, 6 or 9  $\text{m/s}^2$  with an initial speed of 50 km/h. This effect produces an undesirable distortion in the inductive signature.

## 4.3. Proposed Modelling Approach

In this section, we will develop a new model of an inductive sensor, which, as we will see throughout the following subsections, clearly outperforms performances achieved by the standard solution above explained. This advanced approach considers the concentric rectangular shape of the induced currents on the vehicle undercarriage, and both longitudinal and transversal displacements of the vehicle with respect to the road coil and the effect of the pieces of the vehicle undercarriage out of the road coil.

The road inductive loop is simply a buried wire rectangular coil connected to an alternating current source, which also creates an alternating magnetic field and, as we have explained before, the currents induced on the vehicle undercarriage can be shaped like a rectangle [45–47].

Figure 4.16 shows the inductive loop and the rectangular multi-loop currents induced in the vehicle undercarriage, where  $N$  is the number of loops;  $L_C$  and  $L_i$ ,  $i = 1, \dots, N$ , are the coil and the multi-loop self-inductances, respectively;  $M_i$ ,  $i = 1, \dots, N$ , are the mutual inductances between the inductive loop and each vehicle loop;  $M_{ij}$  are the multi-loop mutual cross inductances; and  $d$  is the distance between the inductive loop under the road pavement and the multi-loop currents in the vehicle.

These parameters are calculated as follows.

### 4.3.1. Calculation of the Mutual Inductances $M_i$ and $M_{ij}$

Firstly, we will obtain the expressions for the mutual inductances  $M_i$  and  $M_{ij}$  as derived in Appendix A. Using the formula of A.6 for the mutual inductance of two rectangular, transversely centred loops [50], we will have

$$M_i = M_{\text{rec}}(a, w, l_i, b_i, s_i, d), \quad (4.19)$$

$$M_{ij} = M_{\text{rec}}(l_i, b_i, l_j, b_j, s_{ij}, 0), \quad (4.20)$$

where  $s_i$  is the longitudinal displacement of the road loop with respect to vehicle loop  $i$ , and  $s_{ij}$  is the longitudinal displacement of the  $i$ -th vehicle loop with respect to the  $j$ -th one.

### 4.3.2. Calculation of the Self-inductance $L_C$

The coil self-inductance  $L_C$  is calculated by the Niwa equation for single-layer coils on rectangular winding forms [51]. That equation was obtained by firstly integrating the expression of Eq. A.6 over the length of the coil, so that we obtain the mutual inductance between one rectangular turn and the rest of the coil, and a second integration over the length of the coil gives the self-inductance of the rectangular coil. You can see the details in Appendix B.

Accordingly to Eq. B.3, the coil self-inductance  $L_C$  is given by

$$L_C = L_{\text{coil}}(a, w, a_l, N_C), \quad (4.21)$$

with a single-layer rectangular coil of length  $a$ , width  $w$ , axial length  $a_l$ , and  $N_C$  being the number of turns of the inductive loop.

### 4.3.3. Calculation of the Multi-loop Self-inductances $L_i$

Finally, the multi-loop self-inductances  $L_i, i = 1, \dots, N$ , are also calculated by the Niwa equation [51, 52] as follows

$$L_i = L_{\text{coil}}(l_i, w_i, b_l, 1), \quad (4.22)$$

where  $l_i$  and  $w_i$  are respectively the length and the width of the  $i$ -th vehicle loop,  $b_l$  is the axial length, and the turn number is equal to one for each single-loop.

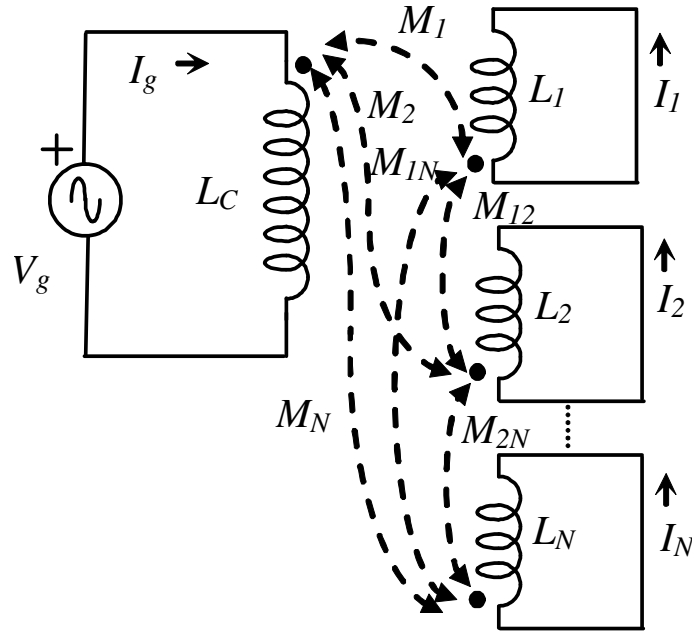


Figure 4.17: Multi-loop equivalent circuit.

The axial length  $b_l$  can be approximated by the classical equation of the current penetration depth in conductors, which is known as *skin effect*, in this way

$$b_l = \frac{1}{\sqrt{\pi f \mu \sigma}}, \quad (4.23)$$

where  $f$  is the oscillation frequency,  $\mu$  is the magnetic permeability, and  $\sigma$  is the material conductivity. Some conductive materials used for vehicle construction are non-magnetic metals, like as aluminium or copper, have a permeability about  $\mu = \mu_0$ , while other conductive materials are ferromagnetic metals, like as steel or iron, which are not linear but because of the low value of current, only few milliamperes are applied to the inductive loop, so that they are able to maintain their permeability approximately constant, with values of  $\mu = 2\,000\mu_0$  for the case of steel or  $\mu = 1\,000\mu_0$  for the iron one.

The system of Figure 4.16, constituted by an inductive loop excited by a sinusoidal oscillator (or generator) and multi-loops, can be modelled by the equivalent circuit of Figure 4.17, i.e. by an air core transformer with an inductance  $L_C$  in the primary circuit and  $N$  secondary circuits in short circuit with inductances  $L_i$ , coupled by mutual inductances  $M_i$  between the road inductive loop and the  $i$ -th loop of the multi-loop, and mutual inductances  $M_{ij}$  between the  $i$ -th and the  $j$ -th loops.

Let  $\mathbf{V} = (V_g, 0, \dots, 0)^\top$  and  $\mathbf{I} = (I_g, I_1, I_2, \dots, I_N)^\top$ . The equations for the sinusoidal

steady-state are given by  $\mathbf{V} = \mathbf{Z}\mathbf{I}$ , where

$$\mathbf{Z} = j\omega \begin{pmatrix} L_C & -M_1 & -M_2 & \cdots & -M_N \\ -M_1 & L_1 & M_{12} & \cdots & M_{1N} \\ -M_2 & M_{12} & L_2 & \cdots & M_{2N} \\ \vdots & \vdots & \vdots & \ddots & \vdots \\ -M_N & M_{1N} & M_{2N} & \cdots & L_N \end{pmatrix}, \quad (4.24)$$

being  $j$  the imaginary unit and  $\omega$  the oscillation frequency.

Let  $\mathbf{Z}_1$  be matrix obtained from  $\mathbf{Z}$  as a result of applying Cramer's rule. Thus, we obtain

$$L_{eq} = \frac{z_{eq}}{j\omega} = \frac{V_g/I_g}{j\omega} = \frac{|\mathbf{Z}|}{|\mathbf{Z}_1|}, \quad (4.25)$$

so for an equivalent oscillation circuit capacity  $C_T$ , we have

$$\Delta T = T_{nv} - T_v = 2\pi \left( \sqrt{L_C C_T} - \sqrt{L_{eq} C_T} \right), \quad (4.26)$$

as was shown in Chapter 4.

The sensitivity  $S$  obtained using this multi-loop inductive model is given by

$$S = \frac{\Delta L}{L_C} = \frac{L_C - L_{eq}}{L_C} = \frac{L_C - \frac{L_T}{L_s}}{L_C}, \quad (4.27)$$

where  $L_T = |\mathbf{Z}|/j\omega$  is the determinant of the total inductance matrix of primary and secondary circuits, and  $L_s = |\mathbf{Z}_1|/j\omega$  is the determinant of the secondary inductance matrix.

From Fig. 4.18, we can deduce a formula that approximates this behaviour based on the dependence between the sensitivity  $S$  and the distance  $d$ , which is

$$S = S_0 10^{-\frac{d}{d_0}}, \quad (4.28)$$

where  $S_0$  and  $d_0$  depend on the inductive loop detector dimensions, frequency, etc., which can be experimentally calculated for each case.

#### 4.3.4. Experiment Results

In this section we have developed some experiments to show the performance of our proposed model.

First, the vehicle inductive signatures will be obtained using Eq. 4.26 with the new multi-loop model for flat vehicle profiles at different positions on the road loop, accordingly to the sampling frequency, the vehicle length, and its speed. Let  $a = 2$  m,  $w = 2$  m,  $a_l = 5$  cm,  $N_C = 5$ , and  $C_T = 50$  nF the road inductive loop parameters, and  $l = 4$  m,  $b = 2$  m,  $d = 25$  cm, and  $v = 72$  km/h the vehicle parameters.

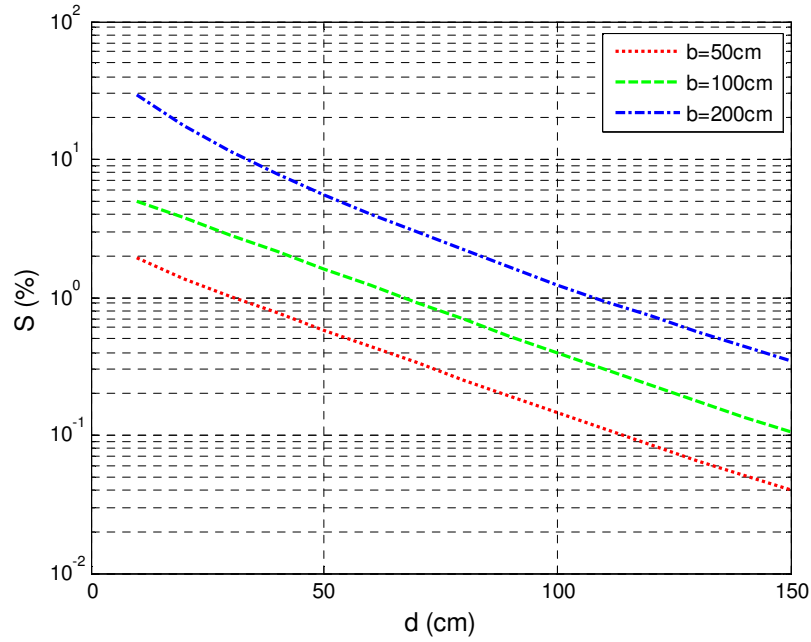


Figure 4.18: Sensitivity (in %) as a function of the distance  $d$  in cm between the road loop and the vehicle undercarriage for a vehicle with a length  $l = 200$  cm and three widths:  $b = 50$  cm, 100 cm and 200 cm.

### Influence of the Vehicle Position

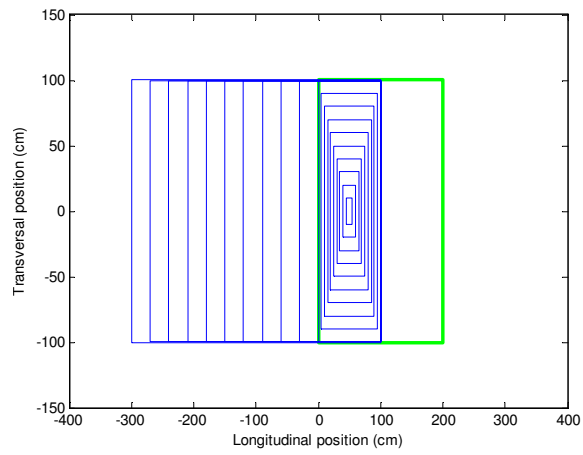
Figures 4.19(a), 4.19(b), and 4.19(c) show the distribution of the multi-loop currents for  $N = 20$  considering three different positions of the vehicle on the coil, i.e. for a vehicle entering 1 m into the loop, for a vehicle entering 2 m into the loop, and for a vehicle centred on the loop.

### Influence of the Number of Loops

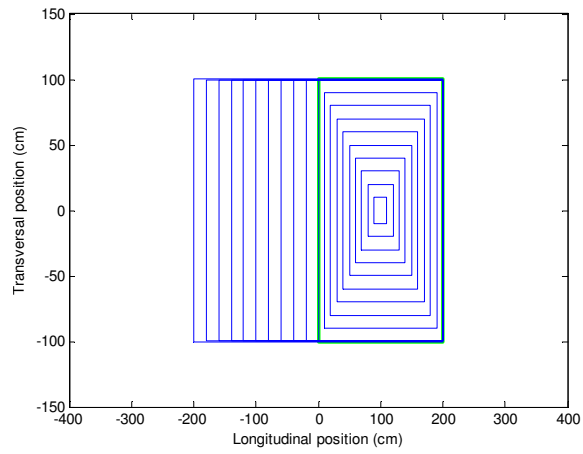
Figure 4.20 shows the vehicle inductive signatures obtained using Eq. 4.26 for a number of loops  $N$  varying from 10 to 400. It is important to remark that there is a very good amplitude convergence when increasing  $N$ , while at the same time the signature shape is maintained even for  $N = 10$ .

### Influence of the Vehicle Length

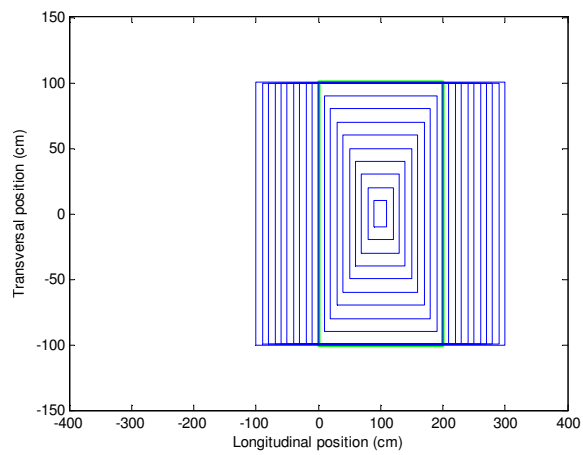
Figure 4.21 was obtained for vehicle lengths from 1 m to 20 m, with  $N = 200$ . As it is expected, this figure shows a significant distortion in the signature shape with length but also very good amplitude convergence.



(a) 1 m of the vehicle length on the road loop.



(b) 2 m of the vehicle length on the road loop.



(c) Vehicle centred on the road loop.

Figure 4.19: Multi-loop current distributions.

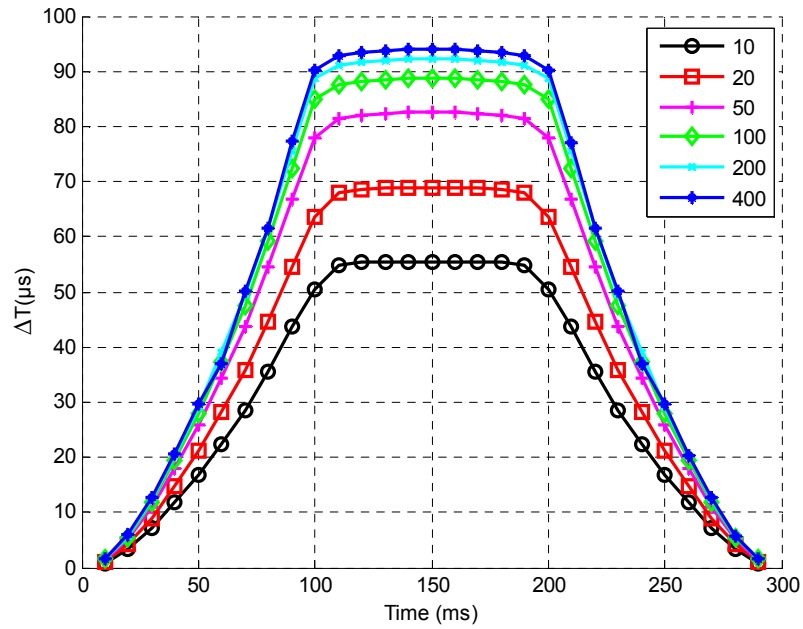


Figure 4.20: Inductive signatures for different values of the number of loops  $N$ .

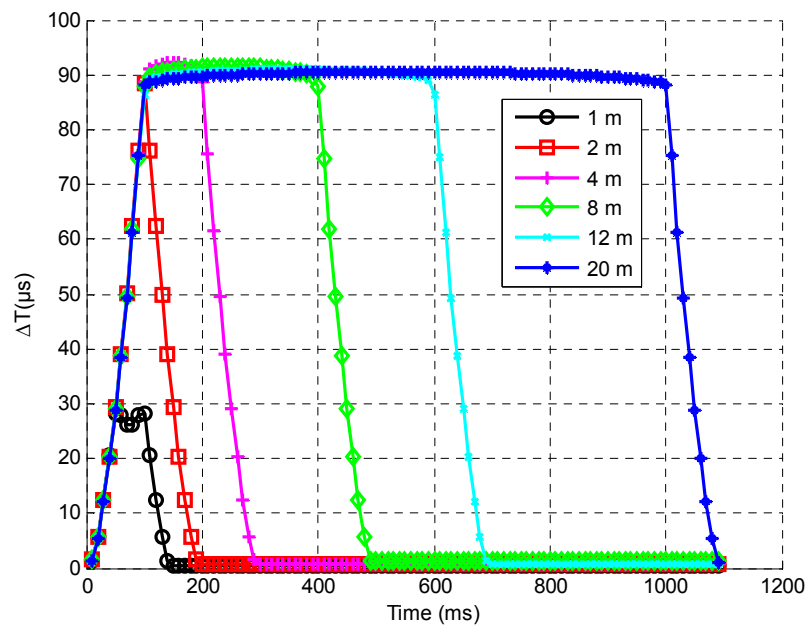


Figure 4.21: Inductive signatures for different values of the vehicle length  $l$ , with  $N = 200$ .

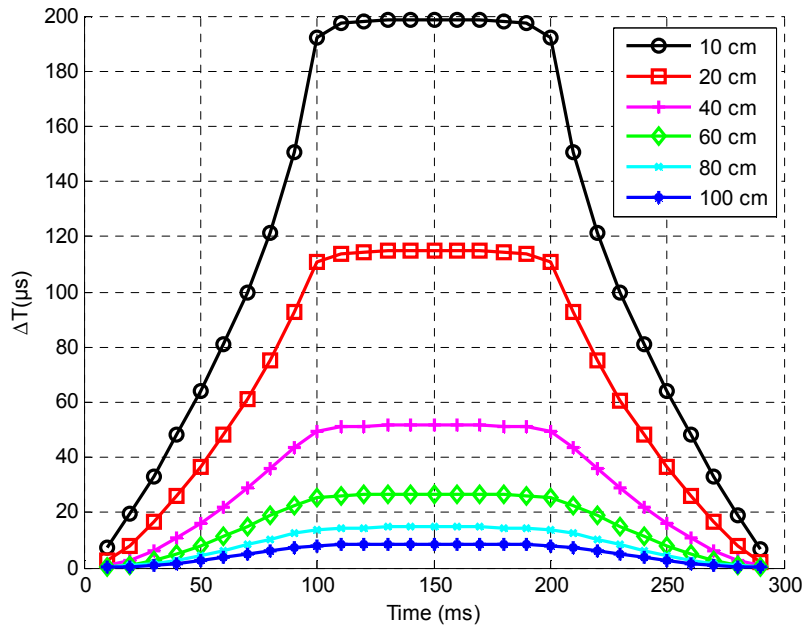


Figure 4.22: Inductive signatures for different values of the distance  $d$ , with  $N = 200$ .

### Influence of the Distance Vehicle-Loop

Figure 4.22 depicts the inductive signatures obtained for distances  $d$  between the vehicle undercarriage and the loop under the road pavement varying from  $d = 10$  cm to  $d = 100$  cm. As it can be observed from the figure, there exists an approximated proportionality of the signature amplitude with the inverse of the distance, as opposed to the behaviour appeared using the standard model, in which that proportionality was with the inverse of the squared distance (see Fig. 4.12).

### Influence of the Vehicle Width

Figure 4.23 has been obtained for vehicle widths  $b$  from 0.5 m to 3 m, with  $N = 200$ . For widths  $b \leq 2$  m there exists an approximated proportionality between the vehicle width and the amplitude of the inductive signature. For  $b > 2$  m the amplitudes converge to a maximum value, which was not adequately modelled using the standard approach.

### Influence of the Vehicle Speed

Figure 4.24 shows the inductive signatures obtained considering speeds from 50 km/h to 200 km/h, with  $N = 200$ . We can see in the figure the corresponding scaled replicas in time resulting from such variations in speed.

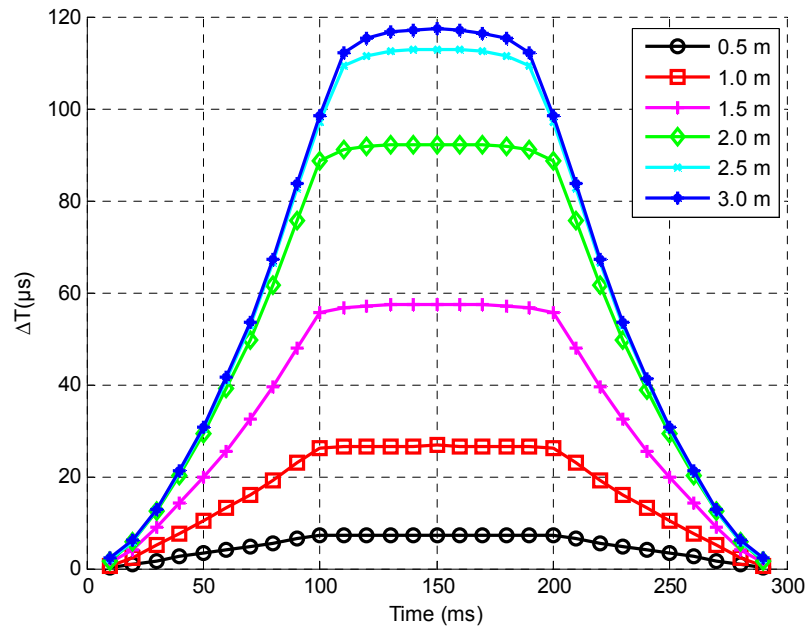


Figure 4.23: Inductive signatures for different values of the vehicle width  $b$ , with  $N = 200$ .

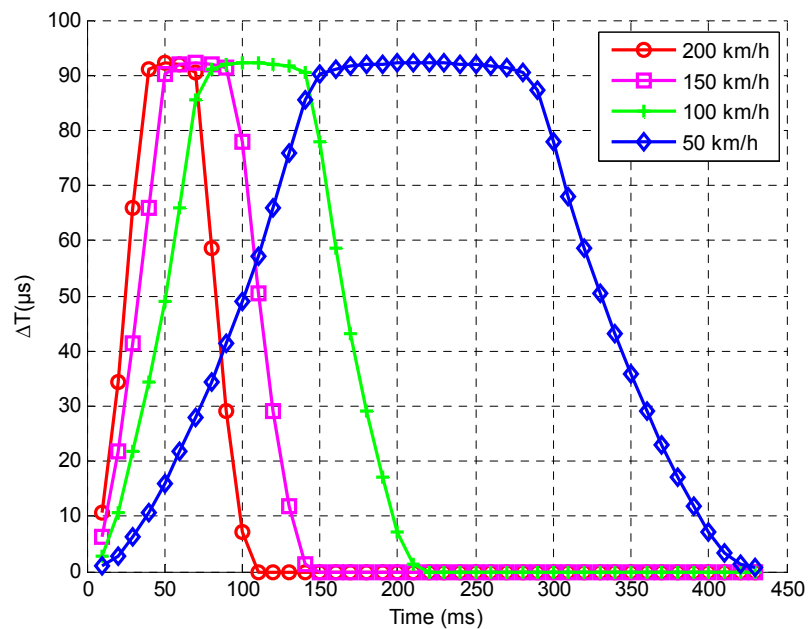


Figure 4.24: Inductive signatures for different values of the vehicle speed  $v$ , with  $N = 200$ .

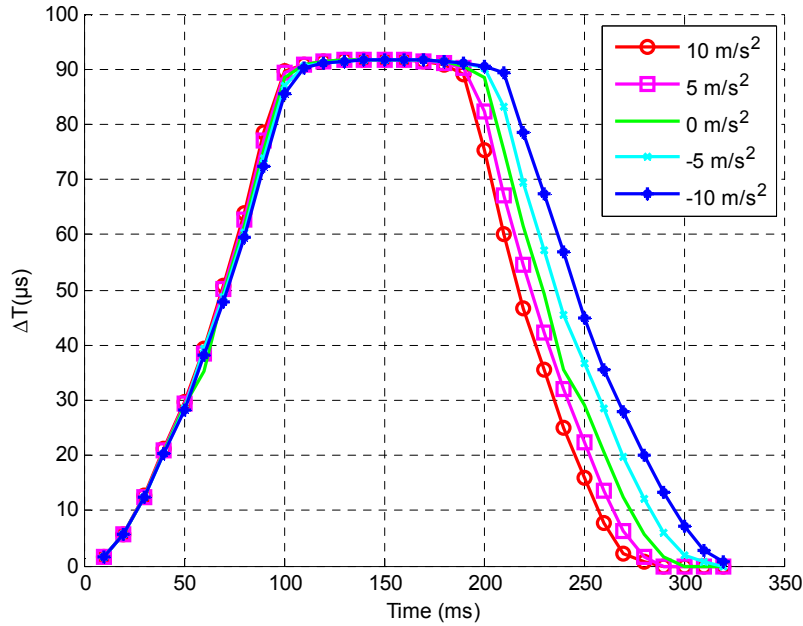


Figure 4.25: Inductive signatures for different values of the vehicle acceleration  $a$ , with  $N = 200$ .

### Influence of the Vehicle Acceleration

Figure 4.25 has been obtained when different values for the vehicle acceleration are considered. In particular, five accelerations ranged from  $-10 \text{ m/s}^2$  to  $10 \text{ m/s}^2$ , with  $N = 200$ , have been considered. As we can observe in the figure, it appears an undesirable distortion in the inductive signature caused by those non-zero constant accelerations.

## 4.4. Comparison of Performances using Real Inductive Signatures

In order to test the proposed model we use a rectangular single-layer coil with  $N_C = 20$  wire turns on an insulating core, with  $a = 18 \text{ cm}$ ,  $w = 17 \text{ cm}$ ,  $a_c = 2 \text{ cm}$ , and a rest oscillation frequency of  $56.60 \text{ kHz}$ . As shown in Fig.4.26, we place  $2 \text{ mm}$  thick rectangular aluminium plates in successive positions parallel to the coil, measuring the magnitude of the inductive signature  $\Delta T$  at each one.

### 4.4.1. Experiment 1: Real Inductive Signatures

Figures 4.27, 4.28, 4.29, 4.30, and 4.31 show an excellent match between signatures obtained with the new multi-loop model for  $N = 200$  and the real measured signatures,

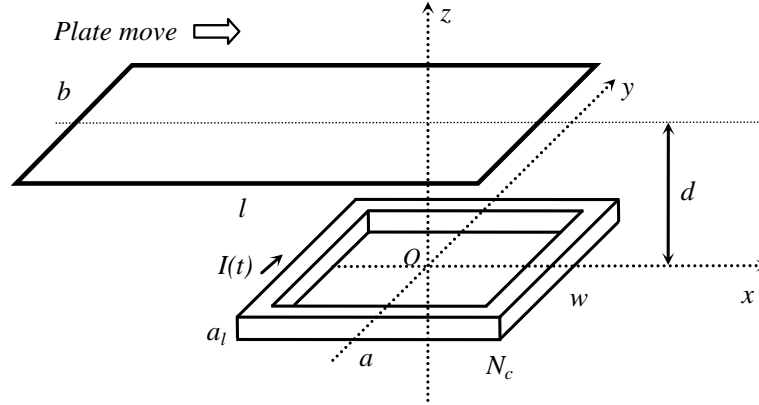


Figure 4.26: Rectangular single-layer coil with  $N_C$  wire turns on an insulating core, with length  $a$ , width  $w$ , and axial length  $a_l$ , with a flat parallel plate of length  $l$  and width  $b$ .

while those obtained with the widely-used models in [1, 22, 23] are significantly different.

Figure 4.27 shows for the new multi-loop model an approximated proportionality of the amplitude of the real inductive signature with the inverse of the distance, as opposed to the standard method, which depended on the squared distance.

Figures 4.28 and 4.29 show the influence of the longitudinal displacement into the coil of a plate of  $l = 9$  cm in length on the real inductive signature, which gives lower real signature amplitudes for a centred plate position. This effect was not modelled by the standard approach.

Figures 4.30 and 4.31 show that the new multi-loop model gives an inductive signature with the peak just in the centre of the road loop, contrary to the old standard model.

#### 4.4.2. Experiment 2: Real Loop Sensitivity

Lastly, for testing the sensitivity measurement performed by this proposed model, we have used our experimental loop formed by a rectangular single-layer coil with  $N_C = 20$  wire turns on an insulating core, with  $a_C = 18$  cm,  $w = 17$  cm,  $a_l = 2$  cm, a rest oscillation frequency of 56.60 kHz, and a parallel rectangular aluminium plates of 2 mm thick and centred for obtaining maximum sensitivity, and with a distance  $d$  between them ranged from 1.5 cm to 5.5 cm.

Figure 4.32 shows that the new multi-loop model much better match the maximum sensitivity obtained from measurements with the real experimental inductive loop at different distances  $d$  compared to the old standard model.

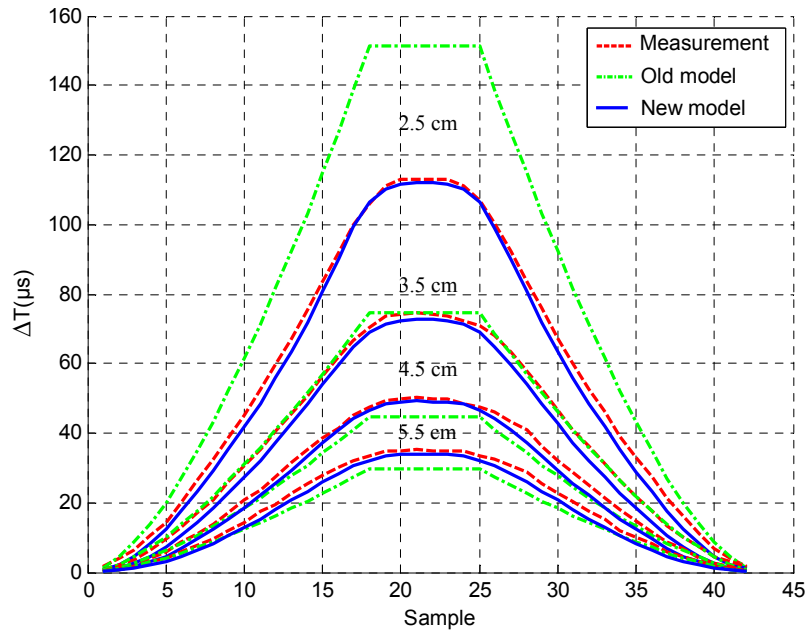


Figure 4.27: Inductive signatures for different values of the loop distance  $d$  ( $d = 2.5, 3.5, 4.5, 5.5$  cm), for a plate of  $25 \text{ cm} \times 16 \text{ cm}$ .

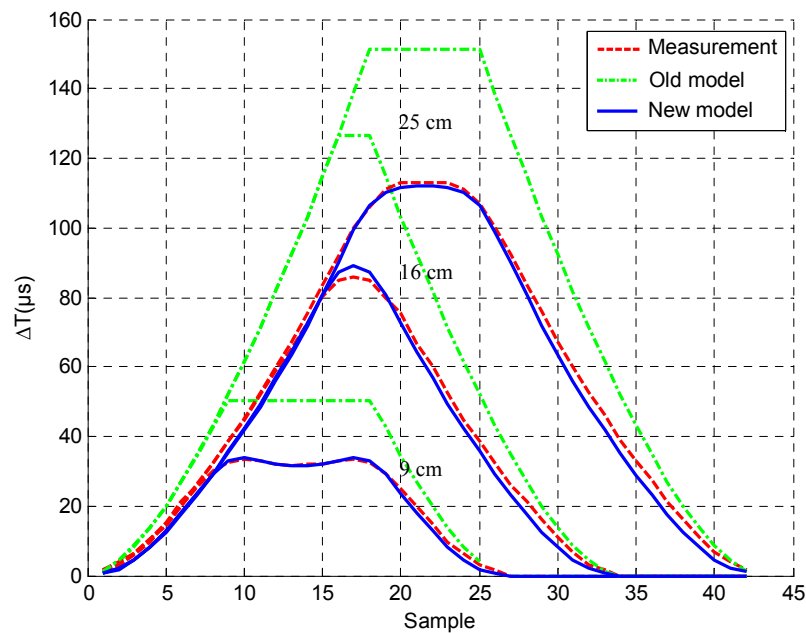


Figure 4.28: Inductive signatures for different values of the plate length  $l$  ( $l = 9, 16, 25$  cm), with  $b = 16 \text{ cm}$  and  $d = 2.5 \text{ cm}$ .

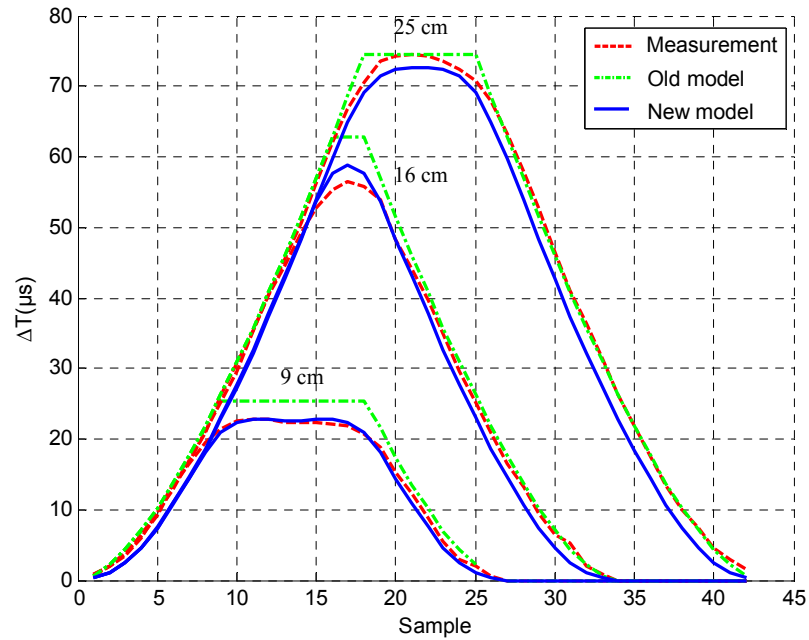


Figure 4.29: Inductive signatures for different values of the plate length  $l$  ( $l = 9, 16, 25$  cm), with  $b = 16$  cm and  $d = 3.5$  cm.

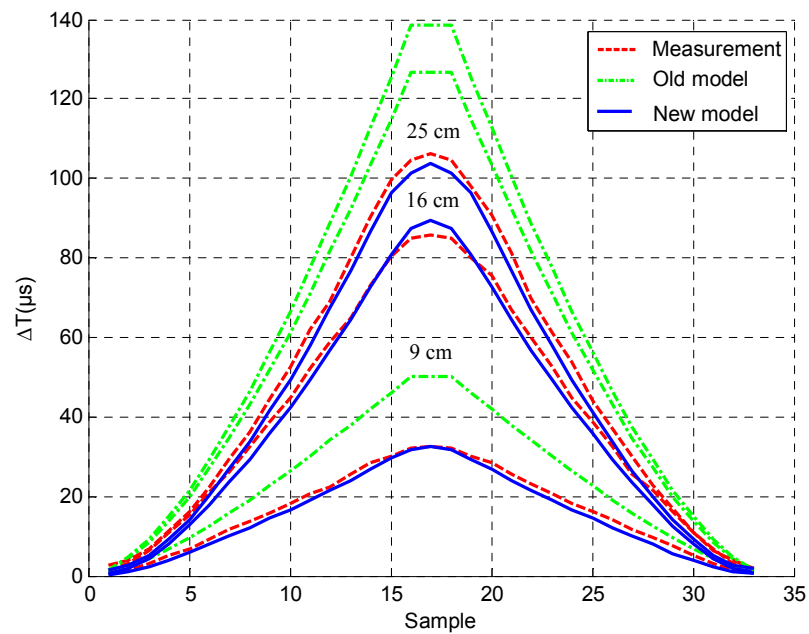


Figure 4.30: Inductive signatures for different values of the plate width  $b$  ( $b = 9, 16, 25$  cm), with  $l = 16$  cm and  $d = 2.5$  cm.

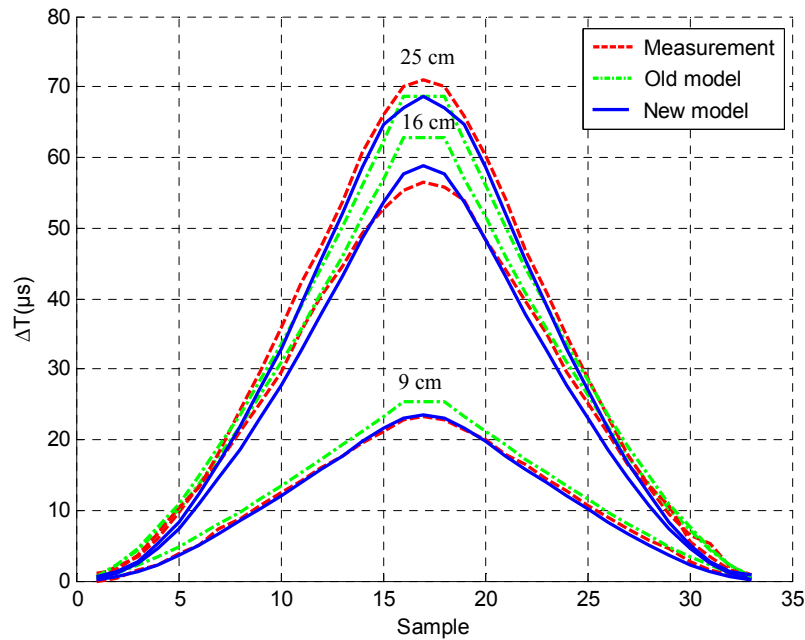


Figure 4.31: Inductive signatures for different values of the plate width  $b$  ( $b = 9, 16, 25$  cm), with  $l = 16$  cm and  $d = 3.5$  cm.

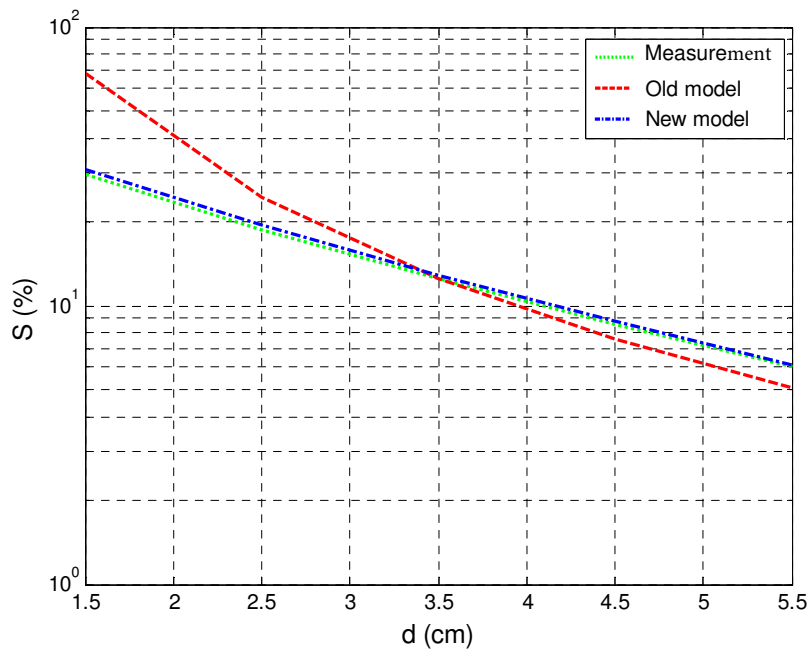


Figure 4.32: Maximum sensitivity (in %) as a function of the distance  $d$  between the experimental inductive loop and the  $25$  cm  $\times$   $16$  cm aluminum plate.

## 4.5. Conclusions

Throughout this chapter we have developed a standard model of an inductive loop detector based on standard approaches. The purpose of such modelling is studying the influence of significant vehicle characteristics on the obtained inductive signatures. Since this model will allow us to obtain the vehicle inductive signatures by means of a simulator without making use of expensive, not only in time but also in resources, tests in real scenarios, we will have a powerful tool to test some features of our inductive sensor prototype in advance. As it is shown with the results obtained using the prototype and the inductive sensor simulator, the vehicle signatures in time domain exhibit similar characteristics, which validates the model used in this work. Moreover, several simulation results have shown the impact of some physical parameters, such as the distance between the vehicle undercarriage and the loop under the road pavement, vehicle length or width, and its speed or acceleration, on their corresponding time inductive signatures.

Also in this chapter we have developed a more accurate model for ILDs that will allow both a much more accuracy in obtaining the inductive signatures compared to real measured ones and a better extraction of features from them than the standard approach, as has been shown with several simulation results. In addition, the response to changes in length or width of the vehicle, distance between the its undercarriage and the inductive road loop, vehicle speed or acceleration, is adequate, as expected. The better performance exhibited by the proposed multi-loop method can be explained by taking into account those parts of the vehicle that fall out of the road coil, and also by the longitudinal and lateral displacement of the vehicle with respect to the road coil, which are not included in the standard approach. However, this multi-loop model was only developed considering flat vehicle profiles, although it could be extended to other types of profiles.



## Chapter 5

# Advanced Methods for Vehicle Traffic Monitoring

Speed measuring is a fundamental task in traffic management systems. In this chapter, we will develop a new algorithm for calculating the vehicle speed with dual loop inductive detectors. This technique will use the mean in time from the measurements obtained using both loops instead of the mean in speed traditionally used in standard methods. Some experimental results will be performed to illustrate the improvement produced by this speed estimate.

We will also present a method for vehicle identification based on analysing the inductive signatures in the frequency domain instead of working in the time domain. The proposed descriptor in the transform domain will be used for vehicle classification by means of a simple threshold-based method. We will show some experimental results obtained with two different methods. The first set of experiments has been performed using a powerful testing tool developed by us based on [1], as was explained in Chapter 4. Its main advantage is that it provides us useful prior information before the actual testing in a real scenario, thus reducing the necessary time and resources. The second set of experiments uses a hardware prototype capable of obtaining simultaneous inductive signatures of vehicles travelling on a road with minimal cost. Based on Time-Division Multiplexing (TDM) with multiple oscillators, one for each inductive loop, the system detects the presence of vehicles by means of a shift in the oscillation period of the selected loop and registers the signature of the detected vehicles.

This chapter is organized as follows. Section 5.1 presents the model for time estimation using a dual loop per road lane. Section 5.2 presents the proposed method for speed estimation using dual loop inductive detectors, and several results are performed to validate the algorithm working. In Section 5.3, we show the proposed method for feature extraction from inductive signatures based on a descriptor obtained by means of a spectral analysis. Our method is introduced as opposed to the standard and well-known strategy

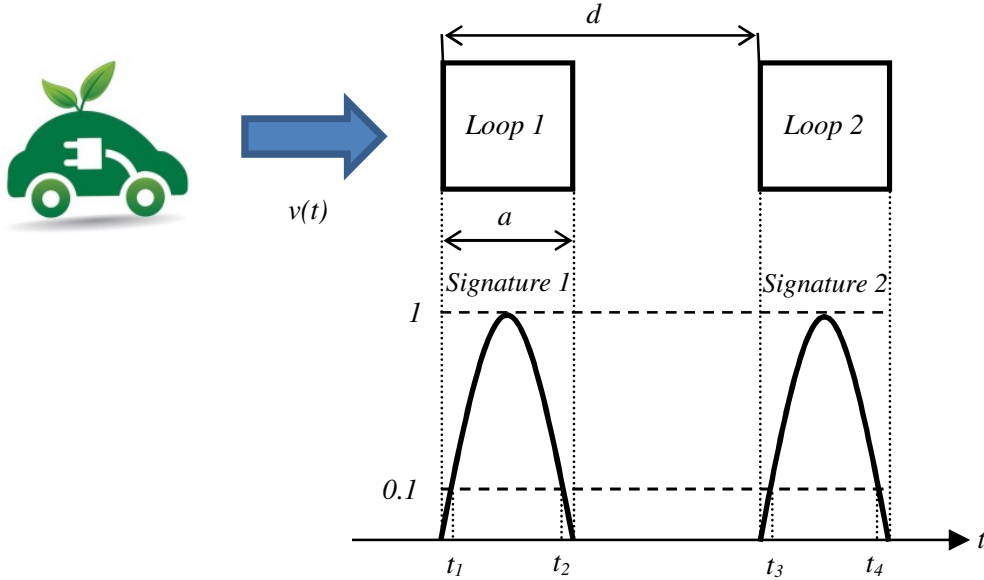


Figure 5.1: Scheme for dual loop time.

based on the vehicle length estimate. Also this section shows the experiment results, where a novel threshold-based method for vehicle classification using the proposed tool is presented. Finally, Section 5.4 is devoted to the concluding remarks.

## 5.1. Model for Time Estimation

In this work, we study *Inductive Loop Detectors* (ILDs) based on period shift. As explained in Chapter 2, these ILDs use a reference clock signal whose frequency is of several MHz, typically between 20 and 1000 times greater than the oscillation frequency of the inductive loop we are employing for measurement. The period of the oscillation signal is calculated as the number of cycles  $N$  of the reference clock signal in  $m_c$  cycles of the oscillation signal. When a vehicle stops or passes over the loop the oscillation frequency increases, so the period (and thus the number of cycles  $N$ ) decreases. The pulses from the oscillation loop are carried to a counter input, so that when a fixed number of pulses  $m_c$  is reached, the measured value  $N$  is captured from a timer working at the frequency  $f_r$  of the reference clock signal. The amplitude of the signatures is determined by means of the difference between the measured value  $N$ , obtained every 10 ms, and that obtained at rest, which is calculated and registered by the measurement equipment. This value is referred to as  $\Delta N$ , so the oscillation period shift is given by  $\Delta T = \Delta N / m_c$ . This parameter  $\Delta T$  gives us the amplitude of the vehicle inductive signature at a time instant.

A dual loop consists of two single loops identical in length placed in line, but separated a distance  $d$  (see Fig. 5.1). When a vehicle passes over the loops two similar signatures are captured accordingly to the procedure above explained and using the signature detector equipment described in Chapter 3 [53]. Accordingly to Fig. 5.1, the following time instants are determined when the vehicle signatures reach as threshold value the percentage of 10 % of its maximum value:

- $t_1$ : Input time instant of the normalized vehicle signature 1 corresponding to the 10 % of its amplitude;
- $t_2$ : Output time instant of the normalized vehicle signature 1 corresponding to the 10 % of its amplitude;
- $t_3$ : Input time instant of the normalized vehicle signature 2 corresponding to the 10 % of its amplitude;
- $t_4$ : Output time instant of the normalized vehicle signature 2 corresponding to the 10 % of its amplitude.

## 5.2. Speed Estimation

An ILD is the most used sensor for traffic monitoring, and an accurate vehicle speed measurement is fundamental in traffic management systems. Although it is possible to measure vehicle speeds with a single loop per lane [54–59], a double loop per lane is necessary for maximum accuracy [60–62]. In recent years there are many works devoted to improve the vehicle speed estimate using dual loop inductive sensors. In [61], algorithms for vehicle filtering were proposed to correct *Irregular Driving Vehicles* (IDVs) and also the presence of *Multiple Vehicles in the Detection Zones* (MVDZs), both compatibles with our algorithm, proposed in this section. Also the *Maximum-Likelihood* (ML) estimator of the vehicle speed was presented in [62], but assuming a constant vehicle speed.

Taking into account the time instants indicated in Section 5.1, we can measure two speed values: the first one, referred to as *vehicle input speed*, and denoted as  $v_I$ , which uses the input time difference  $t_3 - t_1$ ; and the second one, referred to as *vehicle output speed*, and denoted as  $v_O$ , which uses the output time difference  $t_4 - t_2$ . Thus, we have [60,61]

$$v_I = \frac{d}{t_3 - t_1}, \quad (5.1)$$

$$v_O = \frac{d}{t_4 - t_2}. \quad (5.2)$$

Since the digital inductive sensors work with the sampling period,  $T$ , typically ranged between 1 and 10 ms (see Chapter 2), the time instants  $t_1$ ,  $t_2$ ,  $t_3$ , and  $t_4$  are integer multiples of  $T$ , i.e.  $\Delta t = NT$ , with  $N \in \mathcal{Z}$ . Consequently, both speeds  $v_I$  and  $v_O$  are also discrete, so that Eqs. 5.1 and 5.2 can be rewritten as

$$v_I(\Delta t = N_I T) = v_{N_I} = \frac{d}{N_I T}, \quad (5.3)$$

$$v_O(\Delta t = N_O T) = v_{N_O} = \frac{d}{N_O T}, \quad (5.4)$$

where  $N_I, N_O \in \mathcal{Z}$ .

Moreover, the relative quantization errors can be respectively calculated as

$$e_I = \frac{v_{N_I} - v_{N_I+1}}{v_{N_I}} = \frac{1}{N_I + 1},$$

$$e_O = \frac{v_{N_O} - v_{N_O+1}}{v_{N_O}} = \frac{1}{N_O + 1}. \quad (5.5)$$

This shows us that an increase in  $N$  leads to lower errors, which can be reached when  $T$  decreases for a given speed.

### 5.2.1. Standard Method

The vehicle speed could vary when the vehicle on the loops, i.e. the speed could not be constant. Thus, the speed could be calculated as the mean value of the speeds  $v_I$  and  $v_O$ , which will be denoted as  $v_M$  and calculated as follows [60, 61]

$$v_M = \frac{v_I + v_O}{2}, \quad (5.6)$$

which gives us

$$v_M = \frac{\frac{d}{N_I T} + \frac{d}{N_O T}}{2} = \frac{d}{N_M T}, \quad (5.7)$$

where

$$N_M = 2 \frac{N_I N_O}{N_I + N_O}, \quad (5.8)$$

is a real number.

### 5.2.2. Proposed Method

We propose an alternative way of estimating the vehicle speed by calculating the mean in time, i.e.

$$t_P = \frac{(t_3 - t_1) + (t_4 - t_2)}{2}, \quad (5.9)$$

or, equivalently, in the discrete domain

$$N_P = \frac{N_I + N_O}{2}. \quad (5.10)$$

Accordingly to that, the speed estimate is expressed as

$$\begin{aligned} v_P &= \frac{d}{N_P T} = \frac{d}{\left(\frac{N_I + N_O}{2}\right) T} = \frac{2d}{N_I T + N_O T} = \frac{2 \frac{d}{N_I T} \frac{d}{N_O T}}{\frac{d}{N_I T} + \frac{d}{N_O T}} \\ &= \frac{2v_I v_O}{v_I + v_O}, \end{aligned} \quad (5.11)$$

and therefore,  $v_P$  can be seen as the inverse of the mean of the inverse speeds, i.e.

$$v_P = \frac{1}{\frac{\left(\frac{1}{v_I} + \frac{1}{v_O}\right)}{2}}. \quad (5.12)$$

This expression for  $v_P$  can be redefined as

$$v_P = \frac{d}{N'_P T'}, \quad (5.13)$$

with  $T' = T/2$  being the sampling period and

$$N'_P = N_I + N_O \in \mathcal{Z}. \quad (5.14)$$

Let  $v_N = d/(NT)$  be the vehicle speed that both loops would measure. Let  $v_I = d/(N - k)T$  and  $v_O = d/(N - p)T$ , with  $k, p \in \mathcal{Z}$ , be the speed estimates obtained using the dual loop inductive sensor. Figures 5.2 and 5.3 show the sign of  $e_M - e_P$ , respectively given by  $e_M = |v_N - v_M|$  and  $e_P = |v_N - v_P|$ , for  $v_N = 100$  km/h,  $d = 5$  m, and  $T = 10$  ms and  $T = 4$  ms, respectively. In both figures, the region in red corresponds to greater errors if the standard approach is used, i.e.  $e_M > e_P$ ; the region in blue corresponds to lower errors for that standard approach, i.e.  $e_M < e_P$ , and the diagonal region in green corresponds to  $k = p$  and therefore,  $e_M = e_P$ . In other words, from the figure we can say that most scenarios lead to greater errors if the standard speed estimation is used, specially for higher speeds.

### 5.2.3. Speed Estimation Results

In this Subsection, we develop two experiments that allow us to test the performance of the proposed algorithm: the first one compares the aforementioned speed estimates obtained from real measurements; and the second one determines the average estimation error across a range of speeds or accelerations.

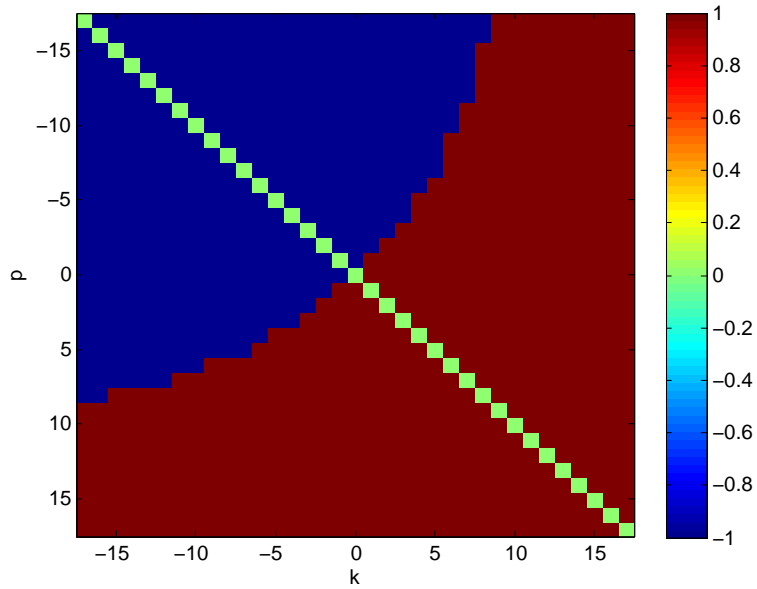


Figure 5.2: Sign of  $e_M - e_P$ : positive (1), zero (0), or negative (-1), considering  $v_N = 100$  km/h and  $T = 10$  ms.

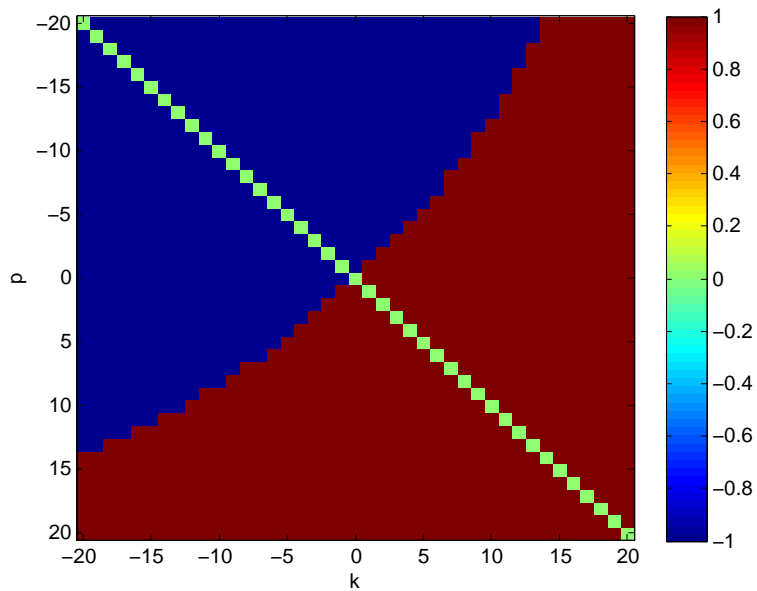


Figure 5.3: Sign of  $e_M - e_P$ : positive (1), zero (0), or negative (-1), considering  $v_N = 100$  km/h and  $T = 4$  ms.

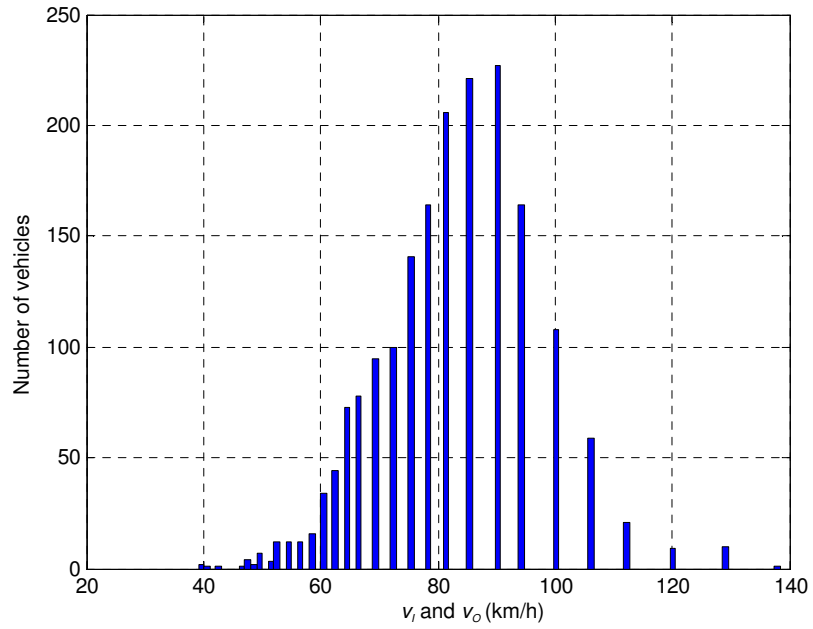
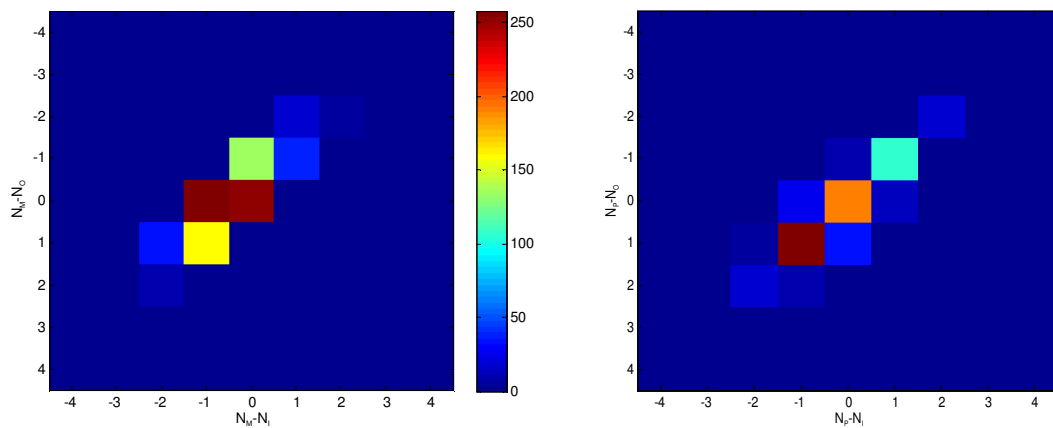


Figure 5.4: Histogram of speeds  $v_I$  and  $v_O$ .



(a) Time index distribution of pairs  $(v_I, v_O)$  with respect to  $v_M$ .

(b) Time index distribution of pairs  $(v_I, v_O)$  with respect to  $v_P$ .

Figure 5.5: Time index distributions of mean speeds considering data of Río Anllóns station.

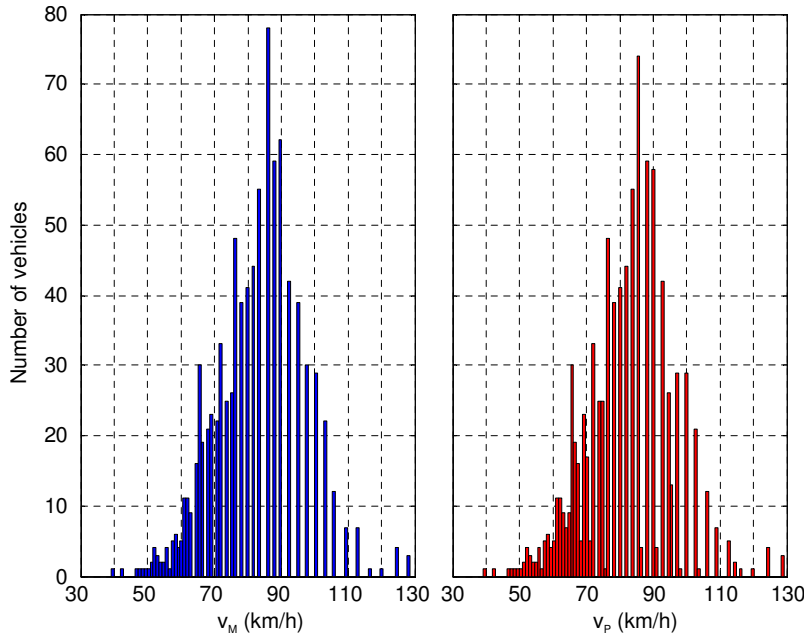


Figure 5.6: Histogram of speeds  $v_M$  and  $v_P$ .

### Experiment 1: Comparison of Speed Real Measurements

For this experiment, we have captured inductive signatures of 914 vehicles in the AC-523 road (Río Anllóns, Ledoño-Meirama, Spain) using our detector as described in Chapter 3 and working at a sampling period of  $T = 10$  ms. We will use the loop configuration pictured in Fig. 5.1, with squared loops of  $a = 2$  m in length and a distance between their centres of  $d = 5$  m.

Figure 5.4 shows the histogram of the vehicle speeds  $v_I$  and  $v_O$  given in Eqs. 5.3 and 5.4, respectively, so that the relative quantization error is given by Eq. 5.5. Figure 5.5(a) shows the difference between the integer multiples of  $T$  measured for the standard method, i.e.  $N_M$  (see Eq. 5.8) and for the vehicle output speed, i.e.  $N_O$ , as a function of that difference with respect to the vehicle input speed, i.e.  $N_I$ . This graph gives us an idea of the number of vehicles corresponding to each pair of speeds  $(v_I, v_O)$  with respect to  $v_M$ , or, equivalently, to each pair of integer indices  $(p, q)$  denoting the mismatch of  $N_I$  and  $N_O$  with respect to  $N_M$ . Figure 5.5(b) depicts that distribution but with respect to  $v_P$ , i.e. using the proposed discrete mean in time  $N_P$  (see Eq. 5.10). In both cases, as we can see from the figures,  $p, q \in \mathcal{Z} = \{-4, \dots, -1, 0, 1, \dots, 4\}$ .

Figure 5.6 shows the histograms corresponding to the standard method for speed estimation (left), i.e., for  $v_M$ , and to the proposed one, i.e. for  $v_P$  (right). Table 5.1 collects the statistical parameters of both distributions, obtained accordingly to the following

Table 5.1: Statistical parameters for  $\mathbf{v}_M$  and  $\mathbf{v}_P$  distributions

Statistical parameters	$\mathbf{v}_M$	$\mathbf{v}_P$
M (km/h)	81.89	81.82
$\mu$ (km/h)	81.74	81.65
$\sigma$ (km/h)	13.38	13.35
$\kappa$	3.37	3.36

formulas

$$\begin{aligned}
\text{Median } (M) &= \begin{cases} \mathbf{v} \left( \frac{n+1}{2} \right) & \text{if } n \text{ is odd,} \\ \frac{1}{2} \left( \mathbf{v} \left( \frac{n}{2} \right) + \mathbf{v} \left( \frac{n+1}{2} \right) \right) & \text{otherwise;} \end{cases} \\
\text{Mean}(\mu) &= \frac{1}{n} \sum_{i=1}^n \mathbf{v}(i); \\
\text{Variance}(\sigma^2) &= \frac{1}{n} \sum_{i=1}^n (\mathbf{v}(i) - \mu)^2; \\
\text{Kurtosis}(\kappa) &= \frac{\frac{1}{n} \sum_{i=1}^n (\mathbf{v}(i) - \mu)^2}{\sigma^4}, \tag{5.15}
\end{aligned}$$

where  $n$  is the length of speed vector, denoted as  $\mathbf{v}$ , and that corresponds to the vectors  $\mathbf{v}_M$  or  $\mathbf{v}_P$  containing the speed values obtained accordingly to the standard and proposed methods, respectively. As we can see from the table, the statistical parameters of both distributions are quite similar.

Moreover, two statistical hypothesis tests have been used to determine if both sets of data are different from each other: the *t-test* [63], which tests if two normally distributed data have the same mean; and the *F-test* [64], for testing if they have the same variances. We can see the results of such tests in Table 5.2. Since the *t-test* provides a  $p$ -value of  $0.88 > \alpha = 0.05$ , the null hypothesis  $H_0$  is not rejected with a 5% of significance level, and since zero falls into the confidence interval there is not a significant difference between  $\mu_M$  and  $\mu_P$ . Therefore,  $\mathbf{v}_M$  and  $\mathbf{v}_P$  are normally distributed with equal mean. Also from Table 5.2 we can see that the *F-test* provides a  $p$ -value of  $0.94 > \alpha = 0.05$ , and then the null hypothesis  $H_0$  is not rejected with a 5% of significance level, so that  $\mathbf{v}_M$  and  $\mathbf{v}_P$  are normally distributed with also equal variances.

Table 5.2: Statistical hypothesis tests

Test	Hypothesis H0	Hypothesis H1	Result	p-value	Confidence Interval
t-test	$\mu_M = \mu_P$	$\mu_M \neq \mu_P$	H0	0.88	-1.13 to 1.32
F-test	$\sigma_M^2 = \sigma_P^2$	$\sigma_M^2 \neq \sigma_P^2$	H0	0.94	0.88 to 1.14

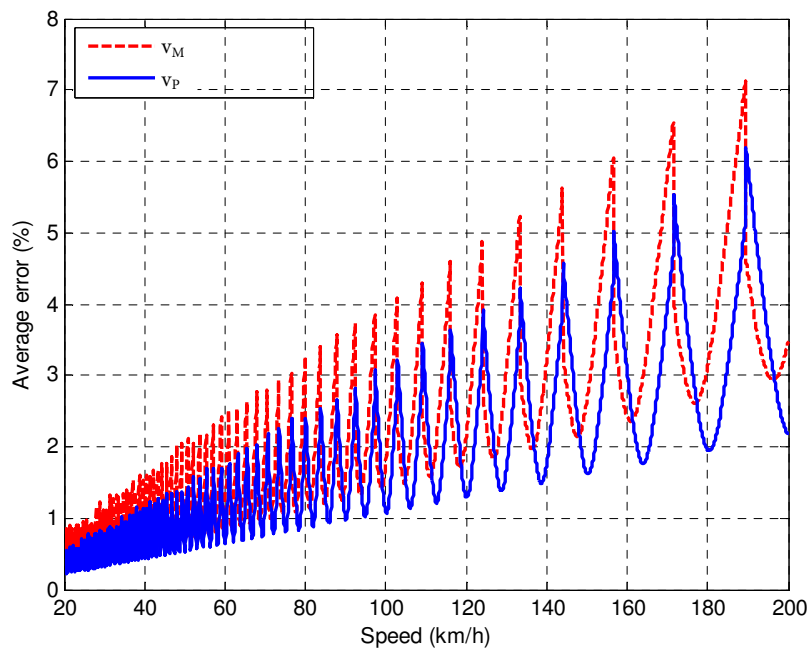


Figure 5.7: Average error (%) in speed estimation.

### Experiment 2: Comparison of Speed Estimation Errors

For the calculation of the speed estimation error we have considered speeds only ranged from 20 km/h to 200 km/h, since speeds lower than 20 km/h cause negligible differences in terms of estimation error when standard and proposed methods are applied. For each speed value, denoted as  $v_e$ , the nearest discrete speed,  $v_N$ , is obtained as

$$v_N = \frac{d}{NT} = \frac{d}{\text{round}\left(\frac{d}{v_e T}\right) T}, \quad (5.16)$$

where  $\text{round}(x)$  provides the nearest integer  $N$  to  $x$ . Remember that the sampling period is  $T = 10$  ms.

Taking into account the time index distribution of pairs  $(v_I, v_O)$  shown in Fig. 5.5, we can consider the measured values for the input and output speeds as follows

$$\begin{aligned} v_I &= v_{N-p}, & p &\in \mathcal{Z} = \{-4, \dots, -1, 0, 1, \dots, 4\}, \\ v_O &= v_{N-q}, & q &\in \mathcal{Z} = \{-4, \dots, -1, 0, 1, \dots, 4\}, \end{aligned} \quad (5.17)$$

and then, considering the  $9^2 = 81$  possible pairs  $(v_I, v_O)$ , the speed estimates for each pair  $(p, q)$ ,  $v_{M,(p,q)}$  and  $v_{P,(p,q)}$ , can be obtained accordingly to Eqs. 5.6 and 5.11, respectively.

The average estimation errors, expressed in %, using the standard and the proposed estimation methods, i.e.  $e_M$  and  $e_P$ , for each value of  $v_e$ , are calculated using the *Weighted Root Mean Square Error* (WRMSE) as follows

$$e_M(\%) = \frac{100}{v_e} \sqrt{\frac{\sum_{p=-4}^{p=+4} \sum_{q=-4}^{q=+4} w_{(p,q)} (v_e - v_{M,(p,q)})^2}{\sum_{p=-4}^{p=+4} \sum_{q=-4}^{q=+4} w_{(p,q)}}}, \quad (5.18)$$

$$e_P(\%) = \frac{100}{v_e} \sqrt{\frac{\sum_{p=-4}^{p=+4} \sum_{q=-4}^{q=+4} w_{(p,q)} (v_e - v_{P,(p,q)})^2}{\sum_{p=-4}^{p=+4} \sum_{q=-4}^{q=+4} w_{(p,q)}}}, \quad (5.19)$$

where  $w_{(p,q)}$  is the  $(p, q)$ -th weight obtained from Fig. 5.5 as

$$w_{(p,q)} = \frac{n_{(p,q)}}{n_T}, \quad (5.20)$$

with  $n_{(p,q)}$  being the number of vehicles corresponding to the pair  $(p, q)$  and  $n_T$  the total number of vehicles. Figure 5.7 depicts the estimation errors of Eqs. 5.18 and 5.19. As it can be seen from the figure, the estimation error produced when the standard method is used is greater than that obtained from the proposed approach for most speeds, although the mean of standard estimation error is always higher.

Figure 5.8 shows the influence of the vehicle acceleration in the speed estimation obtained using the two methods above explained. For the simulation we have considered a dual loop constituted by two coils of  $a = 2$  m in length, separated by a distance of  $d = 5$  m, and a vehicle length of  $l = 5$  m which enters in the first loop with an initial speed  $v_i$  of 100 km/h. Moreover, we assume the linear equation of motion with constant acceleration, denoted as  $a_c$ , with initial time and position conditions  $t_i = 0$  and  $x_i = 0$ , respectively, so the vehicle position at the time instant  $t$ ,  $x(t)$ , is given by

$$x(t) = v_i t + \frac{1}{2} a_c t^2, \quad (5.21)$$

and  $t$  is directly obtained as

$$t = \frac{-v_i + \sqrt{v_i^2 - 2x(t)a_c}}{a_c}. \quad (5.22)$$

The input time instants are given by  $t_1 = 0$  and  $t_3$ , where  $t_3$  is the time instant when  $x = d$ . The output time instants are given by  $t_2$  and  $t_4$ , which represent the time instants corresponding to  $x = l + a$  and  $x = l + a + d$ , respectively. Using Eqs. 5.3, 5.4, 5.6, and 5.11, the speed estimates  $v_M$  and  $v_P$  are calculated for each acceleration value  $a_c$ , and the average speed, denoted as  $v_A$ , is obtained by dividing the distance travelled by the vehicle and the time interval used for that travel, as follows

$$v_A = \frac{l + a + d}{t_4}. \quad (5.23)$$

The error percentages  $e_M$  and  $e_P$  are then calculated as

$$e_M(\%) = 100 \frac{|v_M - v_A|}{v_A}, \quad (5.24)$$

$$e_P(\%) = 100 \frac{|v_P - v_A|}{v_A}. \quad (5.25)$$

Figure 5.8 shows that the influence of a constant acceleration is negligible in terms of error in speed estimation, independently of the method used. However, as we can see it in the figure, the error is again greater for the standard method than for the proposed one in this work.

Therefore, this new algorithm for estimating the vehicle speed using dual loop inductive detectors clearly outperforms the standard one, as was validated observing the significant reduction in the speed miscalculation and the minimum influence of the vehicle acceleration.

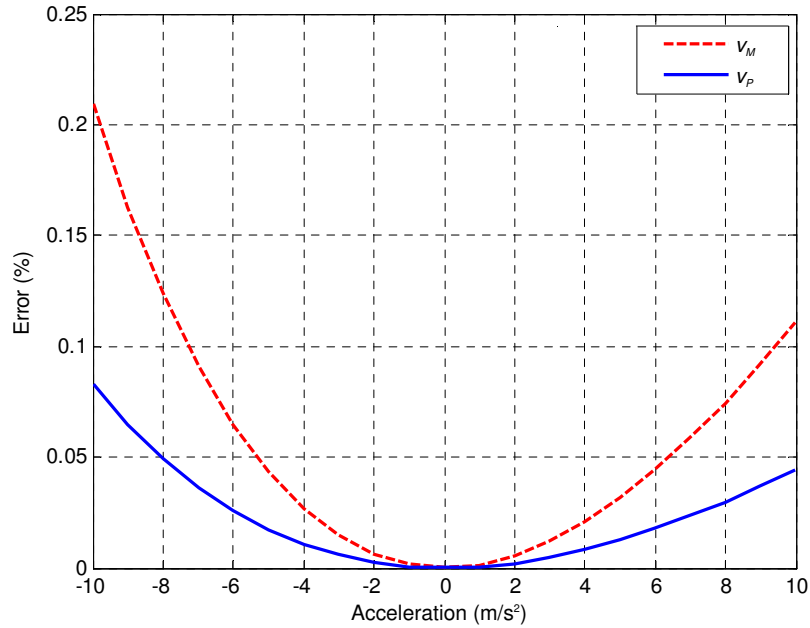


Figure 5.8: Influence of acceleration on speed estimation.

### 5.3. Vehicle Classification

ILDs are usually employed in traffic management systems to estimate vehicle parameters such as speed and length, which are basic requirements for planning, project, and operation of roads, streets or complementary works for transport systems. These sensors mostly need accuracy and reliability when estimating such parameters with a minimum delay in control strategies. The estimate obtained from dual loop detectors is usually accurate [31–34] but it requires a proper maintenance of both loops, which implies that it is not the optimum solution in terms of cost. Moreover, only one loop is available in most of traffic systems. Although some algorithms have already been developed for single-loop classification [35–37] and single-loop speed estimation [38, 39], how to achieve enough accuracy using only one loop is still an open question. In this section we will present a method for vehicle identification based on analysing the inductive signatures in the frequency domain instead of working in the time domain using only a single loop for this purpose.

The vehicles passing on the road will be classified using a threshold-based criterion. We will show results obtained when those vehicles are classified according to three types: cars, vans and trucks. We have used a threshold-based criterion as follows

$$\hat{p} \leq \epsilon_1 \rightarrow \text{Car}; \quad \epsilon_1 < \hat{p} \leq \epsilon_2 \rightarrow \text{Van}; \quad \hat{p} > \epsilon_2 \rightarrow \text{Truck}, \quad (5.26)$$

where  $\hat{p}$  is the descriptor to be considered according to the criterion. This criterion can

be employed for both length-based classification and frequency domain descriptor-based classification, since there is a direct relationship between them. Both prefixed thresholds,  $\epsilon_1$  and  $\epsilon_2$ , are obtained empirically from a training stage.

### 5.3.1. Standard Method

Figure 3.8 of Chapter 3 shows the typical system employed to capture vehicle signatures with two inductive loop sensors per road lane. It is apparent that, using such a configuration, two signatures are registered per vehicle. These sensors are squares with a side length denoted by  $w$  and a distance  $d$  between their centers. The standard methods for vehicle classification are based on estimating both the speed and length of the vehicle using the following expressions [53], accordingly, to the aforementioned notation in Section 5.1

$$\hat{s} = \frac{1}{2} \left( \frac{d}{t_3 - t_1} + \frac{d}{t_4 - t_2} \right), \quad (5.27)$$

$$\hat{L} = \hat{s} \times \frac{(t_2 - t_1) + (t_4 - t_3)}{2} - w. \quad (5.28)$$

### 5.3.2. Proposed Method

Let  $r^l(t)$  be the inductive signature captured in loop  $l$ , with  $l = 1, 2$  in lane 1 and  $l = 3, 4$  in lane 2. These inductive signatures are composed of the sequence of  $\Delta T$  values obtained by the method again described in Section 5.1. In this work we conversely propose to compute the  $L$ -point *Discrete Fourier Transform* (DFT) of the  $M$  samples of  $r^l(t)$  obtained between the corresponding initial and final time instants of each loop  $l$ . Therefore, we will obtain the frequency domain signature

$$r^l[\omega_k] = \sum_{m=0}^{M-1} r^l(m) e^{-j\omega_k m}, \quad k = 0, \dots, L-1, \quad (5.29)$$

where  $\omega_k = 2\pi k/L$  denotes the frequency bin. Throughout this work, we will always assume that the number of frequency bins  $L$  is greater than the window size  $M$ . After normalizing the absolute values by the first coefficient at  $k = 0$ , i.e.  $\omega_0$ , we get the normalized DFT

$$R^l[\omega_k] = \frac{|r^l[\omega_k]|}{|r^l[\omega_0]|}. \quad (5.30)$$

Considering  $\omega_k > 0$ , we obtain the descriptor parameter proposed in this work by finding the first local maximum of  $R^l[\omega_k]$ . The frequency bin of

such peak will be denoted by  $n$ , and thus the descriptor that will be used in the classification of the vehicle is given by  $R^l[\omega_n]$ . As we demonstrate in Appendix C, this parameter is independent of the speed of the vehicle and of its lateral displacement over the inductive loop. In addition, in Section 5.3.3, we show that the descriptor will provide us with enough information to perform the classification of the vehicles with high accuracy.

In the following, we will study the behaviour of the proposed descriptor against different vehicle characteristics. For such purpose, we present three experiments that allow us to ensure the convenience of using this descriptor for vehicle classification tasks.

### **Experiment 1: Examples obtained using the Inductive Standard Model**

Firstly, we apply the inductive sensor model proposed in Chapter 4 since provides us a tool for testing without the need for actual on-site measurements.

Figure 5.9 shows an example of the results obtained for vehicles of 4 m and 6 m in length with this model. The top figure shows the simulated vehicle profile, which represents the distance between the vehicle undercarriage and the road loop. The figure also represents the signatures obtained for vehicle speeds of 50 km/h and 100 km/h. It is interesting to note that the signature shape depends on the vehicle length, and that the signature length depends on the vehicle speed, but the shape remains mostly constant [30]. The bottom figure shows the DFT of the aforementioned simulated signatures with  $L = 4096$ , although only the DFT central part is shown in the figure. Obviously, the vehicle speed has an influence on the DFT length, but the descriptor  $R^l[\omega_n]$  is invariant to speed changes since the magnitude scaling is eliminated by the normalization in the frequency domain (see Appendix C). It is also significant to note that the values of the proposed descriptor are greater for vehicles of 6 m in length than for those of 4 m.

Figure 5.10 shows the value of that descriptor  $R^l[\omega_n]$  when the vehicle length is varying from 4 m to 10 m, and also the speed from 20 km/h to 120 km/h. The figure shows the obtained values and their corresponding mean value given the vehicle length. We can observe that their length produces significant changes in  $R^l[\omega_n]$ . On the other hand, the impact of speed changes is relatively small if the length remains unchanged. The figure shows a clear relationship between length and  $R^l[\omega_n]$ . The anomaly between 4 and 4.5 m is caused by the choice of vehicle undercarriage profile (shown in Fig. 5.9) and the model employed for the simulation [1]. In our simulations we have observed that different vehicle profiles can cause different anomalies in the low length region, but in all cases the relationship between the DFT descriptor and the vehicle length remains significant.

Finally, in order to test the robustness of the descriptor against noise, we perform tests adding white Gaussian noise to the inductive signature signal. The impact of the Additive

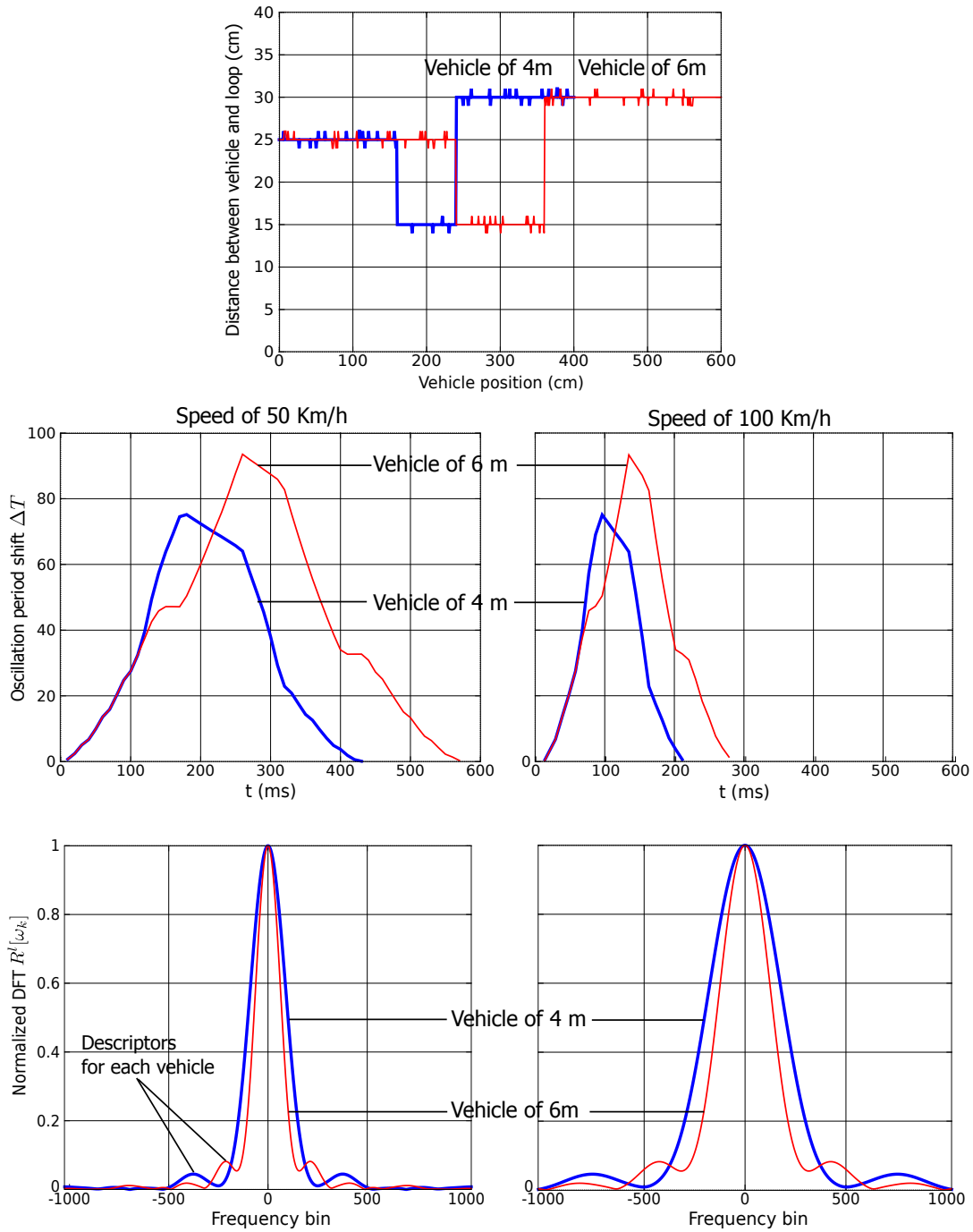


Figure 5.9: Software simulator: Examples of profiles (**Top**), signatures (**Middle**) and normalized DFT (**Bottom**) for two vehicles of 4 m and 6 m in length and for different speeds.

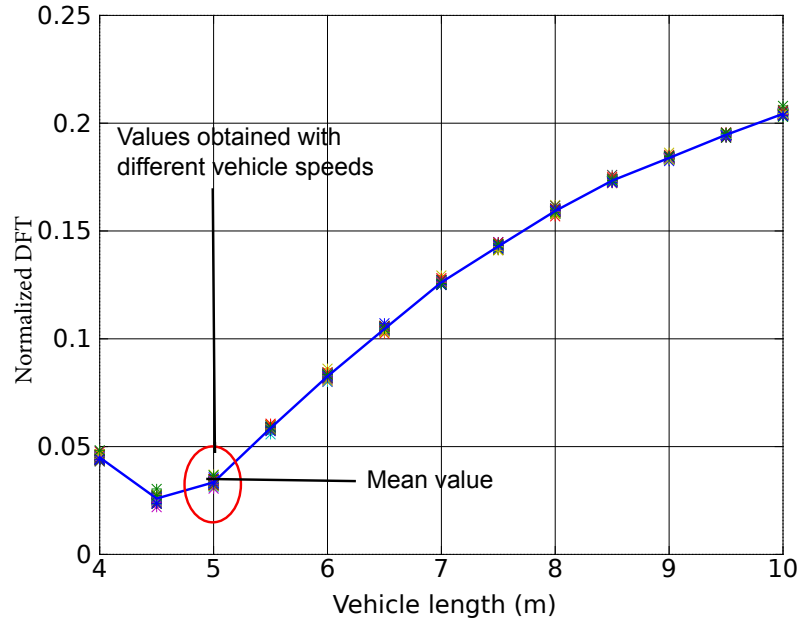


Figure 5.10: Software simulator: Signature descriptor for vehicle length from 4 m to 10 m, and speed from 20 km/h to 120 km/h.

White Gaussian Noise (AWGN) on the DFT descriptor is shown in Fig. 5.11. The noise is applied to inductive signatures obtained from three vehicles of 4 m, 6 m and 8 m in length using the vehicle profile depicted at the top of Fig. 5.9. As can be seen in the figure, no significant effects on the DFT descriptor can be observed for Signal-to-Noise Ratios (SNRs) greater than 20 dB.

### **Experiment 2: Influence of Vehicle Characteristics on $R^l[\omega_n]$ using the Standard Inductive Sensor Model**

Figure 5.13 plots the normalized DFT of the inductive signatures for the profile of a vehicle of 6 m in length shown in Fig. 5.12 scaled to 4, 6, 10 and 16 meters in length. As it can be seen from the figure, an increase in the vehicle length affects the amplitude of the first peak of the DFT given by Eq. (5.30), as it occurs with real acquired signatures (see Chapter 3). This effect can be more clearly seen in Table 5.3.

On the other hand, Tables 5.3, 5.4, 5.5, 5.6 and 5.7 show the spectral feature  $R^l[\omega_n]$  of Eq. (5.30) as a function of the vehicle length and width, the distance between the vehicle undercarriage and the loop under the road pavement, the vehicle speed and the vehicle acceleration, respectively. This frequency domain study is similar to the time domain study performed in Chapter 4. As can be seen in the tables, although the vehicle length

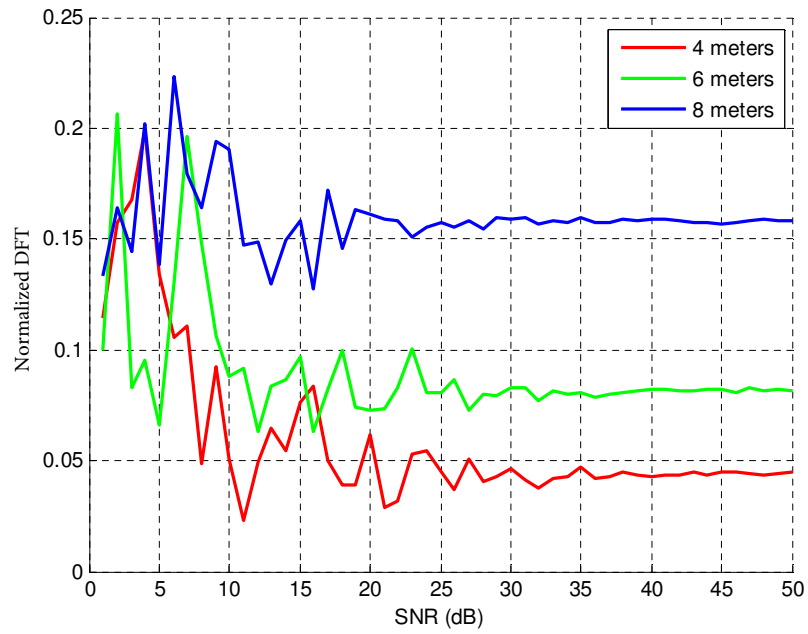


Figure 5.11: Impact of additive white Gaussian noise on the DFT descriptor.

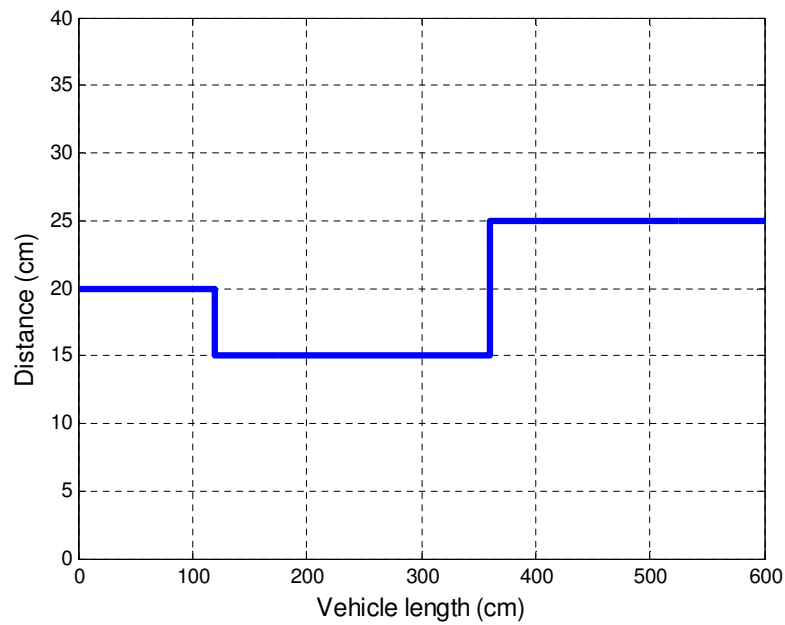


Figure 5.12: Vehicle profile.

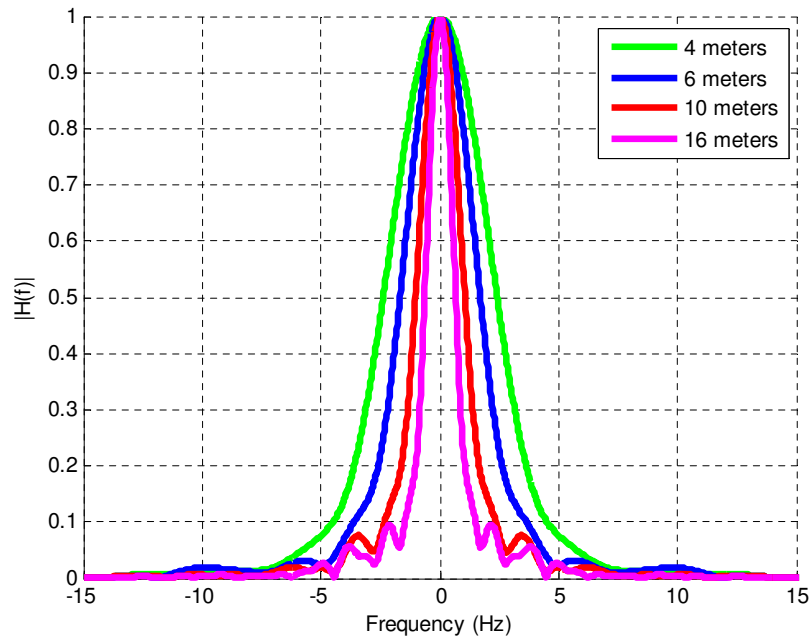


Figure 5.13: Inductive signatures in the frequency domain as a function of the vehicle length.

Table 5.3:  $R^l[\omega_n]$  parameter for vehicles without acceleration and 50 km/h of speed as a function of the vehicle length (in m)

4	6	10	16
0.0190	0.0273	0.0745	0.0946

Table 5.4:  $R^l[\omega_n]$  parameter as a function of the vehicle width (in cm)

50	100	150	180	200
0.0305	0.0287	0.0278	0.0273	0.0271

(which is directly related to the type of vehicle) produces significant changes in  $R^l[\omega_n]$ , the other parameters do not have significant influence on this parameter.

Table 5.5:  $R^l[\omega_n]$  parameter as a function of the distance vehicle-road loop (given by the profile in Fig. 5.12)

Original	$\times 2$	$\times 3$	$\times 4$
0.0273	0.0277	0.0278	0.0278

Table 5.6:  $R^l[\omega_n]$  parameter as a function of the vehicle speed (in km/h)

50	100	150	200
0.0273	0.0280	0.0263	0.0273

Table 5.7:  $R^l[\omega_n]$  parameter as a function of the vehicle acceleration (in  $\text{m/s}^2$ )

0	3	6	9
0.0273	0.0292	0.0304	0.0313

### **Experiment 3: Influence of Vehicle Characteristics on $R^l[\omega_n]$ using Experimental Coil Measurements, and Standard or Multi-Loop Inductive Sensor Models**

In order to test the performance of the DFT descriptor  $R^l[\omega_n]$  of Eq. 5.30, we will compare the values obtained for this descriptor using the inductive signatures captured with our prototype, described in Chapter 3, for the experimental coil shown in Subsection 4.4.1 of Chapter 4, and those obtained by modelling this coil with both standard and proposed models.

Tables 5.8, 5.9, and 5.10 show this spectral descriptor as a function of both length and width of the plate and of the distance between plate and loop, respectively. As it can be seen from the tables, while the plate length causes important changes in  $R^l[\omega_n]$ , the other two parameters do not have significant influence on this descriptor. We can also see from the results shown in these tables that the multi-loop model proposed in Chapter 4 is better fit to the experimental data obtained from the measurements than the standard model for all cases.

From these experiment results, we can say that the proposed descriptor exhibits robustness against variations in most vehicle physical characteristics, as vehicle width,

Table 5.8:  $R^l[\omega_n]$  for a plate width of  $w = 16$  cm and a distance between plate and loop of  $d = 2.5$  cm, as a function of the plate length  $l$ .

<b>Length (cm)</b>	<b>9</b>	<b>16</b>	<b>25</b>
$R^l[\omega_n]$ from measurements	0.1094	0.0327	0.0177
$R^l[\omega_n]$ from multi-loop modelling	0.1139	0.0406	0.0175
$R^l[\omega_n]$ from standard modelling	0.0878	0.0439	0.0106

Table 5.9:  $R^l[\omega_n]$  for a plate length of  $l = 16$  cm and a distance between plate and loop of  $d = 2.5$  cm, as a function of the plate width  $w$ .

<b>Width (cm)</b>	<b>9</b>	<b>16</b>	<b>25</b>
$R^l[\omega_n]$ from measurements	0.0379	0.0327	0.0329
$R^l[\omega_n]$ from multi-loop modelling	0.0413	0.0406	0.0334
$R^l[\omega_n]$ from standard modelling	0.0400	0.0439	0.0446

Table 5.10:  $R^l[\omega_n]$  for a plate length of  $l = 16$  cm and a plate width of  $w = 16$  cm, as a function of the distance  $d$  between plate and loop.

<b>Distance (cm)</b>	<b>2.5</b>	<b>3.5</b>	<b>4.5</b>	<b>5.5</b>
$R^l[\omega_n]$ from measurements	0.0177	0.0047	0.0158	0.0204
$R^l[\omega_n]$ from multi-loop modelling	0.0175	0.0012	0.0090	0.0136
$R^l[\omega_n]$ from standard modelling	0.0106	0.0102	0.0008	0.0013

distance, speed, or acceleration. However, the impact of their length is very important, which could be used in vehicle classification strategies, as we will see in the next section.

### 5.3.3. Vehicle Classification Results

We are interested in assessing the vehicle classification capacity of the descriptor  $R^l[\omega_n]$ . For this purpose, we have developed two experiments using real vehicle inductive signatures captured with our inductive detector prototype: the first one will allow us to validate the proposed DFT descriptor, and the second one, the evaluation of this descriptor for vehicle classification applications [65].

In order to confirm the validity of the proposed classification method we have performed an experiment using a hardware implementation of an ILD [53]. This experiment will allow us to determine whether the actual profile of the car and its mass distribution affect the classification using the DFT descriptor. For the experiment we captured more than one thousand inductive signatures in two real scenarios: In the AC-523 road (Ledoño-Meirama, Spain), and in the AC-415 road (Pastoriza-Arteixo, Spain). A picture of the first location is shown in Fig. 3.7 of Chapter 3. This photo shows the detector equipment located inside the cabinet of Río Anllóns. Both scenarios present the configuration shown in Fig. 3.8 with square loop sensors with a side length of  $w = 2$  m and a distance between their centers of  $d = 5$  m.

At the same place where the inductive signatures were captured, we placed a video camera for the recording of the passing vehicles. Using the signatures and the video, an expert has classified all the signatures into the three different types considered in this work (cars, vans and trucks). Note that although in our work this process is manually performed by the expert, computer vision techniques could be used for the task [66, 67]. In the AC-523 road, we have a total of 909 vehicles: 680 cars, 61 vans and 168 trucks. In AC-415 road, we have registered a total number of 1180 vehicles: 1022 cars, 79 vans and 79 trucks.

Figure 5.14 shows two real signatures as an example, which correspond to a car and a van. The sampling interval is 10 ms. Since two signatures have been acquired for each vehicle, we have estimated speed and length using Eqs. (5.27) and (5.28). The car is 4.7 m in length passing with a speed of 67 km/h. The van is 6.7 m in length passing with a speed of 71 km/h. Similarly to the simulated signatures plotted in Fig. 5.9, the largest signature produces the highest value of our descriptor  $R^l[\omega_n]$ .

Considering the signatures acquired in the loop 1 of the AC-523 road, the descriptor values  $R^1[\omega_k]$  given by the expression of Eq. (5.30) with the vehicle length obtained as detailed in Eq. (5.28) are computed. Figure 5.15 plots the values obtained in this way. The results in Fig. 5.10, obtained using the software simulator, show that the proposed frequency domain descriptor depends on the vehicle length but not on their speed. These

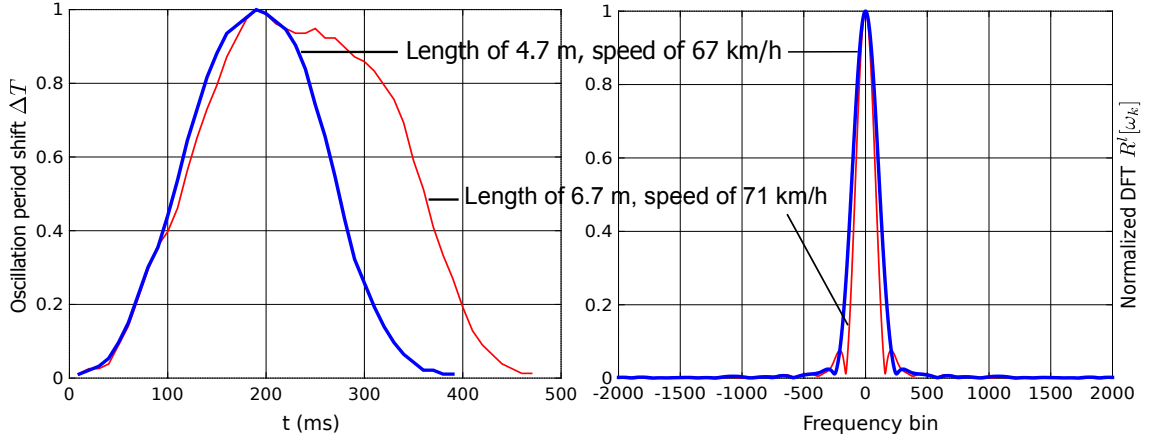


Figure 5.14: Experimental results: Examples of captured signatures.

results have been confirmed with those obtained from real signatures measured with our sensor prototype, as it can be seen in Fig. 5.15. This figure also shows that some van signatures present a frequency domain descriptor similar to those corresponding to car or truck signatures, which makes the task of identification of this type of vehicles quite difficult.

Now, we will obtain some results when the descriptors aforementioned are used for applications of vehicle classification. In the training stage, we have considered the signatures captured in the AC-523 road. All the loops have been employed to compute both length and speed, and only the loops 1 and 3 have been used for calculating the DFT descriptor. The value corresponding to the threshold  $\epsilon_1$  is obtained when only cars and vans are considered, while the threshold value  $\epsilon_2$  is obtained when only vans and trucks are computed. Figure 5.16 shows the success rate in vehicle classification, *i.e.*, the fraction or percentage of success in classifying a real car, van or truck passing on the road as car, van or truck, respectively, obtained for different threshold values. From this figure we conclude that the optimum values for those thresholds are  $\epsilon_1 = 5.6$  and  $\epsilon_2 = 6.5$  if the length-based method is used, and  $\epsilon_1 = 0.06$  and  $\epsilon_2 = 0.11$  if the DFT-based method is applied instead.

For the evaluation of the performance of both classification methods, we have considered the two experimental scenarios, *i.e.*, AC-523 and AC-415 roads. Table 5.11 shows the confusion matrices for each type of vehicle obtained in the AC-523 road, from the training phase (using the loops 1 and 3), and from considering the loops 2 and 4. Table 5.12 shows the results corresponding to the AC-415 road.

The results obtained for vehicle classification are shown in Tables 5.11 (AC-523 road) and 5.12 (AC-415 road) in terms of the confusion matrices. Note that the diagonal entries correspond to correct identifications and that the off-diagonal elements of the confusion

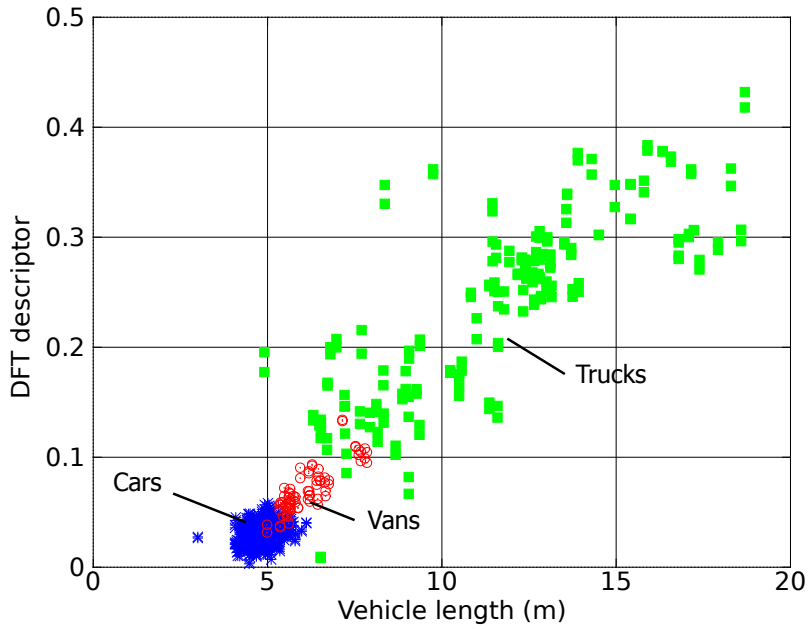


Figure 5.15: Experimental results: DFT descriptor versus vehicle length, computed from acquired signatures.

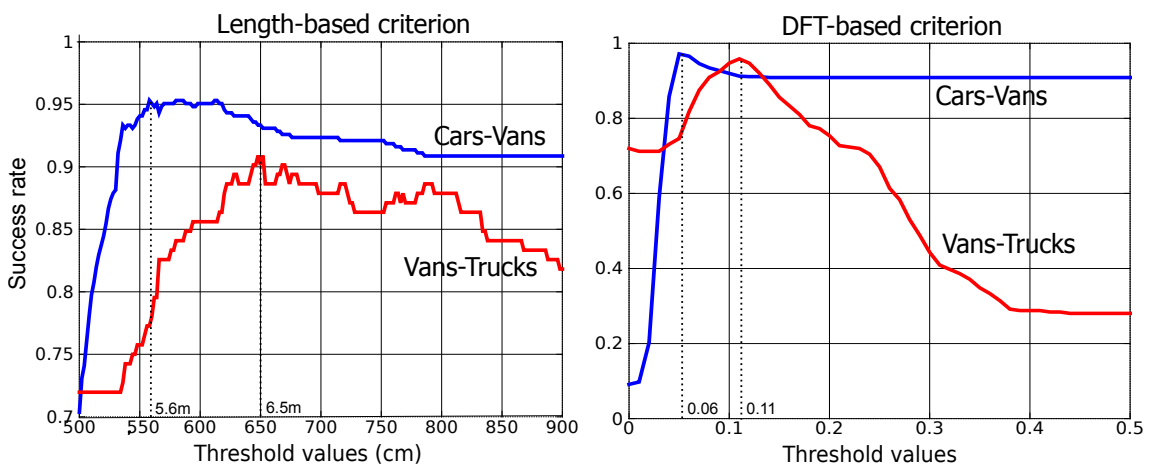


Figure 5.16: Experimental results: Success rates for different threshold values.

Table 5.11: Confusion matrices for AC-523 road.

	Length				Total
	Car	Van	Truck	%	
Car	666	14	0	<b>97.94</b>	680
Van	13	27	21	<b>44.26</b>	61
Truck	2	5	161	<b>95.83</b>	168
Total	681	46	182	<b>93.95</b>	909

	DFT (Loops 1 and 3)				DFT (Loops 2 and 4)				Total
	Car	Van	Truck	%	Car	Van	Truck	%	
Car	669	11	0	<b>98.38</b>	666	14	0	<b>97.94</b>	680
Van	12	42	7	<b>68.85</b>	16	41	4	<b>67.21</b>	61
Truck	1	7	160	<b>95.24</b>	1	13	154	<b>91.67</b>	168
Total	682	60	167	<b>95.82</b>	683	68	158	<b>94.72</b>	909

Table 5.12: Confusion matrices for AC-415 road.

	Length				Total
	Car	Van	Truck	%	
Car	1013	7	2	<b>99.12</b>	1022
Van	30	33	16	<b>41.77</b>	79
Truck	3	14	62	<b>78.48</b>	79
Total	1046	54	80	<b>93.90</b>	1180

	DFT (Loops 1 and 3)				DFT (Loops 2 and 4)				Total
	Car	Van	Truck	%	Car	Van	Truck	%	
Car	998	22	2	<b>97.65</b>	1013	6	3	<b>99.12</b>	1022
Van	11	64	4	<b>81.01</b>	15	61	3	<b>77.22</b>	79
Truck	0	17	62	<b>78.48</b>	0	15	64	<b>81.01</b>	79
Total	1009	103	68	<b>95.25</b>	1028	82	70	<b>96.44</b>	1180

Table 5.13: Comparison with other related literature works in terms of success rates.

Road	Oh <i>et al.</i> [30]	Ki and Bai [35]	Meta and Cinsdikici [36]
AC-523	88.45%	94.17%	95.05%
AC-415	88.98%	95.34%	95.68%

Road	DFT Loops 1 and 3	DFT Loops 2 and 4
AC-523	95.82%	94.72%
AC-415	95.25%	96.44%

matrix correspond to crossed classifications or errors. The smallest number of errors is obtained when the proposed DFT-based criterion is applied, compared to the length-based one. Since car and van signatures are very similar, most classification errors are produced for vans but note that the DFT-based criterion proposed in this work leads to lower error percentages in such case than those corresponding to the length-based criterion.

Finally, we compare the results obtained by our system with previous single-loop methods in the literature. Table 5.13 shows the different success rates extrapolated from the confusion matrices of those works when classifying cars, vans and trucks and applied to our vehicle distributions. Although the real scenarios are not the same and the vehicles are different, if we compare the results obtained from all the tests, the performance of our proposal is similar or better, with the additional advantage of using a very simple method.

Note that although more than three vehicle types have been considered in some of those works, we restrict ourselves to the classification results achieved for cars, vans, and trucks.

## 5.4. Conclusions

In this chapter, we have developed a new algorithm for calculating the vehicle speed using dual loop inductive detectors and using for this purpose the mean in time from the measurements obtained from the two loops instead of the mean in speed, as made in standard algorithms used for speed estimation. All the results shown throughout this chapter allow us to validate the proposed method for speed estimation, with significant performance improvements, especially for high vehicle speeds.

This chapter has also shown that the DFT is an adequate tool to classify vehicles from inductive signatures because of the spectral features extracted from the frequency domain

analysis. This analysis exhibits interesting properties. Firstly, it can be used with only one loop, as it is shown in the results section. Secondly, the DFT has been demonstrated to be independent to variations in the vehicle speed. Moreover, the experimental results performed with real signatures captured with our inductive sensor prototype have shown that the proposed DFT-based criterion obtains a significant reduction of the total error percentage when compared with the standard criterion based on estimating both speed and length of passing vehicles with two loops and with other methods in the literature.



# Chapter 6

## Conclusions and Future Work

To conclude this work, in this chapter we will summarize the main contributions of our work in Section 6.1, and some future work lines are shown in Section 6.2.

### 6.1. Conclusions

*Inductive Loop Detectors* (ILDs) are the sensors most commonly used in traffic management systems. ILDs show an adequate compromise between reliability and cost, which determines that such sensors have been widely used for traffic monitoring in Spain during last years. For that reason, we have focused our work on the improvement of ILDs, taking into account both aspects, i.e. their hardware design and also the development of signal processing methods for traffic monitoring.

Throughout this work, we have presented a simple module for the capture of inductive vehicle signatures based on *Time-Division Multiplexing* (TDM). This system performs a sequential scanning using analogue multiplexing of up to eight oscillators and detects the presence of a vehicle by means of a shift in the period of the signals from the selected oscillator. It subsequently captures the inductive signature of the detected vehicle by measuring the time needed to count a fixed number of pulses. In the experimental results obtained from measurements in a real scenario using dual loops, we observed a good similarity between the pair of signatures obtained from the same vehicle and a significant difference between the signatures corresponding to different vehicles, which validates the good performance of our implementation and enables its use in applications such as vehicle classification, speed and length measurement using only one loop, and re-identification of vehicles for supervision and control tasks in vehicular traffic.

In this work we have also developed a standard model of an inductive loop detector based on standard approaches. The purpose of such modelling is studying the influence of significant vehicle characteristics on the obtained inductive signatures. Since this model

allowed us to obtain the vehicle inductive signatures by means of a simulator without making use of expensive, not only in time but also in resources, tests in real scenarios, we have got a powerful tool to test some features of our inductive sensor prototype in advance. However, we have developed a more accurate model for ILDs that allowed both a much more accuracy in obtaining the inductive signatures compared to real measured ones and a better extraction of features from them than the previous standard approach, as has been shown throughout several simulation results. In addition, the response to changes in length or width of the vehicle, distance between the undercarriage and the inductive road loop, vehicle speed or acceleration, was much more adequate, as expected. The better performance exhibited by the proposed multi-loop method can be explained by taking into account those parts of the vehicle that fall out of the road coil, and also by the longitudinal and lateral displacement of the vehicle with respect to the road coil, which were not included in the standard approach.

In this work we have also developed a new algorithm for calculating the vehicle speed using dual loop inductive detectors and using for this purpose the mean in time from the measurements obtained using two loops instead of the mean in speed, as was used in standard algorithms of speed estimation. All the results included in this work have validated the proposed method with significant performance improvements, especially for high vehicle speeds.

Finally, we have shown that the *Discrete Fourier Transform* (DFT) is an adequate tool to classify vehicles from inductive signatures because of the spectral features extracted from the frequency domain analysis. This analysis exhibits interesting properties: firstly, it can be used with only one loop, and secondly, the DFT has been demonstrated to be independent against variations in vehicle speed. Moreover, the experimental results performed with real signatures and captured with our inductive sensor prototype have shown that the proposed DFT-based criterion obtains a significant reduction of the total error percentage when is compared to the standard criterion based on estimating both speed and length of passing vehicles using two loops and to other methods appeared in the literature.

## 6.2. Future Work

In the ensuing sections we describe some future lines of work to continue the research contained in this dissertation.

### 6.2.1. Multi-loop Model for Non-Flat Profiles

The new multi-loop model here presented has been developed and tested for only flat vehicle profiles, i.e. flat conductive plates. It is clear that the vehicle undercarriages are not generally flat. Thus, we are interested in extending this multi-loop model for not flat profiles so that it could withstand all the types of vehicle profiles. For such purpose, we will have to decompose that profile in horizontal and vertical flat sections. Through this multi-loop extended model we could generate inductive vehicle signatures for any given vehicle profile.

### 6.2.2. Capturing of Vehicle Profiles from Inductive Signatures

Using the multi-loop extended model developed in Subsection 6.2.1, we firstly propose to obtain the simulated vehicle profiles from a single inductive signature given by simulation. Then, our goal would be to get vehicle profiles from single inductive signatures in real scenarios. This would allow us to simultaneously estimate the vehicle speed, since achieving enough accuracy in speed measurement using only one loop is still an open question. The process of capturing the vehicle profile from inductive signatures is computationally complex, which will force that the model for the extended multi-loop approach be as simple as possible.

### 6.2.3. Increasing Classification Categories

Using the obtained vehicle profile, new types of vehicles, such as buses or motorbikes, could be added to the classification algorithm and also improve the success rates for the classification of vans and trucks. Furthermore, the vehicle profile extraction could provide the number of axles of the vehicle, which would serve to incorporate additional types to the classification, such as was made by the American *Federal Highway Administration* (FHWA). FHWA establishes 13 categories, primarily based on the number of axles. The combined use of the vehicle profile and the number of axles would provide a very comprehensive classification method.

### 6.2.4. Re-identification and Travel Time Estimation

Following the future work suggested in Subsection 6.2.2, the availability of real vehicle profiles could significantly improve other important aspects of vehicle traffic monitoring in *Intelligent Transportation Systems* (ITS) as, for example, vehicle re-identification and travel time estimation, as was defined in Chapter 2. The vehicle re-identification would be not only based on matching signatures as usual, but inductive vehicle profiles would also be used to improve the re-identification for anonymous vehicle

tracking. A good re-identification would provide a better estimate of travel times or measurements of the vehicle transit time between two points on the road, thus improving traffic operations, planning, information, and control.

# Appendix A

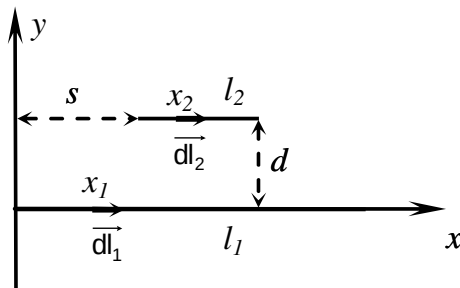
## Calculation of the Mutual Inductance of Two Rectangular Loops

The concept of inductance is defined based on the magnetic fields caused by currents flowing through closed conductor loops. For general three-dimensional interconnects, however, partial inductances are defined to represent the loop interactions among conductors, each forming its own return loop with infinity [68]. In the following discourse, we use mutual inductance to refer strictly to partial mutual inductance and self-inductance to refer strictly to partial self-inductance.

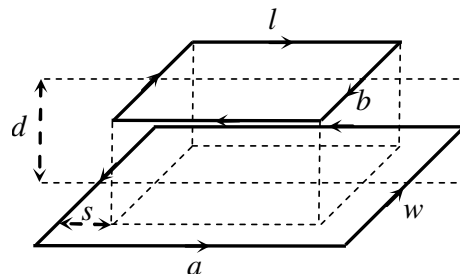
For obtaining the mutual inductance of two rectangular loops, we firstly need to determine the expression of the mutual inductance between two parallel and straight line segments with lengths  $l_1$  and  $l_2$ , with a shift  $s$  and a distance  $d$  between them, as you can see in Fig. A.1(a). This mutual inductance will be denoted as  $M_{\text{seg}}$ .

Applying Neumann's integral, we will have

$$M_{\text{seg}} = \frac{\mu_0}{4\pi} \int_{l_1} \int_{l_2} \frac{d\vec{l}_1 d\vec{l}_2}{r}, \quad (\text{A.1})$$



(a) Picture of two straight line segments.



(b) Picture of two rectangular loops.

Figure A.1: Pictures of the multiloop inductive model.

where  $\mu_0 = 4\pi 10^{-7}$  H/m is the permeability of the material, essentially air, and  $r$  is the distance between two differential elements of  $l_1$  and  $l_2$  with lengths  $dl_1$  and  $dl_2$ , respectively, so that

$$\vec{dl}_1 \vec{dl}_2 = dl_1 dl_2 = dx_1 dx_2. \quad (\text{A.2})$$

Thus, we can obtain the expression of  $M_{\text{seg}}$  as follows

$$\begin{aligned} M_{\text{seg}}(l_1, l_2, s, d) &= \frac{\mu_0}{4\pi} \int_{l_2} dx_2 \int_{l_1} \frac{dx_1}{r} = \frac{\mu_0}{4\pi} \int_s^{l_2+s} dx_2 \int_0^{l_1} \frac{dx_1}{\sqrt{(x_1 - x_2)^2 + d^2}} \\ &= \frac{\mu_0}{4\pi} \int_s^{l_2+s} \left[ \sinh^{-1} \frac{x_1 - x_2}{d} \right]_0^{l_1} dx_2 = \frac{\mu_0}{4\pi} \int_s^{l_2+s} \left( \sinh^{-1} \frac{l_1 - x_2}{d} + \sinh^{-1} \frac{x_2}{d} \right) dx_2 \\ &= \frac{\mu_0}{4\pi} \left[ - (l_1 - x_2) \sinh^{-1} \frac{l_1 - x_2}{d} + d \sqrt{1 + \left( \frac{l_1 - x_2}{d} \right)^2} + x_2 \sinh^{-1} \frac{x_2}{d} - d \sqrt{1 + \left( \frac{x_2}{d} \right)^2} \right]_s^{l_2+s}, \end{aligned} \quad (\text{A.3})$$

where we have used Dwight's integral tables [69] that apply

$$\int \sinh^{-1} \frac{x}{x_0} dx = x \sinh^{-1} \frac{x}{x_0} - x_0 \sqrt{1 + \left( \frac{x}{x_0} \right)^2}. \quad (\text{A.4})$$

Finally, we have

$$\begin{aligned} M_{\text{seg}}(l_1, l_2, s, d) &= \frac{\mu_0}{4\pi} \left( - (l_1 - l_2 - s) \sinh^{-1} \frac{l_1 - l_2 - s}{d} + d \sqrt{1 + \left( \frac{l_1 - l_2 - s}{d} \right)^2} \right. \\ &\quad + (l_2 + s) \sinh^{-1} \frac{l_2 + s}{d} - d \sqrt{1 + \left( \frac{l_2 + s}{d} \right)^2} + (l_1 - s) \sinh^{-1} \frac{l_1 - s}{d} - d \sqrt{1 + \left( \frac{l_1 - s}{d} \right)^2} \\ &\quad \left. - (s) \sinh^{-1} \frac{s}{d} + d \sqrt{1 + \left( \frac{s}{d} \right)^2} \right). \end{aligned} \quad (\text{A.5})$$

Since the induced currents by a rectangular coil on a flat parallel plate are rectangular-shaped [45–47], we will determine the expression of the mutual inductance  $M_{\text{rec}}$  between two rectangular loops of dimensions  $a \times w$  and  $l \times b$ , respectively, which are placed parallel to each other at a distance  $d$ , longitudinally shifted  $s$  and transversely centred (see Fig.

A.1(b)) using the  $M_{\text{seg}}$  expression of Eq. A.5 as follows

$$\begin{aligned}
M_{\text{rec}}(a, w, l, b, s, d) &= 2M_{\text{seg}}\left(a, l, s, \sqrt{d^2 + \left(\frac{w-b}{2}\right)^2}\right) \\
&- 2M_{\text{seg}}\left(a, l, s, \sqrt{d^2 + \left(\frac{w+b}{2}\right)^2}\right) + M_{\text{seg}}\left(w, b, \frac{w-b}{2}, \sqrt{d^2 + s^2}\right) \\
&- M_{\text{seg}}\left(w, b, \frac{w-b}{2}, \sqrt{d^2 + (s+l)^2}\right) - M_{\text{seg}}\left(w, b, \frac{w-b}{2}, \sqrt{d^2 + (a-s)^2}\right) \\
&+ M_{\text{seg}}\left(w, b, \frac{w-b}{2}, \sqrt{d^2 + (a-s-l)^2}\right). \tag{A.6}
\end{aligned}$$



## Appendix B

# Calculation of the Inductance of a Single-layer Rectangular Coil of $N_C$ Turns

Figure B.1 shows a single-layer rectangular coil with length  $a$ , width  $w$ , and axial length  $a_l$ , with  $N_C$  being the number of turns of the inductive loop.

First, we will determine the expression of the mutual inductance  $M_{\text{rec}}$  between a rectangular loop of sides  $a$  and  $w$ , and a confronted and parallel identical loop also rectangular with the same dimensions  $a \times w$ , being  $z$  the distance between both loops (see Fig. B.1). For this purpose, we use the  $M_{\text{seg}}$  expression given as follows

$$M_{\text{rec}}(a, w, a, w, 0, z) = 2M_{\text{seg}}(a, a, 0, z) - 2M_{\text{seg}}\left(a, a, 0, \sqrt{z^2 + w^2}\right) \\ + 2M_{\text{seg}}(w, w, 0, z) - 2M_{\text{seg}}\left(w, w, 0, \sqrt{z^2 + a^2}\right)$$

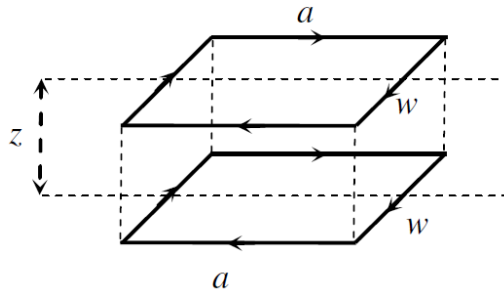


Figure B.1: Picture of two identical rectangular loops.

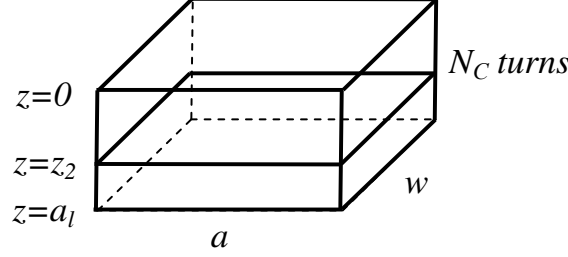


Figure B.2: Rectangular coil and one loop at a  $z$  position.

$$\begin{aligned}
&= \frac{\mu_0}{2\pi} \left( z - \sqrt{z^2 + a^2} + a \sinh^{-1} \frac{a}{z} + \sqrt{z^2 + w^2} - \sqrt{z^2 + w^2 + a^2} \right. \\
&\quad \left. + a \sinh^{-1} \frac{a}{\sqrt{z^2 + w^2}} + z - \sqrt{z^2 + w^2} + w \sinh^{-1} \frac{w}{z} + \sqrt{z^2 + a^2} \right. \\
&\quad \left. - \sqrt{z^2 + w^2 + a^2} + w \sinh^{-1} \frac{w}{\sqrt{z^2 + a^2}} \right) \\
&= \frac{\mu_0}{2\pi} \left( 2z + a \sinh^{-1} \frac{a}{z} + w \sinh^{-1} \frac{w}{z} - 2\sqrt{z^2 + w^2 + a^2} + a \sinh^{-1} \frac{a}{\sqrt{z^2 + w^2}} \right. \\
&\quad \left. + w \sinh^{-1} \frac{w}{\sqrt{z^2 + a^2}} \right). \tag{B.1}
\end{aligned}$$

The self-inductance  $L_C$  is calculated using the Niwa equation for a rectangular loop of single-layer coils. We can think about the self-inductance of a conductor as the mutual inductances between two identical conductors, which are coincident. Then, the Niwa equation is obtained by integrating the expression of Eq. B.1 on the length of the coil, which gives as a result the mutual inductance between one rectangular loop and the rest of the coil, and by a second integration over the length of the coil, which provides the self-inductance of the rectangular coil, i.e.

$$\begin{aligned}
L_C &= L_{\text{coil}}(a, w, a_l, N_C) = N_C^2 \int_0^{a_l} \left( \int_0^{a_l} M_{\text{rec}}(a, w, a, w, 0, |\Delta z|) dz_1 \right) dz_2 \\
&= \frac{\mu_0}{2\pi} N_C^2 \int_0^{a_l} \left( \int_0^{a_l} \left( 2|\Delta z| + a \sinh^{-1} \frac{a}{|\Delta z|} + w \sinh^{-1} \frac{w}{|\Delta z|} - 2\sqrt{(\Delta z)^2 + w^2 + a^2} \right. \right. \\
&\quad \left. \left. + a \sinh^{-1} \frac{a}{\sqrt{(\Delta z)^2 + w^2}} + w \sinh^{-1} \frac{w}{(\Delta z)^2 + a^2} \right) dz_1 \right) dz_2, \tag{B.2}
\end{aligned}$$

where  $\Delta z = z_1 - z_2$ , with  $z_1$  being the  $z$  position of a generic rectangular loop on the coil, and  $z_2$  the  $z$  position of one rectangular loop (see Fig. B.2).

Such an integral calculation can be performed using standard methods, although not

in a simple way. Therefore, here we will indicate only the final result [51, 52]

$$\begin{aligned}
L_{\text{coil}}(a, w, a_l, N_C) = & 2 \frac{\mu_0}{\pi} N_C^2 \frac{aw}{a_l} \times \\
& \left[ \frac{a_l}{2w} \sinh^{-1} \frac{a}{a_l} + \frac{a_l}{2a} \sinh^{-1} \frac{w}{a_l} - \frac{a_l}{2w} \left( 1 - \frac{w^2}{a_l^2} \right) \sinh^{-1} \frac{a}{a_l \sqrt{1 + \frac{w^2}{a_l^2}}} \right. \\
& - \frac{a_l}{2a} \left( 1 - \frac{a^2}{a_l^2} \right) \sinh^{-1} \frac{w}{a_l \sqrt{1 + \frac{a^2}{a_l^2}}} - \frac{w}{2a_l} \sinh^{-1} \frac{a}{w} - \frac{a}{2a_l} \sinh^{-1} \frac{w}{a} \\
& + \left( \frac{\pi}{2} - \tan^{-1} \frac{aw}{a_l^2 \sqrt{1 + \frac{g^2}{a_l^2}}} \right) + \frac{a_l^2}{3aw} \sqrt{1 + \frac{g^2}{a_l^2}} \left( 1 - \frac{g^2}{2a_l^2} \right) + \frac{a_l^2}{3aw} \\
& - \frac{a_l^2}{3aw} \sqrt{1 + \frac{a^2}{a_l^2}} \left( 1 - \frac{a^2}{2a_l^2} \right) - \frac{a_l^2}{3aw} \sqrt{1 + \frac{w^2}{a_l^2}} \left( 1 - \frac{w^2}{2a_l^2} \right) \\
& \left. + \frac{a_l}{6aw} \left( \frac{g^3 - a^3 - w^3}{a_l^2} \right) \right], \tag{B.3}
\end{aligned}$$

where  $g^2 = a^2 + w^2$ .



# Appendix C

## DFT Descriptor Properties

In this appendix, we demonstrate the independence of the proposed descriptor in Chapter 5 on the vehicle speed and on the lateral displacement over the inductive loop.

### C.1. Independence on Speed

Let  $r(t)$  be the inductive signature obtained for a constant vehicle speed  $v$ , which corresponds to a Fourier transform  $r[\omega]$ . Thus, the DFT descriptor proposed in the work is given by

$$R[\omega_n] = \frac{|r[\omega_n]|}{|r[\omega_0]|}. \quad (\text{C.1})$$

Let  $r(t_i)$  the inductive signature in the time instant  $t = t_i$  and  $d = vt_i$  the distance travelled by the vehicle. For a vehicle speed  $v' = av$ , where  $a$  is a positive real value, the distance travelled by the vehicle is  $d' = avt_i$ , which corresponds to a time instant  $t' = d'/v = at_i$ . Thus, we obtain an inductive signature  $r'(t) = r(at)$ , which gives us the Fourier transform  $r'[\omega]$ . Using the scaling property of the Fourier transform,  $r'[\omega]$  is scaled by  $1/a$  in both amplitude and frequency. That means that if a vehicle is travelling with speed  $v$  and the Fourier transform of its inductive signature has a local maximum at the frequency bin  $\omega_n$ , for a vehicle with speed  $v' = av$ , that maximum appears at the frequency bin  $\omega_n/a$  and its amplitude is divided by  $a$ . Thus, we have

$$r' \left[ \frac{\omega_n}{a} \right] = \frac{1}{a} r[\omega_n]. \quad (\text{C.2})$$

Therefore, the DFT descriptor corresponding to a vehicle with speed  $v'$  is expressed as

$$R' \left[ \frac{\omega_n}{a} \right] = \frac{|r'[\frac{\omega_n}{a}]|}{|r'[\frac{\omega_0}{a}]|} = \frac{|ar'[\frac{\omega_n}{a}]|}{|ar'[\frac{\omega_0}{a}]|} = \frac{|r[\omega_n]|}{|r[\omega_0]|} = R[\omega_n]. \quad (\text{C.3})$$

## C.2. Independence on Lateral Displacement

Considering now that a lateral displacement can cause a partial coverage of the vehicle on the coil, we will see how our descriptor responds to variations in lateral displacement using our physical model. Let  $b$  be the vehicle coverage or its effective width on the coil, which is less than or equal to the coil width, denoted by  $a$ . Suppose that the vehicle is completely on the coil and that produces the maximum amplitude of inductive signature  $\Delta T$ . Thus, we have

$$L_1 = \frac{\mu_0 N_1^2 a^2 F_1}{l_1}, \quad (\text{C.4})$$

$$L_2(b) = \frac{\mu_0 ab F_2}{l_2}, \quad (\text{C.5})$$

$$M(b) = \frac{\mu_0 N_1 ab F_1}{d(b)}, \quad (\text{C.6})$$

$$L_{eq}(b) = L_1 - \frac{M^2(b)}{L_2(b)} = L_1 - \frac{\mu_0 N_1^2 a F_1^2 l_2 b}{F_2 d^2}, \quad (\text{C.7})$$

$$\begin{aligned} \Delta T &= 2\pi \left( \sqrt{L_1 C_T} - \sqrt{L_{eq}(b) C_T} \right) = 2\pi \left( \sqrt{L_1 C_T} - \sqrt{\left( L_1 - \frac{\mu_0 N_1^2 a F_1^2 l_2 b}{F_2 d^2} \right) C_T} \right) \\ &= 2\pi \left( \sqrt{L_1 C_T} - \sqrt{L_1 C_T \left( 1 - \frac{l_1 l_2 F_1 b}{a F_2 d^2} \right)} \right) = 2\pi \sqrt{L_1 C_T} \left( 1 - \sqrt{1 - \frac{l_1 l_2 F_1 b}{a F_2 d^2}} \right), \end{aligned} \quad (\text{C.8})$$

where  $\mu_0 = 4\pi \times 10^{-7}$  H/m,  $N_1$  is the number of turns,  $a^2$  is the cross sectional area of the coil,  $l_1$  is the axial length of the coil,  $F_1$  is a factor used to consider the non uniform flux in the roadway inductive loop,  $l_2$  is the axial length of the loop, and  $F_2$  is the same factor as  $F_1$  but referred to the vehicle inductive loop. The average distance from the road loop to the vehicle undercarriage is denoted by  $d$ . Only one turn is considered in our model, *i.e.*,  $N_2 = 1$ .

Since  $l_1 l_2 F_1 / a F_2 d^2 \ll 1$ , we can make an approximation of the square root by the first two terms of the Taylor series as follows

$$\Delta T \cong 2\pi \sqrt{L_1 C_T} \left( 1 - \left( 1 - \frac{l_1 l_2 F_1 b}{2 a F_2 d^2} \right) \right) = \pi \sqrt{L_1 C_T} \frac{l_1 l_2 F_1}{a F_2 d^2} b. \quad (\text{C.9})$$

Let  $r(t)$  be the vehicle inductive signature of a vehicle with effective width  $b$ . For an effective width  $b' = cb$ , where  $c$  is a positive real value, we obtain an inductive signature  $r'(t) = cr(t)$ , since each point  $\Delta T$  conforming the signature is linearly dependent on  $b$  as shown in Eq. (C.9). The Fourier transform of this inductive signature, denoted as  $r'[\omega]$ , is

thus given by

$$r'[\omega] = cr[\omega], \quad (\text{C.10})$$

due to the linearity of the DFT. The corresponding descriptor is then given by

$$R'[\omega_n] = \frac{|r'[\omega_n]|}{|r'[\omega_0]|} = \frac{|cr[\omega_n]|}{|cr[\omega_0]|} = \frac{|r[\omega_n]|}{|r[\omega_0]|} = R[\omega_n]. \quad (\text{C.11})$$



# Appendix D

## Resumen extendido

Uno de los aspectos más importantes de los sistemas de transporte inteligente, en inglés *Intelligent Transportation Systems* (ITS), es la monitorización del tráfico de vehículos, fundamentalmente aquellas aplicaciones cuyo objetivo es contar el número de vehículos en una carretera o conocer su velocidad, ocupación, o características estructurales como densidad y tipo. Los sensores son elementos imprescindibles en los sistemas modernos de monitorización de tráfico, puesto que maximizar la eficiencia y capacidad de las redes de transporte existentes es crucial debido al incremento exponencial del volumen de tráfico de vehículos en los últimos años, y a la limitación en la construcción de nuevas carreteras. Aunque se han utilizado diferentes tipos de sensores para la detección de vehículos, como detectores de bucles inductivos, en inglés *Inductive Loop Detectors* (ILDs), magnetómetros, sensores térmicos de imagen en infrarrojos, etc., desde su presentación en los años 60, los ILDs son los sensores más usados habitualmente en los sistemas de gestión de tráfico para tareas tales como clasificación de vehículos, reconocimiento de vehículos, y estimación de velocidad con un solo bucle. Los ILDs han de proporcionar precisión y fiabilidad con mínimo retardo cuando estiman velocidades en estrategias de control. Las estimaciones obtenidas en dobles bucles son usualmente precisas, pero requieren instalaciones con dos bucles por carril y un mantenimiento adecuado, lo que implica que no es la solución óptima en términos de coste. Además, hay instalaciones donde sólo hay un bucle por carril. Aunque ya han sido desarrollados algoritmos para clasificación y estimación de velocidad con un único bucle, cómo conseguir suficiente precisión es todavía un tema sin resolver.

Los sensores inductivos están basados en el principio de la inducción electromagnética. Se realizan mediante ranuras en el pavimento, por ejemplo, cuadradas de 2 m de lado, donde a continuación se inserta un cable creando una bobina de 3 a 5 vueltas que se conecta al detector, y después se rellenan con resina epoxi. Cuando un vehículo pasa sobre la bobina, sobre su masa metálica se inducen corrientes de Foucault que son interpretadas por el detector como el paso del mismo. La duración

de estas corrientes puede ser usada para medida de la ocupación del carril. También pueden ser fácilmente calculadas la velocidad y la longitud mediante detectores de doble bucle por carril permitiendo realizar una clasificación según la longitud del vehículo. Este tipo de detectores son los más habituales en las carreteras de España, por ser una tecnología altamente desarrollada, de operación sencilla, y costes bajos de instalación. Aunque estos sensores inductivos presentan un reemplazamiento difícil en caso de rotura, necesitan calibración regular, y la inevitable interrupción del tráfico en caso de labores de mantenimiento, su diseño flexible se puede adaptar a una gran variedad de aplicaciones, incluso haciendo uso del bucle simple, proporcionando mejor precisión en clasificación de tráfico que otras técnicas.

Los detectores de bucles inductivos modernos son digitales porque proporcionan más fiabilidad y precisión en la medida que los antiguos detectores analógicos. La mayoría de los detectores miden indirectamente las variaciones de inductancia de la bobina causadas por la presencia del vehículo en el área de detección del bucle inductivo, que produce una disminución de inductancia. Se usan dos métodos para medir tales variaciones: el primero, se basa en la medida de los cambios de la frecuencia o del período de un circuito oscilador resonante, y el segundo, en la medida de los cambios de la amplitud de la tensión en un circuito RLC excitado a una frecuencia fija de operación. La mayoría de los detectores inductivos pueden operar sobre cuatro o más bobinas. En los detectores resonantes el problema de la interferencia entre bucles, en inglés *crosstalk*, se soluciona separando dichos bucles mediante multiplexado por división en el tiempo, en inglés *Time-Division Multiplexing* (TDM). Los detectores multiplexados alimentan y analizan secuencialmente los canales más de cien veces por segundo y miden el desplazamiento del período de oscilación del oscilador resonante. En los detectores inductivos de amplitud los cambios de inductancia del bucle debido a la presencia del vehículo modulan la amplitud de la señal obtenida a una frecuencia fija. En otras palabras, el voltaje de la señal de salida está modulado en amplitud, en inglés *Amplitude Modulation* (AM), por la huella del vehículo. Entonces, la demodulación de la forma de onda AM proporciona la huella inductiva del vehículo y mediante su conversión a digital, los valores de la misma. El ancho de banda de la huella inductiva del vehículo es principalmente función de su velocidad, de la geometría del bucle y de las características del fondo del vehículo. El problema de la interferencia entre bucles en los ILDs de amplitud que trabajan con cuatro o más bobinas se resuelve introduciendo un circuito RLC por cada bucle, con frecuencias portadoras diferentes para cada uno, separadas lo suficiente para incluir el ancho de banda de cada huella, y usando un demodulador síncrono sintonizado a cada frecuencia portadora.

El objetivo principal de este proyecto es el desarrollo de técnicas avanzadas para gestión del tráfico de vehículos usando un ILD. Vamos a tener en cuenta dos aspectos: en primer lugar, el desarrollo del hardware del ILD, y en segundo lugar, el desarrollo

de métodos de procesamiento de señal para monitorización del tráfico. Para ello, en primer lugar se desarrolla e implementa un ILD que va a proporcionar huellas inductivas de los vehículos que transitan por una vía. Además de las funciones tradicionales de medida de aforamientos de tráfico, tales como densidad, ocupación y clasificación de vehículos, se pretende conseguir el reconocimiento de los mismos mediante el análisis de la señal de su huella. Basándose en la infraestructura existente en las carreteras para realizar los aforamientos de tráfico que usa fundamentalmente bucles inductivos, modificaciones de los equipos detectores van a permitir incluir además la función de re-identificación, para su uso en aplicaciones de control y supervisión de tráfico de vehículos. Por lo tanto, y aunque la tecnología de los detectores de bucles inductivos está totalmente extendida y en uso en este momento, se le añade una función de captura de las huellas inductivas del vehículo que permite aplicaciones adicionales de reconocimiento de los mismos para mejorar la clasificación, detección de velocidad con una sola espira, y re-identificación para aplicaciones de control y supervisión del tráfico rodado. Nuestra implementación práctica de un ILD está basada en un detector resonante que mide la huella inductiva mediante desplazamiento del período de oscilación y multiplexa hasta ocho canales usando TDM, permitiendo el registro de huellas inductivas de hasta cuatro carriles con doble bucle, o hasta ocho carriles con un solo bucle en cada carril. Esto cubre muchos de los tipos existentes de carreteras y hace el sistema fácil de construir gracias a la disponibilidad de gran número de circuitos estándar con ocho canales, como multiplexores, decodificadores, buffers, etc. Los ILDs resonantes que miden desplazamiento de período usan una señal de reloj de referencia cuya frecuencia es de varios MHz, típicamente entre 20 y 1000 veces mayor que la frecuencia de oscilación del bucle inductivo usado para medir. El período de la señal de oscilación del bucle inductivo se calcula como el número de ciclos  $N$  de la señal de referencia en  $m$  ciclos de la señal de oscilación. Cuando un vehículo se detiene o pasa sobre el bucle, la frecuencia de oscilación se incrementa, y el período disminuye (y también disminuye el número  $N$  de ciclos). Los pulsos del circuito de oscilación se llevan a la entrada de un contador, así que cuando éste alcanza un número de pulsos  $m$ , el valor  $N$  se captura de un temporizador que trabaja a la frecuencia de la señal de referencia. La amplitud de las huellas inductivas se determina por la diferencia entre el valor medido  $N$ , obtenido cada  $t$  milisegundos, típicamente entre 1 y 10, y el valor de  $N$  obtenido en reposo, que es calculado y registrado por el equipo detector. Este valor es referido por  $\Delta N$ , así que el desplazamiento del período de oscilación viene dado por  $\Delta T = \Delta N/m$ . Este parámetro  $\Delta T$  nos da la amplitud de la huella inductiva en cada instante de muestreo. En los resultados experimentales obtenidos con nuestro prototipo de ILD a partir de medidas realizadas en escenarios reales usando doble bucle, hemos observado una gran coincidencia entre el par de huellas obtenidas de un mismo vehículo y una diferencia significativa entre huellas correspondientes a vehículos diferentes, que valida las buenas prestaciones de

nuestra implementación y habilita su uso para aplicaciones de clasificación de vehículos, medidas de velocidad y longitud usando un único bucle, y reconocimiento de vehículos en labores de supervisión y control de tráfico de vehículos. Además hemos realizado una comparativa de prestaciones de los dos tipos de detectores estudiados, resonante y de amplitud, con respecto a su comportamiento al aplicar una perturbación de ruido blanco gaussiano, en inglés *Additive White Gaussian Noise* (AWGN), superpuesta a la señal de entrada de los sensores inductivos, observando la relación SNR obtenida a la salida en la huella inductiva del detector. Se ha constatado un buen comportamiento del detector resonante para entradas con SNR mayor que 15 dB, incluso mejor que el de los detectores de amplitud. Sin embargo, para entradas con una SNR por debajo de 15 dB el detector resonante es muy sensible al ruido y no es útil para los propósitos descritos en este trabajo.

Por otro lado, dado el elevado coste de las pruebas en escenarios reales cada vez que una nueva técnica está siendo estudiada, hemos desarrollado un modelo avanzado del detector de bucles inductivos que claramente supera los modelos que se han usado tradicionalmente con unos resultados muy similares a los obtenidos directamente usando el prototipo de ILD que hemos desarrollado. En primer lugar presentamos un modelo de sensor de bucles inductivos estándar, propuesto en la literatura, que será empleado para estudiar la influencia de distintos parámetros, tales como velocidad, aceleración, anchura y longitud del vehículo, en las estrategias de clasificación de los vehículos. Mediante este modelo podemos obtener huellas inductivas de vehículos de cualquier perfil por medio de un simulador, y estudiar la influencia de las características significativas del vehículo sobre las huellas inductivas obtenidas. Se demuestra, mediante una comparación de los resultados obtenidos con el simulador y con el detector prototipo desarrollado, que las huellas inductivas de vehículos obtenidas presentan características similares en el dominio del tiempo, lo que valida el modelo presentado en este trabajo. Además, los resultados de varias simulaciones han mostrado el impacto de algunos parámetros físicos, tales como la separación entre el fondo del vehículo y la bobina bajo el pavimento de la carretera, la longitud o la anchura del vehículo, y su velocidad o aceleración, en sus correspondientes huellas inductivas. El modelo estándar de sensor presentado no tiene en cuenta la distribución de las corrientes inducidas en el fondo del vehículo, que para bobinas rectangulares son también rectangulares y concéntricas, ni el desplazamiento longitudinal o transversal del vehículo sobre la bobina, ni tampoco la influencia de las partes del fondo del vehículo que caen fuera de la bobina. Es por ello que hemos desarrollado un nuevo modelo de sensor más sofisticado que el estándar y que se adapta mejor a todos los posibles casos. Este modelo para sensores de bucles inductivos está basado en multiespiras rectangulares y puede ser empleado en la adquisición de huellas inductivas por los sistemas de gestión de tráfico de vehículos. Además, hemos verificado experimentalmente que nuestro nuevo modelo propuesto proporciona mejores características que el modelo estándar. Podemos asegurar entonces que el nuevo modelo

multiespira desarrollado para ILDs permite obtener huellas inductivas más precisas si las comparamos con medidas de huellas reales, y una mejor extracción de parámetros característicos a partir de las mismas que el modelo estándar, que ha sido mostrado en varios resultados. Adicionalmente se ha comprobado que la respuesta a variaciones de longitud o de anchura del vehículo, distancia entre fondo de vehículo y bucle inductivo, y velocidad y aceleración, es adecuada, como se esperaba. Las mejores prestaciones observadas con el modelo propuesto basado en multiespiras pueden ser explicadas porque en este modelo se tienen en cuenta aquellas partes del fondo del vehículo que caen fuera de la bobina, y también el desplazamiento longitudinal o transversal del fondo del vehículo con respecto a la bobina, que no están incluidas en la aproximación estándar. No obstante, este nuevo modelo multiespira ha sido desarrollado y probado considerando únicamente perfiles planos de vehículos, aunque podría ser extendido para soportar otros tipos de perfiles.

La medida de velocidad es una tarea fundamental en los sistemas de gestión de tráfico. En este trabajo hemos desarrollado un nuevo algoritmo para calcular el valor de la velocidad con detectores de doble bucle inductivo. Esta técnica usa la media temporal de las medidas obtenidas usando los dos bucles en lugar de la media de velocidades usada tradicionalmente en el método estándar. Los resultados experimentales obtenidos muestran una clara mejora en la determinación de las velocidades estimadas con este nuevo método. Para probar el nuevo algoritmo, hemos realizado una estimación de las velocidades a partir de las huellas reales obtenidas, y se ha comparado la distribución de velocidades obtenida con la del método estándar. Hemos comprobado que parámetros estadísticos tales como la media, la mediana, la varianza y la kurtosis de ambas distribuciones son muy similares. Además, se han realizado dos test basados en hipótesis estadísticas para determinar si ambas distribuciones de datos son o no diferentes: el t-test, que comprueba si dos distribuciones normales tienen la misma media, y el test-F, que comprueba si tienen la misma varianza. Por otra lado, hemos realizado una estimación del error medio obtenido para velocidades comprendidas entre 20 km/h y 200 km/h usando como referencia la distribución de velocidades obtenida en un escenario real, y hemos visto que la estimación de error usando el método estándar es mayor que la obtenida usando el método propuesto para la mayor parte de las velocidades, mientras que el error medio de la estimación estándar es siempre mayor. Asimismo también hemos verificado que la influencia de la aceleración sobre el error en las velocidades estimadas mediante ambos algoritmos es prácticamente despreciable, pero el error es un poco mayor en el método estándar que en el método propuesto en este trabajo.

Este trabajo presenta un sistema completo para clasificación de vehículos compuesto de un detector de bucles inductivos y los correspondientes algoritmos off-line. El sistema detecta la presencia de vehículos mediante un desplazamiento en el período de oscilación del bucle seleccionado de forma que las huellas de los vehículos detectados se registran

mediante la duración de un número prefijado de pulsos de oscilación. En este trabajo nos centraremos en la cuestión, todavía no resuelta a día de hoy, de contar el número de vehículos (clasificándolos en tres tipos, coches, furgonetas y camiones) que circulan por una carretera. El método clásico para tal propósito consiste en la estimación de la longitud del vehículo usando las huellas inductivas obtenidas en dos bucles y, a continuación, las clasifica de acuerdo con un umbral preestablecido. Para la clasificación de los vehículos que circulan por una vía, presentamos un sistema bastante simple que usa esas huellas inductivas y la transformada discreta de Fourier (DFT, del inglés *Discrete Fourier Transform*). Para abordar el problema de clasificación en tres tipos de vehículos (como mencionábamos antes, coches, furgonetas y camiones) se propone un algoritmo heurístico basado en decisión por umbrales y en la magnitud del primer máximo espectral obtenido aplicando el análisis DFT a la huella inductiva del vehículo obtenida a partir de un único bucle. Además, el método aquí desarrollado puede aplicarse a huellas de vehículos capturadas con otros tipos de sensores. En este trabajo hemos comparado nuestro sistema con métodos de clasificación clásicos basados en la estimación de la longitud del vehículo obtenida a partir de dos bucles. Los resultados experimentales muestran que el criterio basado en la magnitud de la DFT exhibe un error de clasificación más bajo que el alcanzado con dichos métodos, con la enorme ventaja de la utilización de un único bucle. Finalmente hemos hecho una comparativa entre los resultados obtenidos con nuestro sistema de clasificación con otros métodos de clasificación publicados previamente, para lo cual hemos extrapolado las matrices de confusión de aciertos obtenidos por esos trabajos en la clasificación de coches, furgonetas y camiones, aplicándolos a nuestra distribución de vehículos. Aunque los escenarios reales y los vehículos son diferentes, de la comparación de resultados obtenidos a partir de estas pruebas, podemos deducir que las prestaciones de nuestro sistema de clasificación son similares o mejores, con la ventaja adicional de ser un método más simple.

Hemos visto que el nuevo modelo multiespira presentado aquí ha sido desarrollado y probado para perfiles de vehículos planos, es decir, placas conductoras planas. Está claro que el fondo de los vehículos no es generalmente plano. Así es que estamos interesados en extender este modelo multiespira para perfiles no planos soportando cualquier tipo de perfil de vehículo. Para tal propósito será necesario descomponer ese perfil en secciones planas horizontales y verticales. Mediante este modelo multiespira extendido podremos generar huellas inductivas de vehículos para cualquier perfil de vehículo. Usando el modelo multiespira extendido presentado anteriormente, nuestro objetivo será obtener perfiles de vehículos a partir de las huellas inductivas generadas por simulación, y a continuación se pretende obtener perfiles reales de vehículos a partir de sus huellas reales. Esto además permitiría simultáneamente estimar con precisión la velocidad del vehículo a partir de una sola huella, un tema todavía no resuelto. El proceso de capturar el perfil del vehículo a partir de la huella inductiva es complejo computacionalmente, y llevará consigo

la simplificación al máximo del modelo multiespira extendido. El uso del perfil del vehículo obtenido proporcionará la posibilidad de mejorar el algoritmo de clasificación para nuevos tipos de vehículos como motocicletas y autobuses, y además mejorar el acierto en la clasificación de furgonetas y camiones. Adicionalment, el perfil podría proporcionar el número de ejes del vehículo, que serviría para incorporar tipos adicionales a la clasificación de vehículos. La combinación del perfil del vehículo y el número de ejes proporcionaría un método de clasificación muy eficiente. Y por último, la disponibilidad de perfiles reales de vehículos podría mejorar significativamente otros aspectos de la monitorización del tráfico de vehículos en los ITS como, por ejemplo, el reconocimiento de vehículos y la estimación del tiempo de recorrido. El reconocimiento de vehículos no estaría basado únicamente en el análisis comparativo de huellas inductivas, sino que mediante los perfiles obtenidos se podría mejorar el seguimiento anónimo de los mismos. Un buen reconocimiento de vehículos proporcionaría además una mejor estimación de los tiempos de recorrido o de tránsito de vehículos entre dos puntos de una carretera, y se verían mejoradas las operaciones de tráfico, planificación, información y control.



# Appendix E

## List of Acronyms

**AC** A Coruña

**FHWA** Federal Highway Administration

**AM** Amplitude Modulated

**ADC** Analogue-to-Digital Conversion

**AWGN** Additive White Gaussian Noise

**ANN** Artificial Neural Network

**BEM** Boundary Element Method

**DC** Direct Current

**DFT** Discrete Fourier Transform

**EM** ElectroMagnetic

**FDD** Frequenz-Division Duplex

**FDM** Finite Difference Method

**FEM** Finite Element Method

**FFT** Fast Fourier Transform

**FT** Fourier Transform

**GPS** Global Positioning System

**ILD** Inductive Loop Detector

**IR** InfraRed

**ITS** Intelligent Transportation Systems

**IDVs** Irregular Driving Vehicles

**Hz** Hertz

**LIDAR** LIght Detection And Ranging or Laser Imaging Detection And Ranging

**LOS** Line-Of-Sight

**MAC** Media Access Control

**ML** Maximum-Likelihood

**MVDZs** Multiple Vehicles in the Detection Zones

**NEMA** National Electrical Manufacturers Association

**QS** Quasi-Static

**P-EM-QS** Quasi-Static ElectroMagnetic Solvers

**RADAR** RAdio Detection And Ranging

**RF** Radio Frequency

**rms** root mean square

**sps** samples per second

**SNR** Signal-to-Noise Ratio

**SiDIVS** Simple Detection of Inductive Vehicle Signatures

**TDD** Time-Division Duplex

**TV** TeleVision

**WRMSE** Weighted Root Mean Square Error

## References

- [1] L. Klein, D. Gibson, and M. Mills, *Traffic Detector Handbook: Third Edition*. Federal Highway Administration, Turner-Fairbank Highway Research Center, 2006, vol. 1, FHWA-HRT-06-108.
- [2] T. Agarwal, “Best Technical Way to Prevent Accidents Using Speed Checker System.” [Online]. Available: URL{<https://www.elprocus.com/a-technical-way-to-prevent-accidents/>}
- [3] FHWA, “Measurement of Highway-Related Noise.” [Online]. Available: URL{<http://www.fhwa.dot.gov/environment/noise/measurement/mhrn03.cfm>}
- [4] SYSCOM, “MR3000TR. Traffic and Railways.” [Online]. Available: URL{<http://www.syscom.ch/products/mr3000tr/>}
- [5] FHWA, “A Summary of Vehicle Detection and Surveillance Technologies use in Intelligent Transportation Systems.” [Online]. Available: URL{<https://www.fhwa.dot.gov/policyinformation/pubs/vdstits2007/05.cfm>}
- [6] M. D. of Public Safety, “Understanding Traffic Radar.” [Online]. Available: URL{<http://www.mendonpublicsafety.com/ondutyradar.htm>}
- [7] T. Harris, “How Red-light Cameras Work.” [Online]. Available: URL{<http://auto.howstuffworks.com/car-driving-safety/safety-regulatory-devices/red-light-camera1.htm>}
- [8] Plan-Bravo, “Traffic Loop Sensor Activator.” [Online]. Available: URL{<http://www.plan-bravo.com/lefty.html>}
- [9] C. Sun and S. Ritchie, “Individual vehicle speed estimation using single loop inductive waveforms,” *Journal of Transportation Engineering*, vol. 125, no. 6, pp. 531–538, November 1999.
- [10] Z. W. et al., “Constrained total least-squares calibration of three-axis magnetometer for vehicular applications,” *Measurement Science and Technology*, vol. 24, no. 9, September 2013.
- [11] Y. I. et al., “Robust vehicle detection even in poor visibility conditions using infrared thermal images and its application to road traffic flow monitoring,” *Measurement Science and Technology*, vol. 22, no. 8, August 2011.

- [12] J. Gajda, R. Sroka, M. Stencel, A. Wajda, and T. Zeglen, "A vehicle classification based on inductive loop detectors," in *Instrumentation and Measurement Technology Conference, 2001. IMTC 2001. Proceedings of the 18th IEEE*, vol. 1, May 2001, pp. 460–464.
- [13] S.-T. Jeng, L. Chu, and S. Hernandez, "Wavelet-k nearest neighbor vehicle classification approach with inductive loop signatures," *Transportation Research Record: Journal of the Transportation Research Board*, vol. 2380, pp. 72–80, 2013.
- [14] S.-T. Jeng and S. Ritchie, "Real-time vehicle classification using inductive loop signature data," *Transportation Research Record: Journal of the Transportation Research Board*, vol. 2086, pp. 8–22, 2008.
- [15] Y. Ki and D. Bai, "Vehicle classification model for loop detectors using neural networks," *Transportation Research Record: Journal of the Transportation Research Board*, vol. 1917, pp. 164–172, 2005.
- [16] G. Zhang, Y. Wang, and H. Wei, "Artificial neural network method for length-based vehicle classification using single-loop outputs," *Transportation Research Record: Journal of the Transportation Research Board*, vol. 1945, pp. 100–108, 2006.
- [17] M. Ndoye, V. Totten, B. Carter, D. Bullock, and J. Krogmeier, "Vehicle detector signature processing and vehicle reidentification for travel time estimation," in *Transportation Research Board 87th Annual Meeting*, no. 08-0497, May 2008.
- [18] C. Oh, A. Tok, and S. Ritchie, "Real-time freeway level of service using inductive-signature-based vehicle reidentification system," *Intelligent Transportation Systems, IEEE Transactions on*, vol. 6, no. 2, pp. 138–146, June 2005.
- [19] C. Sun, S. G. Ritchie, K. Tsai, and R. Jayakrishnan, "Use of vehicle signature analysis and lexicographic optimization for vehicle re-identification on freeways," *Transportation Research*, vol. 7C, pp. 167–185, 1999.
- [20] A. Y. Tawfik, B. Abdulhai, A. Peng, and S. M. Tabib, "Using decision trees to improve the accuracy of vehicle signature reidentification," *Transportation Research Record: Journal of the Transportation Research Board*, vol. 1886, pp. 24–33, 2004.
- [21] Y. Wang and N. L. Nihan, "Freeway traffic speed estimation with single-loop outputs," *Transportation Research Record: Journal of the Transportation Research Board*, vol. 1727, pp. 120–126, 2000.
- [22] M. Mills, "Inductive loop detector analysis," in *Vehicular Technology Conference, 1981. 31st IEEE*, vol. 31, April 1981, pp. 401–411.
- [23] —, "Inductive loop system equivalent circuit model," in *Vehicular Technology Conference, 1989, IEEE 39th*, May 1989, pp. 689–700 vol.2.
- [24] P. Cheevarunothai, Y. Wang, and N. Nihan, "Identification and correction of dual-loop sensitivity problems," *Transportation Research Record: Journal of the Transportation Research Board*, vol. 1945, pp. 73–81, January 2006.

- [25] C. Day, T. Brennan, M. Harding, H. Premachandra, A. Jacobs, D. Bullock, J. Krogmeier, and J. Sturdevant, "Three-dimensional mapping of inductive loop detector sensitivity with field measurement," *Transportation Research Record: Journal of the Transportation Research Board*, vol. 2128, pp. 35–47, December 2009.
- [26] M. Martin, "Microprocessor controlled loop detector system," July 14 1987, uS Patent 4,680,717. [Online]. Available: <http://www.google.co.in/patents/US4680717>
- [27] C. Minsen, J. Ngarmnil, and T. Rongviriyapanich, "Embedded adaptive algorithm for multi-lanes-traffic inductive loop detecting system," in *International Conference on Electrical Engineering/Electronics, Computer, Telecommunications and Information Technology*, 2th, May 2005, pp. 359–362 vol.1.
- [28] S. Ali, B. George, L. Vanajakshi, and J. Venkatraman, "A multiple inductive loop vehicle detection system for heterogeneous and lane-less traffic," *Instrumentation and Measurement, IEEE Transactions on*, vol. 61, no. 5, pp. 1353–1360, May 2012.
- [29] B. Coifmanab and S. Neelisettyc, "Improved speed estimation from single-loop detectors with high truck flow," *Intelligent Transportation Systems, IEEE Transactions on*, vol. 18, no. 2, pp. 138–148, May 2014.
- [30] S. Oh, S. Ritchie, and C. Oh, "Real-time traffic measurement from single loop inductive signatures," *Transportation Research Record: Journal of the Transportation Research Board*, vol. 1804, pp. 98–106, 2002.
- [31] S. Sheik Mohammed Ali, B. George, and L. Vanajakshi, "An efficient multiple-loop sensor configuration applicable for undisciplined traffic," *Intelligent Transportation Systems, IEEE Transactions on*, vol. 14, no. 3, pp. 1151–1161, Sept 2013.
- [32] B. Coifman, "Using dual loop speed traps to identify detector errors," *Transportation Research Record: Journal of the Transportation Research Board*, vol. 1683, pp. 47–58, 1999.
- [33] G. Geetharamant, C. Sharmila Devi, and J. Arun Pandian, "Vehicle classification algorithm using fuzzy expert decision set," in *International Journal of Application or Innovation in Engineering and Management (IJAIEM)*, vol. 4, April 2015, pp. 26–32.
- [34] S.-T. Jeng and L. Chu, "Vehicle reidentification with the inductive loop signature technology," *Journal of the Eastern Asia Society for Transportation Studies*, vol. 10, pp. 1896–1915, May 2013.
- [35] Y.-K. Ki and D.-K. Baik, "Vehicle-classification algorithm for single-loop detectors using neural networks," *Vehicular Technology, IEEE Transactions on*, vol. 55, no. 6, pp. 1704–1711, Nov 2006.
- [36] S. Meta and M. Cinsdikici, "Vehicle-classification algorithm based on component analysis for single-loop inductive detector," *Vehicular Technology, IEEE Transactions on*, vol. 59, no. 6, pp. 2795–2805, July 2010.

- [37] G. de Lima, J. Silva, and O. Saotome, "Vehicle inductive signatures recognition using a madaline neural network," *Neural Computing and Applications*, vol. 19, no. 3, pp. 421–436, 2010. [Online]. Available: <http://dx.doi.org/10.1007/s00521-009-0298-3>
- [38] Z. Jia, C. Chen, B. Coifman, and P. Varaiya, "The pems algorithms for accurate, real-time estimates of g-factors and speeds from single-loop detectors," in *ITSC 2001. 2001 IEEE Intelligent Transportation Systems*, vol. 1, August 2001, p. 536541.
- [39] X.-Y. Lu, P. Varaiya, R. Horowitz, Z. Guo, and J. Palen, "Estimating traffic speed with single inductive loop event data," *Transportation Research Record: Journal of the Transportation Research Board*, vol. 2308, pp. 157–166, 2012.
- [40] S. Ali, B. George, L. Vanajakshi, and J. Venkatraman, "A multiple inductive loop vehicle detection system for heterogeneous and lane-less traffic," *Instrumentation and Measurement, IEEE Transactions on*, vol. 61, no. 5, pp. 1353–1360, May 2012.
- [41] S. Hilliard, M. Roberts, and G. Yerem, "Inductive signature measurement system," 2006, US6911829B2 Patent.
- [42] N. Malik, M. García, M. Ordas, and C. Viejo, *Circuitos Electrónicos: Análisis, Diseño y Simulación*, ser. Fuera de colección Out of series. Pearson Educación, 1996. [Online]. Available: <http://books.google.es/books?id=1plpPAAACAAJ>
- [43] R. Blake, *Sistemas electrónicos de comunicaciones*. International Thomson, 2004. [Online]. Available: <http://books.google.es/books?id=53i69LV2ETsC>
- [44] C. Day, T. Brennan, M. Harding, H. Premachandra, A. Jacobs, D. Bullock, J. Krogmeier, and J. Sturdevant, "Three-dimensional mapping of inductive loop detector sensitivity with field measurement," *Transportation Research Record: Journal of the Transportation Research Board*, vol. 2128, pp. 35–47, 2009.
- [45] R. E. Beissner and J. A. G. Temple, *Review of Progress in Quantitative Nondestructive Evaluation*. Boston, MA: Springer US, 1990, ch. Calculation of Eddy Current Fields for Coils of Arbitrary Shape, pp. 257–264. [Online]. Available: [http://dx.doi.org/10.1007/978-1-4684-5772-8\\_31](http://dx.doi.org/10.1007/978-1-4684-5772-8_31)
- [46] T. P. Theodoulidis and E. E. Kriezis, "Impedance evaluation of rectangular coils for eddy current testing of planar media," *NDT & E International*, vol. 35, no. 6, pp. 407 – 414, 2002. [Online]. Available: <http://www.sciencedirect.com/science/article/pii/S0963869502000087>
- [47] J. O. Fava and M. C. Ruch, "Análisis de las corrientes inducidas producidas por bobinas rectangulares planas," in *Conferencia Panamericana de END*, Oct 2007, pp. 1–13.
- [48] T. Itaya, K. Ishida, A. Tanaka, N. Takehira, and T. Miki, "Eddy current distribution for a rectangular coil arranged parallel to a moving conductor slab," *Science, Measurement Technology, IET*, vol. 6, no. 2, pp. 43–51, March 2012.
- [49] G. Pelosi, "The finite-element method, part i: R. l. courant [historical corner]," *Antennas and Propagation Magazine, IEEE*, vol. 49, no. 2, pp. 180–182, April 2007.

- [50] C. R. Paul, *Inductance: Loop and Partial*. John Wiley & Sons, Inc., 2010.
- [51] F. W. Grover, *Inductance Calculations*. Dover Publications, 2009.
- [52] Y. Niwa, *A Study of Coils Wound on Rectangular Frames with Special Reference to the Calculation of Inductance*. Tokyo, Japan: Research of the Electrotechnical Laboratory, 1924, no. 141.
- [53] J. J. Lamas-Seco, A. Dapena, J. P. González-Coma, P. M. Castro, and F. J. Vazquez-Araujo, "System for vehicle classification: Hardware prototype and off-line signal processing," in *IEEE Region 8 EuroCon 2015 Conference*, September 2015, pp. 376–379.
- [54] B. R. Hellinga, "Improving freeway speed estimates from single-loop detectors," *Journal of Transportation Engineering*, vol. 128, no. 1, pp. 58–67, 2002.
- [55] A. Tok, S. V. Hernandez, and S. G. Ritchie, "Accurate individual vehicle speeds from single inductive loop signatures," in *Transportation Research Board 88th Annual Meeting*, vol. 09-3512, January 2009.
- [56] M. L. Hazelton, "Estimating vehicle speed from traffic count and occupancy data," *Journal of Data Science*, vol. 2, pp. 231–244, 2004.
- [57] S. Oh, S. Ritchie, and C. Oh, "Real-time traffic measurement from single loop inductive signatures," *Transportation Research Record: Journal of the Transportation Research Board*, vol. 1804, pp. 98–106, 2002.
- [58] B. Coifman and S. Kim, "Speed estimation and length based vehicle classification from freeway single-loop detectors," *Transportation Research Part C: Emerging Technologies*, vol. 17, no. 4, pp. 349 – 364, 2009. [Online]. Available: <http://www.sciencedirect.com/science/article/pii/S0968090X09000072>
- [59] B. Coifman and S. Neelisetty, "Improved speed estimation from single-loop detectors with high truck flow," *Journal of Intelligent Transportation Systems*, vol. 18, no. 2, pp. 138–148, 2014.
- [60] R. L. Gordon and W. Tighe, *Traffic Control Systems Handbook*. Federal Highway Administration, Report No.: FHWA-HOP-06-006, Washington, DC, 2005.
- [61] Y.-K. Ki and D.-K. Baik, "Model for accurate speed measurement using double-loop detectors," *Vehicular Technology, IEEE Transactions on*, vol. 55, no. 4, pp. 1094–1101, July 2006.
- [62] J. Ernst, M. Ndoye, J. Krogmeier, and D. Bullock, "Maximum-likelihood speed estimation using vehicle-induced magnetic signatures," in *Intelligent Transportation Systems, 2009. ITSC '09. 12th International IEEE Conference on*, Oct 2009, pp. 1–6.
- [63] J. Rice, *Mathematical Statistics and Data Analysis*, ser. Advanced series. Cengage Learning, 2006, no. p. 3.

- [64] R. Lomax, *Statistical Concepts: A Second Course*. Lawrence Erlbaum Associates, 2007.
- [65] J. J. Lamas-Seco, P. M. Castro, A. Dapena, and F. J. Vazquez-Araujo, "Vehicle classification using the discrete fourier transform with traffic inductive sensors," *Sensors*, vol. 15, no. 10, p. 27201, 2015. [Online]. Available: <http://www.mdpi.com/1424-8220/15/10/27201>
- [66] Y. Xia, X. Shi, G. Song, Q. Geng, and Y. Liu, "Towards improving quality of video-based vehicle counting method for traffic flow estimation," *Signal Processing*, *in press*, 2014.
- [67] Y. Xia, C. Wang, X. Shi, and L. Zhang, "Vehicles overtaking detection using RGB-D data," *Signal Processing*, vol. 112, no. 0, pp. 98 – 109, 2015.
- [68] A. Ruehli, "Inductance calculations in a complex integrated circuit environment," *IBM Journal of Research and Development*, vol. 16, no. 5, pp. 470–481, Sept 1972.
- [69] H. B. Dwight, *Tables of Integrals and Other Mathematical Data*, 4th ed. New York: Macmillan, 1961.



